This is to certify that the

dissertation entitled

A NOVEL TOTAL INTERNAL REFLECTION FLUORESCENCE (TIRF) TECHNIQUE FOR INVESTIGATING MACROMOLECULAR ADSORPTION AND INTERACTIONS AT THE LIQUID-LIQUID INTERFACE.

presented by

Arivalagan Gajraj

has been accepted towards fulfillment
of the requirements for

Ph.D. degree in Chemical Engineering

Robert Y. Ofoli
Major professor

Date 12/2/99

A NOVEL TOTAL INTERNAL REFLECTION FLUORESCENCE (TIRF) TECHNIQUE FOR INVESTIGATING MACROMOLECULAR ADSORPTION AND INTERACTIONS AT THE LIQUID-LIQUID INTERFACE.

By

Arivalagan Gajraj

A DISSERTATION

Submitted to
Michigan State University
in partial fulfillment of the requirements
for the degree of

DOCTOR OF PHILOSOPHY

Department of Chemical Engineering

1999

ABSTRACT

A NOVEL TOTAL INTERNAL REFLECTION FLUORESCENCE (TIRF) TECHNIQUE FOR INVESTIGATING MACROMOLECULAR ADSORPTION AND INTERACTIONS AT THE LIQUID-LIQUID INTERFACE.

By

Arivalagan Gajraj

This dissertation presents a total internal reflection fluorescence microscopy (TIRFM) tool that allows for direct, quantitative and *in situ* measurement of molecular-level phenomena at the liquid-liquid interface. The apparatus uses a novel experimental cell designed to create a stable and easily maintained liquid-liquid interface and is completely non-invasive.

Protein adsorption at the liquid-liquid interface plays a significant role in a wide range of biological, pharmaceutical, cosmetic, and food related processes. In the first part of this study, the apparatus was used to measure the equilibrium adsorption isotherms of two proteins (BSA and lysozyme), labeled with fluorescein isothiocyanate (FITC) at the oil-water interface. To evaluate the integrity of the interface, the measured profiles were compared to adsorption data collected independently using interfacial tensiometry. Agreement between these sets of data indicated that, in spite of the thinness of the immiscible liquid layers, the interface behaves energetically like a normal liquid-liquid interface.

An important aspect of the study of protein dynamics is the attachment of an extrinsic fluorescent label to enable tracking of proteins by optical techniques. Consequently, the

effect of labeling on protein dynamics is of considerable scientific interest. Unfortunately, this has not been adequately addressed in the literature to date. In the second part of this work, the effect of FITC labeling on BSA was investigated. Ion-exchange chromatography (IEC) was used to exploit the differences in electronegativity between proteins labeled with various quantities of FITC, to obtain samples with different monodisperse labeling ratios. TIRFM was then combined with fluorescence photobleaching recovery (FPR) to measure the effect of labeling on adsorption kinetics and protein diffusion. The results showed that the attachment of an extrinsic label does have a pronounced effect on both adsorption and diffusion of proteins near the interface. For instance, we estimated that the diffusion coefficient of a BSA molecule conjugated with 2 FITC molecules is 40% greater than that of BSA to which only a single label has been attached.

The last part of this work concerned the development of a calibration protocol to enable quantification of interfacial protein concentrations, based solely on the intensity of fluorescence emission. Photobleaching was used to separate the bulk and surface contributions to the fluorescence signal by exploiting differences in mobilities between free and adsorbed proteins. The procedure is instantaneous and non-invasive, and does not require the use of external standards or additional equipment. The surface coverages measured were lower than the corresponding values reported in the literature for the solid-liquid interface. However, this was attributed to the increased mobility afforded to proteins at a liquid-liquid interface.

Dedicated to my mother and my father.

ACKNOWLEDGEMENTS

Firstly, I would like to thank my beloved advisor, Dr. Bob Ofoli, for his guidance, support, encouragement, and friendship. More than anything, he exposed me to the true philosophy of research and taught me, by example, to be a scientist.

I would also like to thank my committee members Dr. Lira, Dr. Ng and Dr. Scranton for taking the time out of their busy schedules to serve on my committee.

Thanks are also due to Sharon, Ilona and Mary who patiently processed every small materials request and put up with me when I fretted over delays.

Big thanks to all my friends and labmates: Parijat, Shawn, Julie, Sumei, Brian, Jamaica, Avani, Ajeet, Bill, Kiran, ...for the good times and the times wasted, the Tetris competitions and the philosophical discussions.

Special thanks to the food science crew, who shared with me their delicious food (Oh yes!) and their friendship and support: Dr. Ng, Vince, Monica, Alfred, Ryu, Pascal, Ling

Thanks to Nicole for her friendship and for her work on the calibration protocols, Rob, for his tensiometry work and enlightening technical discussions and Margarida, for her life saving help with the SAS programming and so much more.

Finally, a shout out to my boys in the Mau Mau... I'd have probably gone insane if not for the music: Jahyouth, Mo, Ossama, Raja, Richard, Tarig, Temesgen

TABLE OF CONTENTS

LIST OF FIGURES

LIST OF TABLES

NOMENCLATURE

θ	incident angle of laser light
θ_c	critical angle for n_1-n_2 interface
λ_∞	wavelength of incident laser light in free space
A	spectroscopic absorbance
$\overline{C}$	protein concentration before photobleaching
C	concentration of diffusing species
C_S	two-dimensional interfacial concentration of proteins
C_B	bulk concentration of proteins
τ	characteristic diffusion time
$\psi(r)$	dimensionless function of the evanescent intensity profile
D	protein diffusion coefficient
d_p	penetration depth of the evanescent wave
d_f	depth of focus of microscope objective
$\overline{E}_S^t$	perpendicularly polarized component of transmitted electric field
$\overline{E}_{0S}^t$	amplitude of $\overline{E}_S^t$
f	mobile fraction of adsorbed proteins
$\overline{F}$	fluorescence signal before photobleaching
$F(\infty)$	asymptote of the fluorescence recovery curve
$F(t)$	fluorescence signal as a function of time

F_T total fluorescence seen by the PMT

F_{ads} interfacial fluorescence

F_{bulk} bulk fluorescence

$I(z)$ evanescent wave intensity at a depth of z

I_o incident light intensity at a depth of z = 0

$I_p(0)$ p-polarized incident light intensity

$I_s(0)$ s-polarized incident light intensity

k bleaching parameter

k_a adsorption rate constant

k_{d1} slow desorption rate constant

k_{d2} rapid desorption rate constant

k_{PB} photobleaching rate constant

k_T rate constant for inter-fluorophore quenching energy transfer

l depth of aqueous phase in experimental cell

L molar labeling ratio of proteins

n_1 refractive index of the dense media

n_2 refractive index of rare media

n relative refractive index

NA numerical aperture of microscope objective

q overall system constant

q_f quantum yield of fluorophores

q_{fB} quantum yield of bulk fluorophores

q_{fS} quantum yield of adsorbed fluorophores

q_I overall instrument constant

q_r relative quantum yield

r_0 immobile fraction of adsorbed proteins

r_1 slowly desorbing fraction of proteins

r_2 rapidly desorbing fraction of proteins

r radial position vector

R inter-fluorophore separation

R_0 Forster distance

s thickness of adsorbed protein layer at the interface

t time

T duration of photobleaching pulse

w half width at e^{-2} height of the Gaussian intensity profile of the laser beam

z depth coordinate into the rare media

Abbreviations

BSA bovine serum albumin

FITC fluorescein isothiocyanate

FPR fluorescence photobleaching recovery

IEC ion-exchange chromatography

PBS phosphate buffered saline buffer

PEO polyethylene oxide

PMT photomultiplier tube

TIRF total internal reflection fluorescence

1. INTRODUCTION

Proteins are amphiphilic polymers that play crucial roles in all biological processes. The word protein is derived from the Greek word "proteios" which means "of the first rank." The term was coined by Berzelius in 1838 to emphasize the importance of this class of molecules (1). The ability of proteins to influence a variety of interfacial phenomena stems from an amphiphilic nature that makes them highly surface active. Proteins are known to adsorb from solution onto almost any surface. In fact, early studies of protein adsorption at the solid-liquid interface were aimed at the development of non-thrombogenic materials for use in implanted cardiovascular prosthetic devices (2). Furthermore, practical problems such as contact lens fouling, plaque formation on teeth and denitrifices, foaming of protein solutions, and fouling of equipment used in the food processing industry are a direct consequence of the relatively high surface activity of proteins.

Due to the importance of proteins in many practical situations, there is a great interest in the study of their adsorption at a variety of interfaces. A large number of studies have been conducted on equilibrium adsorption as well as interactions of various macromolecules at the fluid-solid interface. A small sampling of these studies include interfacial adsorption (3, 4, 5, 6, 7, 8, 9, 10), equilibrium conformation (11, 12, 13), binding equilibrium (13, 14, 15, 16, 17, 18), and binding kinetics (19, 20, 21, 22, 23, 24). Other studies include adsorption of proteins onto solid surfaces (25) and polymer films

(26, 27, 2), binding of antibody to an immobilized antigen (28), characterization of cell-substrate interactions (29, 30, 31), and surface diffusion of adsorbed species (32, 33).

Proteins at the liquid-liquid interface play a significant role in a wide range of biological, pharmaceutical, cosmetic, and food-related processes. In molecular biology, transmembrane proteins (adsorbed at the lipid bilayer) act as channels or pumps and thus play a vital role in energy transduction, ion exchange, and intercellular communication. Just as important, a wide variety of physiological processes are the result of ligand interactions with transmembrane protein receptors. Receptor-driven cell behavior is now known to be extremely important; for example growth, secretion, contraction, motility, and adhesion are all receptor-mediated functions (34). Also, cytoskeletal components (e.g. spectrin in red blood cells) form attachments to cell membranes to define cell motility, shape and mechanoelastic properties (1).

In biomedical applications, the behavior of drugs at biological membranes is an important factor in determining pharmacological activity (35). In such cases, the oil-water interface can be used as a first approximation to study drug delivery in the human body. The water-hydrocarbon solvent interface is the simplest representation of a biological membrane surface that separates the aqueous cytosol or external medium from the apolar central region of a bilayer membrane (36). In fact, oil-water interfaces have been used to model not only drug delivery (37, 35, 38) but also biological systems such as skin, nerve and biomembranes related to taste and olfaction (39).

In areas related to food and agricultural science, protein adsorption plays an important role in the formation and stability of dispersed systems (foams, emulsions, etc). Protein adsorption affects the processing, rheology, texture, appearance and shelf life of food emulsions like mayonnaise and butter and foams like meringue, whipped cream and bread.

There is now also speculation that oil water interfaces might have played an important role in the origin of life. Deamer and Volkov (40) have theorized that the most basic form of life could have utilized energy trapped at the hydrocarbon/water interface to control photochemical reactions, thus giving rise to the beginning of life as defined by biological science.

1.1 Review of studies at the liquid-liquid interface

Various studies have been performed at the liquid-liquid interface using optical and other techniques. The optical techniques used include resonance Raman spectroscopy for a surface-active dye excited by total internal reflection of incident light (41, 42, 43), total internal reflection fluorescence combined with polarization measurements of bis-ANS at the decalin-water interface (36), total internal reflection sum-frequency vibrational spectroscopy to study the conformational order of sodium dodecyl sulfate (SDS) adsorbed at the D_2O-CCl_4 interface (44), attenuated total internal reflection spectroscopy of the kinetics of metal ion extraction at the decalin-water interface (45), optical second harmonic generation used to determine orientation of molecular monolayers at the decane-water and carbon tetrachloride-water interfaces (46), and surface light scattering to determine the dynamic surface pressure of a spread monolayer (47).

Other techniques that measure macroscopic properties and derive molecular parameters include measurement of interfacial tension (47, 48, 49), measurement of the interfacial concentration of proteins tagged with ^{14}C by scintillation counting (50), measurement of potential drop to characterize ion and electron transfer in phospholipids at the interface between two immiscible electrolyte solutions (ITIES) (51), ion transfer voltametry (35), and measurement of interfacial viscosity and shear (52, 53 48).

Markin and Volkov (54) derived a modified Frumpkin adsorption isotherm in a theoretical study and Leaver et al. (55) used trypsin-catalyzed hydrolysis to study variations in the binding of β-casein to the oil-water interface. Ando et al. (56) have cultured human endothelial cells at the liquid-liquid interface pretreated with proteins to study cell-matrix interactions. Also the partitioning of proteins between two liquid phases has been used to model the transfer of membrane proteins into membranes (57).

More recently, Malmsten (58) has combined ellipsometry with TIRF to study adsorption processes in parenteral drug delivery at the liquid-liquid interface. Aoyama et al. (59) have exploited surface mobility at the liquid-liquid interface to develop a new method for two-dimensional crystallization of soluble proteins. Shiba et al. (60) have studied the growth and morphology of anchorage-dependent animal cells. By cultivating the cells at a liquid-liquid interface, they were able to prevent detrimental proteolysis effects usually seen at the solid-liquid interface.

1.2 Challenges and difficulties presented by the liquid-liquid interface

A survey of the literature reveals relatively few optically based techniques for the liquid-liquid interface. This is because of the various difficulties presented by the inherent nature of this interface. Some of the main difficulties and our approaches to dealing with them are discussed below.

1.2.1 Interfacial stability

The interface between two fluids is by nature unstable and susceptible to deformation. For example, room and building vibrations can destabilize the oil-water interface; even convectional currents can induce flow causing the interface to fluctuate. To counteract this tendency, our interface is made up of very thin layers of oil and water (approximately an 80 μm layer of oil on top of a 900 μm layer of water). Thus, from a global or macroscopic point of view, the system functions like a solid-liquid interface. Therefore it does not suffer from the typical vibration-induced instability problems encountered at liquid-liquid interfaces of normal depth. However, in relation to the largest linear dimension of a protein (approximately 15 nm for BSA) an oil layer of 80 μm is sufficiently thick, and should function as a liquid-liquid interface of normal depth. To provide further stability, our entire experimental apparatus is housed on a vibration isolation table.

1.2.2 Reproducibility

Forming a reproducible oil-water interface is nearly impossible as minute changes in shape, size and location are unavoidable. This means that experimental runs made on different days or even at different locations on the same interface may not be comparable.

Therefore, we have been constrained to design our experiments to stand on their own. Our calibration protocol, described in chapter 4 of this dissertation, has been developed to circumvent this problem.

1.2.3 Difficulties in calibration

The common techniques used for quantifying protein adsorption at the solid-liquid interface will not work at the liquid-liquid interface. This is because

1. the exact thickness of the liquid-liquid interface is non-uniform and unknown;
2. the liquid-liquid interface cannot be isolated from the experimental cell; and
3. there is no reliable way to drain species in the aqueous bulk without incorporating species at the interface.

A calibration protocol that enables one to circumvent these liabilities is discussed in further detail in chapter 4 of this dissertation.

1.3 Focus of this dissertation

The primary goal of this dissertation was to design a quantitative tool to study protein adsorption at the liquid-liquid interface to enable non-intrusive, *in situ* investigation of the same. A major portion of the work that went into this project involved the development, design and assembly of the instrumentation of the technique. The basic experimental tool was adapted from various TIRF studies at the solid-liquid interface. However, there were several differences between the two protocols. For example, the nature of the oil-water interface precludes the use of a standard microscope, and the use of an inverted microscope necessitated a total rethinking of the experimental cell and beam optics in

relation to the position of the microscope objective. Several generations of equipment were developed, modified and improved. The key concerns addressed were enhancements of the signal-to-noise ratios of the PMT and improvement of the surface selectivity of the TIRF technique. To illustrate we were able to reduce the noise levels from approximately 40% to 0.5%.

This dissertation was divided into three studies with auxiliary information provided in the appendices. The first study introduces the TIRF technique and provides a description of the development, design criteria, construction, and trouble shooting of the experimental set-up. The study also presents details of the experimental procedure and preliminary results of equilibrium adsorption of BSA and lysozyme. The qualitative agreement of the adsorption curves with the theory, independent interfacial tensiometry experiments and previous results in the literature confirms the integrity of our liquid-liquid interface, and validates the technique.

An important aspect of modern protein chemistry is the attachment of an extrinsic label to proteins. The second study investigates the effect of a label on the adsorption kinetics and diffusion of proteins. Several researchers have discussed the possibility that extrinsic fluorophores affect protein behavior; however, there are no definitive conclusions reported in the literature. This study uses ion-exchange chromatography to obtain protein samples with different monodisperse labeling ratios. Subsequent TIRF experiments on these samples revealed that the label does have a pronounced effect on both diffusion and adsorption kinetics.

The third study presents a calibration protocol for the quantitation of interfacially adsorbed proteins in our system. The method is self-contained, in that no other measuring systems besides the TIRF apparatus is required. The protocol uses an absolute criterion for focusing the microscope that automatically accounts for unevenness of the oil-water interface. Thus, protein concentrations estimated at different locations on the interface are comparable.

2. A TIRF TECHNIQUE FOR INVESTIGATING MACROMOLECULAR ADSORPTION AND INTERACTIONS AT THE LIQUID-LIQUID INTERFACE.

2.1 Introduction and background

The liquid-liquid interface is of considerable importance in biological systems, particularly in biomedical engineering, pharmacology and food processing. The hydrocarbon/water interface provides an excellent first approximation to cellular interfaces where many important biological functions and/or processes occur. These include receptor-ligand interactions, energy transduction, electron transfer, enzyme coupling, and triggering of cells by hormones and neurotransmitters (1). In biomedical applications, the behavior of drugs at biological membranes is an important factor in determining pharmacological activity (35). In such cases, the oil-water interface can be used to characterize and/or understand drug delivery issues, since it can be used to approximate membrane structure and/or activity. In effect, while biomembranes are structurally complex, immiscible oil-water interfaces may be used as simplified models in drug delivery experiments.

The liquid-liquid interface provides an excellent model for interactions of macromolecules at relatively mobile interfaces (61). It also affords enormous flexibility with respect to system complexity. For example, by adding surfactants and ions to a simple oil-water interface and/or controlling the pH, the interface can be made as complex as desirable, enabling one to mimic many biological systems. In particular, the hydrocarbon-water

interface is a simple representation of a biological membrane surface that separates the aqueous cytosol or external medium from the apolar central region of a bilayer membrane (36).

The liquid-liquid interface is also crucial to food systems and food processing. For example, the distribution and/or interactions of proteins and surfactants at this interface greatly influence the properties of food emulsions and microemulsions. The stability of emulsions such as mayonnaise depends to a large extent on the adsorption and/or interactions of proteins and/or surfactants at the oil-water interface. Protein-stabilized emulsions also influence such properties as shelf life and foam stability in many food systems. The food industry (as well as the pharmaceutical industry) also routinely uses proteins to lower the interfacial tension between two immiscible liquid phases, to facilitate the dispersion of one phase in the other (48).

In spite of its considerable importance in biological systems, this interface has, until recently, received relatively little attention. This is primarily due to the lack of appropriate quantitative techniques that may be used to probe the interface at the molecular level. One of our goals in developing the technique described in this chapter was to help mitigate this shortcoming in experimental tools.

2.1.1 Rationale for using TIRFM for the liquid-liquid interface

Total internal reflection fluorescence microscopy (TIRFM) is an invaluable in-situ, non-invasive and non-destructive tool for studying interfacial phenomena at the molecular

level. The ability to directly measure molecular-level phenomena represents an improvement over techniques that measure macroscopic properties and derive microscopic parameters from the data. TIRFM provides the ability to selectively excite species within tens of nanometers from a given interface. It can be used to quantify the concentration of species as a function of distance from a given interface, allowing one to directly determine adsorption and desorption kinetic parameters (62). One of the earliest studies using TIRF for fluid-fluid interfacial adsorption was done by Tweet et al. (63) when they used the technique to measure the emission spectrum and quenching behavior of chlorophyll *a* monolayers at the air-water interface. By using TIRF, the weak fluorescence generated by the dilute monolayer was detected while light from direct and scattered mercury arc excitation was excluded.

There are a few published applications of TIRF at the liquid-liquid interface. Among these, Morrison and Weber (36) studied the adsorption of 4,4'-bis-1-phenylamino-8-naphthalenesulfonate (bis-ANS) at the decalin-water interface; and Takenaka and Nakanaga (42), Nakanaga and Takenaka (41) and Takenaka (43) have presented results of a series of experiments on adsorption of anionic dyes to the water-chloroform interface, using Raman scattering to infer the orientation of dye molecules at the interface. More recently, TIRFS has been used by Wirth and Burbage (64) to study acridine orange reorientation at a water/(octadecylsilyl)silica interface, Besso et al. (65) have studied the microenvironment of 8-anilino-1-naphthalenesulphonate at the heptane/water interface, Watarai and Saitoh (66) have studied the ion-association adsorption of water-soluble

porphyrins at the liquid-liquid interface, and Tupy et al. (67) have studied dynamic adsorption at the oil-water interface.

Several standard (non-TIRF) techniques have also been used to study adsorption at the liquid-liquid interface (68, 69, 70). These techniques include monitoring changes in interfacial tension (48, 71, 72, 73); measuring the interfacial concentration of ^{14}C labeled species by scintillation counting (50); measuring rheological properties such as interfacial viscosity and/or shear (48, 71, 74); monitoring film viscosities and viscous traction (48, 52); evaluating surface voltage potential differences (particularly in the case of spread monolayers); measuring surface diffusion; and characterizing electrokinetic phenomena.

Among other optical studies, Grubb et al. (46) used second harmonic generation to determine the orientation of molecular monolayers of surfactants at various liquid-liquid interfaces, Conboy et al. (44) used sum-frequency vibrational spectroscopy (in TIR geometry) to investigate the conformation and order of sodium dodecyl sulfate adsorbed at the water-carbon tetrachloride interface, and Sauer et al. (47) used quasi-elastic light scattering to determine the dynamic surface pressure of dipalmitoylphosphatidylcholine at the heptane-water interface.

2.2 Objectives

Our goal in this study was to develop a total internal reflection fluorescence microscopy (TIRFM) technique to enable molecular-level investigations of adsorption and interactions of amphiphilic macromolecules at the liquid-liquid interface. In this chapter, we present the details of the experimental set-up and the nature of the interface, and briefly outline the results of experiments on the equilibrium adsorption of a hard protein (lysozyme) and a soft protein (BSA) at the oil-water interface.

2.3 Theory

The theory of total internal reflection has been well treated elsewhere (62, 75, 25, 30). As such, only a brief discussion will be given here. A more detailed description of development of the evanescent wave equation can be found in Chapter 4.

2.3.1 The Evanescent wave

Total internal reflection occurs when a light beam, emanating from an optically dense medium (n_1) reaches the interface between that medium and an optically rarer medium (n_2) at an angle which exceeds a critical angle (θ_c) defined by

$$\theta_c \equiv \sin^{-1}\left(\frac{n_2}{n_1}\right) \qquad n_1 > n_2 \tag{1}$$

where n_1 and n_2 are the refractive indices of the dense and rare media, respectively.

When the beam undergoes total internal reflection, it induces an electromagnetic field in the rarer medium beyond the interface (Figure 2.1). The intensity of this induced electromagnetic field (or evanescent wave) decays exponentially with perpendicular distance z from the interface. As a result, the light impinging on a body in the evanescent wave also decays exponentially with distance from the interface according to the relationship

$$I(z) = I_o e^{-z/d_p} \tag{2}$$

where $I(z)$ is the intensity at any depth z and I_o is the incident light intensity at the interface.

The penetration depth, d_p, of the evanescent wave is given by

$$d_p = \frac{\lambda_o}{4\pi n_1 \sqrt{\sin^2 \theta - n_{21}^2}} \tag{3}$$

where λ_o is the wavelength of the incident radiation in vacuum, θ is the angle of incidence, and $n_{21} = n_2 / n_1$ is the relative refractive index.

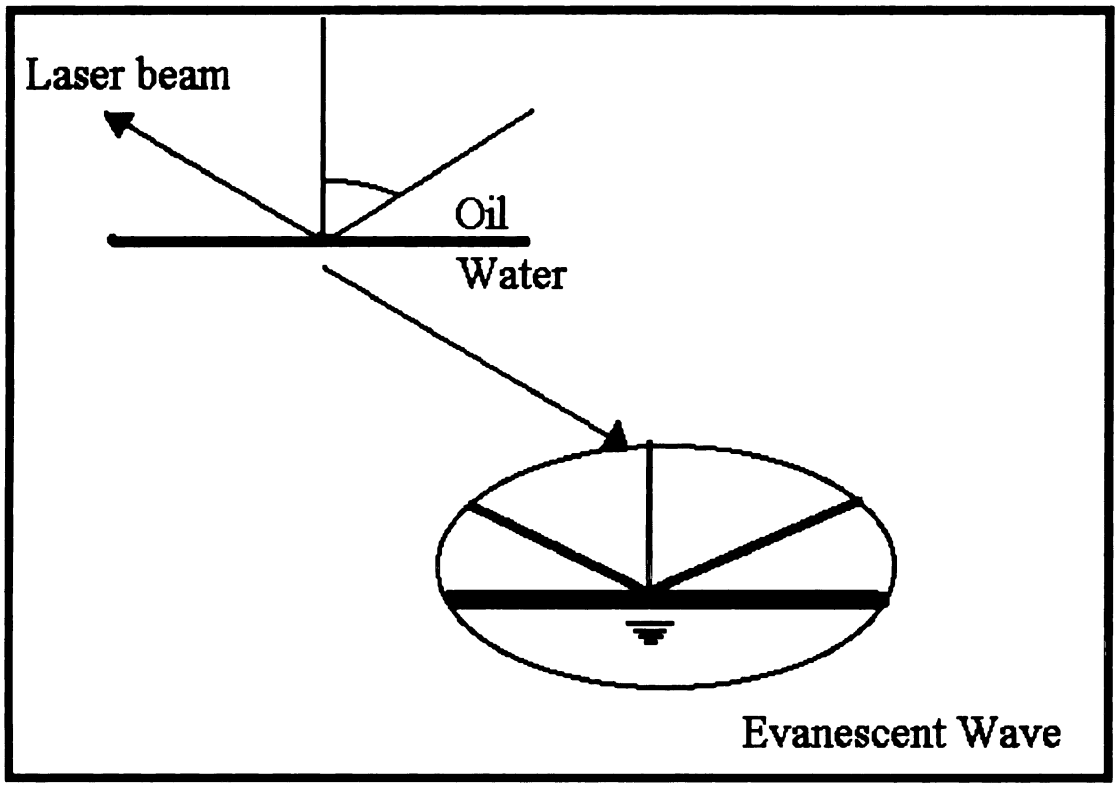

Figure 2.1. Total internal reflection at the oil-water interface. The resulting evanescent wave decays exponentially into the rarer aqueous phase.

There are two optical techniques that exploit the properties of the evanescent wave to measure the sub-micron distances between macromolecules and interfaces. These are total internal reflection microscopy (TIRM) and total internal reflection fluorescence (TIRF). TIRM has been used to measure the energies of interaction between a single particle and a flat surface. By measuring I_o and $I(z)$, the separation distances z between the particle and the surface can be calculated from Eq. (2) and converted to a potential energy of interaction (76). TIRF also exploits the evanescent wave at the interface between two materials with different refractive indices, except that fluorescence emission intensities rather than light scattering intensities are measured. Because TIRFM can accommodate much smaller particles for which light scattering intensities are generally not measurable, it is an important technique for studying protein adsorption.

2.4 Description of apparatus

2.4.1 Developmental challenges

There were several challenges in developing and assembling this apparatus. The first concerned the adaptation of the standard solid-liquid interface TIRF apparatus to the liquid-liquid interface. In particular, several precautions and mechanisms had to be put in place to ensure interfacial stability. The second challenge was to ascertain that the steps taken to help ensure interfacial stability had not modified the interfacial energetics to the point that one could not guarantee the integrity of the interface. The third was to devise a calibration scheme to enable the calculation of interfacial fluorophore concentrations directly from fluorescence intensity data.

2.4.2 TIRFM set-up

The experimental setup is shown in Figure 2.2. In summary, the apparatus uses an inverted microscope (Zeiss Axiovert 135 M, Carl Zeiss, Inc., Thornwood, NY), a 5 W continuous wave argon ion laser (Lexel Lasers Model 95, Fremont, CA), a side-on photomultiplier tube (Hamamatsu R4632, Bridgewater, NJ) jacketed in a thermoelectrically cooled housing (TE177TSRF, Products for Research, Danvers, MA), a CCD camera (MTI, VE1000, Zeiss), a computerized data acquisition system (Viewdac, Keithley/Asyst, Rochester, NY), a modular automation controller with an RS232 interface (MAC 2000, Ludl Electronic Products, Hawthorne, NY), and a double-syringe pump system (Model 551382, Harvard Apparatus, South Natick, MA) used to simultaneously infuse and withdraw samples from the flow cell. The entire assembly of components is mounted on a vibration isolation table (RS 4000, Newport Corporation, Irvine, CA) to ensure interfacial stability.

We use the 488 nm line of an argon ion laser housed in a light-tight box. The laser light is first attenuated using neutral density filters (03FNQ, Melles Griot, Boulder, CO). An optical chopper (SR540, Stanford Research Systems, Sunnyvale, CA) is used to prevent unintended photobleaching of fluorophores during experiments conducted over long periods of time. Our work requires a rapid and reproducible method for instantaneously switching from bleaching laser beam intensities to monitoring beam intensities. This is achieved by a system of two identical optical flats, a programmable shutter (D122, Uniblitz, Vincent Associates, Rochester, NY) and a set of neutral density filters, as described below.

The front of the first flat is coated with magnesium fluoride and the back with aluminum, to discourage and encourage reflection, respectively. The monitoring beam is formed by the weak reflection off the front surface while the photobleaching beam reflects off the aluminized back surface. The second flat is aligned to exactly recombine the two beams to ensure that the monitoring beam is accurately superimposed on the photobleaching beam at the interface. The shutter, placed between the two flats, blocks the photobleaching beam only, but allows for photobleaching with a sub-millisecond laser flash upon activation. A typical bleach pulse duration of 100 msecs is used in our experiments. This was found to be sufficient to entirely bleach the interfacial fluorophores and yet not cause any undesirable heating effects (77). A second shutter placed inside the microscope cavity blocks off the PMT for the duration of the photobleaching pulse. The driver/controllers for the two shutters are wired such that they can be triggered by a single footswitch. By adjusting the delay and exposure times, the two shutters can be exactly synchronized. This is important to prevent damage to the PMT during photobleaching and also aids in the mitigation of light hysteresis of the PMT (see chapter 4 for further discussion). The ratio of photobleaching to monitoring beam intensities can be varied from 1000:1 up to 5000:1, and is typically 4000:1 in our experiments. Beyond the flats, the laser beam is conveyed by a system of mirrors, and finally focused onto the interface in the experimental cell, using a plano-convex lens (f = 200mm, Oriel Corporation, Stratford, CT).

The sample cell (described more fully below) is accessed through a Zeiss Achroplan microscope objective (LD 440651, 32X, 0.4 or 440091, 40X, 0.75, Carl Zeiss Inc.,

Thornwood, NY) focused at the interface. The fluorescence excited by the incident laser light is captured by the objective and can either be viewed by a CCD camera or measured by the PMT. An interference filter (500EFLP-EM, Omega Optical, Brattleboro, VT) placed inside the microscope ensures that only the wavelength range of the emitted fluorescence is transmitted.

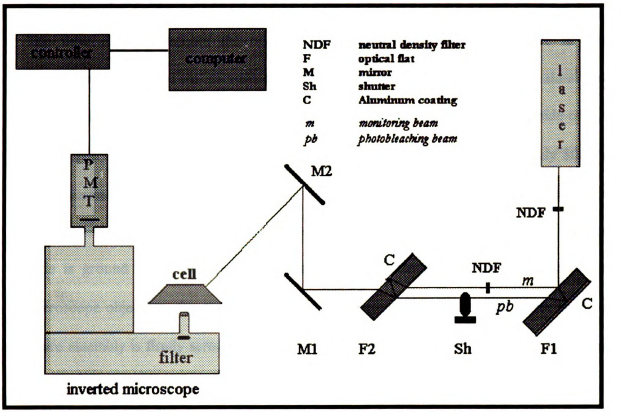

Figure 2.2. Layout of the experimental setup for TIRFM experiments. The double-flat system is used to first separate the incident beam into monitoring and photobleaching streams, and then recombine the two beams. This scheme provides control over beam intensities while ensuring superposition at the interface.

2.4.3 The sample cell

The flow cell that houses the oil-water interface is of crucial importance in this experimental set-up. Two microscope slides are separated by a 1-mm thin aluminum spacer, with an oval cut into it to form the experimental sample cell. The underside of the top microscope slide is coated with a thin layer of oil. This layer, approximately 80 μm thick, forms the oil part of the interface. Two holes drilled in the bottom slide enable infusion and withdrawal of water and/or protein solutions from the apparatus. The bottom slide is ground to a thickness of 0.75 mm to allow for the use of the appropriate microscope objective. The top slide is optically coupled to a 70° dovetail prism and the entire assembly is firmly screwed onto an anodized aluminum shell that sits on top of an inverted microscope stage (Figure 2.3). The microscope stage can be moved precisely and repeatably by a computer, enabling different areas of the interface to be studied in a series of runs.

The double-syringe pump is used to simultaneously infuse and withdraw protein solution into and out of the experimental cell in a controlled manner. The setup can be used for flow-through experiments, but has so far been mostly used in the stopped-flow mode. Prior to each experiment, the chamber is filled with phosphate buffered saline (PBS) buffer, which is replaced by a protein solution of the appropriate concentration for each experiment.

A critical and novel aspect of this setup is that the thickness of the entire oil-water assembly is approximately 1.0 mm. The primary advantage of this construction is that,

from a global or macroscopic point of view, the system functions like a solid-liquid interface. Therefore, it does not suffer from the typical vibration-induced instability problems encountered at liquid-liquid interfaces of normal depth. Thus, interfacial stability is essentially guaranteed. However, from a microscopic or molecular point of view, it behaves as a true liquid-liquid interface since, for a protein molecule with a linear dimension of no more than 20 nm, an 80 μm oil layer is sufficiently thick and should not affect its dynamics. This was the first goal in our apparatus development.

The second goal was to put the thin oil layer in contact with a protein solution approximately 1000 μm thick. This water/solution layer is thin enough to give us an equilibrium adsorption time on the order of minutes rather than hours. In addition, the apparatus makes it possible to use hydrodynamic shear to sweep the interface clean and create a new interface within a reasonable amount of time although, in practice, this has not been very easy to accomplish.

2.4.4 Materials

The proteins used for the study presented in this chapter were essentially fatty acid-free BSA (A-7511, Sigma Chemical Co, St. Louis, MO) and lysozyme (L-2879, Sigma Chemical Co, St. Louis, MO). Protein concentrations in all our regular experiments were kept below the critical micelle concentration, therefore; only single protein interactions are normally characterized with this equipment. In this chapter, however, we present standard protein adsorption data, therefore concentrations range from infinite dilution to above the critical micelle concentration.

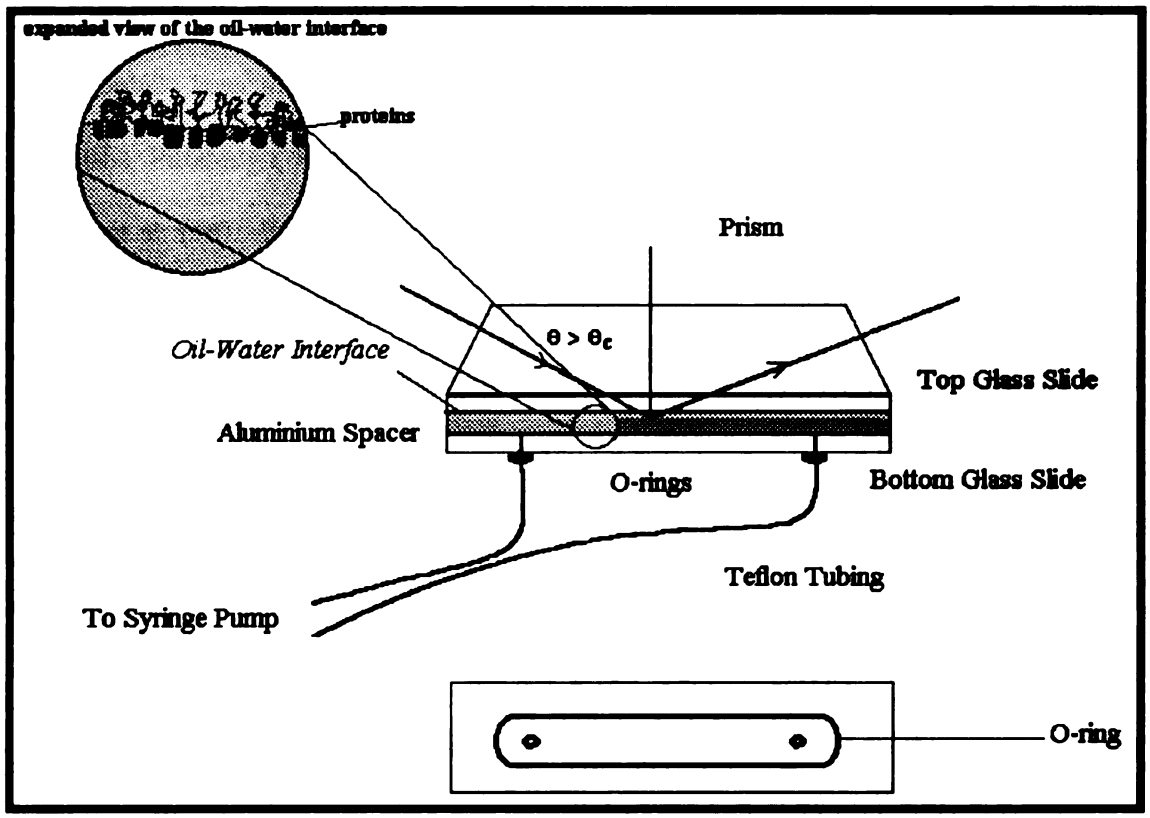

Figure 2.3. The experimental cell, showing the location of the interface. The thickness of the oil-water layer is less than 1.0 mm, which helps to ensure interfacial stability.

2.5 Experimental Procedures

2.5.1 Coating of microscope slide with oil

The lyophilic layer at the interface is formed with Cargille Type A immersion oil (Fisher Scientific, Pittsburgh, PA). The microscope slide is cleaned by the procedure outlined by Cheng et al. (78). Before coating with oil, the slide is first heated for 5 minutes under a heat lamp. Then a drop of oil, of a pre-determined volume, is placed at the top of the slide. A clean cylindrical glass rod is smoothly dragged and gently rolled once over the slide, thereby sweeping the surface of the slide and evenly coating it with oil. The slide is then optically coupled to the prism by applying an appropriate refractive index matching fluid (Cargille Type A immersion oil, Fisher Scientific, Pittsburgh, PA) to the upper surface in contact with the prism. The slide and the prism are then placed on top of a flow cell (initially filled with double de-ionized water or protein solution) to form the oil-water interface. We estimated that the oil layer interacting with the water to form the oil-water interface is approximately 80 μm thick. This was done by carefully comparing the weights of microscope slides, before and after coating with oil, to deduce the weight of the oil layer. The thickness of the oil layer was then deduced from the surface area of the slide and the density of the oil.

2.5.2 Protein labeling

Proteins were labeled with fluorescein-5-isothiocyanate (FITC, F-1907, Molecular Probes, Eugene, OR) in our laboratory, using the techniques outlined by Edidin (79). The unreacted labels were removed by a two-stage dialysis process performed over a period of 24 hours. Absorbance spectroscopy measurements with a diode array spectrophotometer

(8452 A, Hewlett Packard, Brielle, NJ) at 280 nm and 500 nm were used to determine the protein and label concentrations, respectively. The chemistry of the labeling reaction is discussed in chapter 3 of this dissertation.

2.5.3 Beam alignment and microscope focusing protocols

The proper alignment of the TIRF system is primarily dependent on achieving normal incidence of the laser beam on the TIR prism, while simultaneously ensuring that the point of TIR is exactly above the microscope objective. This is not a trivial matter, because the optical alignments required to focus the microscope tend to destroy the normal incidence of the beam and vice versa. However, repeated iterations of the two procedures, along with horizontal translation of the beam steering device, will eventually yield the desired result.

Normal incidence of the laser beam was achieved by tracking the reflection of the beam from the prism surface. The optical components of the system were adjusted till the back reflection of the laser beam re-entered the laser. This indicates that the beam has achieved normal incidence at the prism. Each optical component, starting from the mirror closest to the prism, was adjusted in turn to ensure that the reflection from the next optic exactly retraces the incident beam path. The optical component furthest upstream from the laser was later slightly displaced, to prevent the back reflection from re-entering the laser during the course of the experiments.

The microscope was focussed as follows: a coarse alignment was first performed with the naked eye to roughly place the point of TIR over the microscope objective. Then, looking through the PMT cavity on the microscope (the PMT was removed for this procedure), the top mirror of the beam steering device was adjusted to bring the evanescent wave under the microscope objective. The microscope was then focussed till the evanescent wave fills the objective viewing area. This was performed after removing the interference filter from the microscope at a laser beam intensity of about 0.1 mW.

The PMT was then replaced and minute adjustments were performed to the microscope and the beam steering device to maximize the PMT signal.

2.5.4 Introduction of proteins into the flow cell

The experimental cell was first flushed with pure PBS buffer at a pH of 7.4, for a period of 25 minutes. This served to remove any air bubbles in the tubing and the experimental cell. At this time, the PMT shutter was opened and the background noise present in the system was estimated. This level, usually about 100 arbitrary intensity units, was later subtracted from all PMT readings. The proteins were then injected into the cell using a reciprocating syringe pump that simultaneously withdraws PBS buffer solution. To prevent artifacts due to mechanical shearing of the interface, care was taken to ensure that the flowrate does not exceed ~0.1 mL/min. The solution was allowed to flow into the sample cell until the PBS buffer initially occupying the flow cell had been completely replaced by the protein solution. At this time, the syringe pump was turned off, and a stable interface was re-established.

2.5.5 Experimental precautions

The first concern was with unintended photobleaching of labeled adsorbates. Photobleaching is the random, dynamic process in which fluorophore molecules undergo photo-induced chemical destruction and thus lose their ability to fluoresce. This was always a strong possibility in TIRF experiments when adsorption was slow to reach equilibrium and one continuously monitors the process. We followed the procedure of Lok et al. (27, 2) and used a beam chopper during long experiments. The photobleaching beam was always blocked during periods of fluorescence measurement through the use of the triggered shutter system described earlier. The trigger that activates the photobleaching beam also simultaneously closes an LS6Z2 shutter (Vincent Associates, Rochester, NY) mounted inside the microscope. This serves to protect the PMT from the high power photobleaching flash and prevent PMT hysteresis, which distorts the initial fluorescence recovery curve.

A second experimental necessity was the prevention of photochemically induced cross-linking of proteins at the interface. When this occurs, it was accompanied by a slow continual illumination-dependent increase in the fluorescence signal (62). To prevent this, the samples were deoxygenated before introduction into the sample chamber.

2.6 Problems and opportunities for the liquid-liquid interface

Flow cells are routinely used in studies at the solid-liquid interface without the risk of destroying the interface. With the liquid-liquid interface, however, there is a strong

possibility of sweeping away molecules adsorbed at the interface during continuous flow experiments, as a result of hydrodynamic shear. While this is a potential problem, the fact that the interface can be swept clean is also an advantage of this setup. The ability to use hydrodynamic shear to clear the interface of adsorbates enables us to greatly minimize the time required to create a new interface. By using this clean-in-place strategy, a given quartz slide can be left in place and used to run several experiments without having to change the slide each time a clean interface is required. Our experiments were usually conducted in stopped-flow mode, but we have also determined the maximum flow rate at which flow-through experiments can be conducted without inducing unacceptable levels of hydrodynamic shear at the interface.

2.7 Results and discussion

2.7.1 Timescale of equilibrium adsorption

Figure 2.4 shows the results of a TIRFM experiment to measure the equilibrium adsorption of BSA at the oil-water interface. The bulk protein concentration was 0.01 mM with a labeling ratio of one FITC per BSA. The syringe pump was operated at an injection rate of 0.05 ml/min. To reduce the chances of photobleaching by the monitoring beam, the optical chopper was completely masked with aluminum foil, except for a 1-cm wide slit. This reduced the duration of the monitoring beam incidence on the interface by approximately 95%.

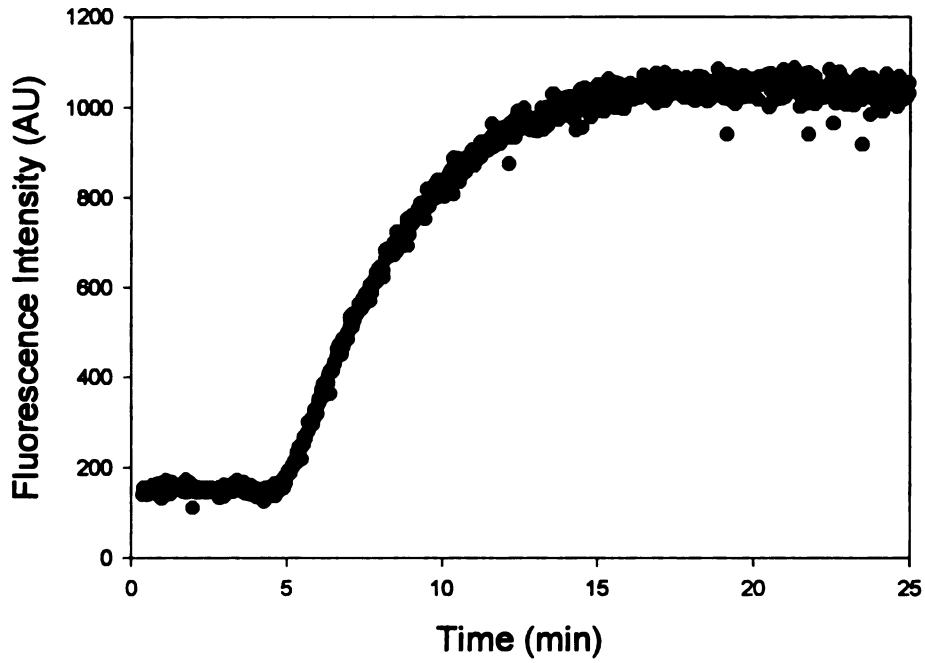

Figure 2.4. Typical TIRFM protein adsorption experiment showing fluorescence intensity versus time during the equilibrium adsorption of BSA at the oil-water interface. From the data, the time required to reach adsorption equilibrium was estimated at about 20 minutes.

At t = 5 min, the flow of protein solution was started. As the protein adsorbed, the fluorescence signal increased steadily and reached a steady-state value at interfacial saturation. This was observed to occur at t ~ 20 minutes. This confirms the fact that the thinness of the oil-water assembly allows for faster equilibrium adsorption times.

Note that the signal to noise ratio (~10%) is larger than what is typically seen in other TIRFM experiments presented in this dissertation. This is due to the presence of the optical chopper. Since PMT data collection is not synchronized with beam chopping frequency, a part of the collection cycle frequently occurs with the incident beam partially blocked. This leads to a random artificial lowering of the PMT signal, which results in an increased signal to noise ratio.

2.7.2 Assessment of interfacial integrity

A key concern of this study was whether a thin oil-water interface, configured to a dimension of no more than 80 μm of oil on top of approximately 1000 μm of water, would behave like a "true" oil-water interface. As already discussed, the thinness of the interface was necessary to ensure interfacial stability, and prevent the interface from shifting or rolling in the presence of vibration. To assess the interfacial integrity of our apparatus, we measured the emitted fluorescence and, from the signal, computed the relative interfacial concentration of adsorbed species. The adsorption isotherms were then compared to isotherms obtained from interfacial tension measurements at a "normal" oil-water interface, using the Krüss 12K Interfacial tensiometer (Krüss, USA). The results for BSA and lysozyme are discussed below.

2.7.2.1 Equilibrium adsorption of BSA at the oil-water interface

Most amphiphilic or surface-active solutes have the property of forming colloid-size clusters called micelles when their concentration in an aqueous solution is at or above the critical micelle concentration (cmc). A graph of most physical properties that are functions of size or number density of solute particles display a break in the neighborhood of the cmc. We postulated that an important test of the integrity of the oil-water interface in our apparatus is whether the apparatus can be used to estimate the cmc. To do this assessment, we measured the interfacial fluorescence intensities as a function of the concentration of FITC-conjugated BSA molecules in solution.

The results are shown in Figure 2.5a. As expected, the fluorescence intensity rises with concentration until the interface approaches saturation. At that point, the fluorescence intensity begins to level off. However, there is a clear break in slope between the region of sharply rising fluorescent intensities and the region where fluorescent intensities appear to be stabilizing with respect to concentration. This break occurs at a BSA concentration of 0.1 mM, which is approximately the cmc of this protein, as determined by interfacial tension measurements. These data provide strong evidence that we are indeed measuring phenomena at a thermodynamically true oil-water interface, and that the thinness of the oil-water layer has not affected protein dynamics.

a.

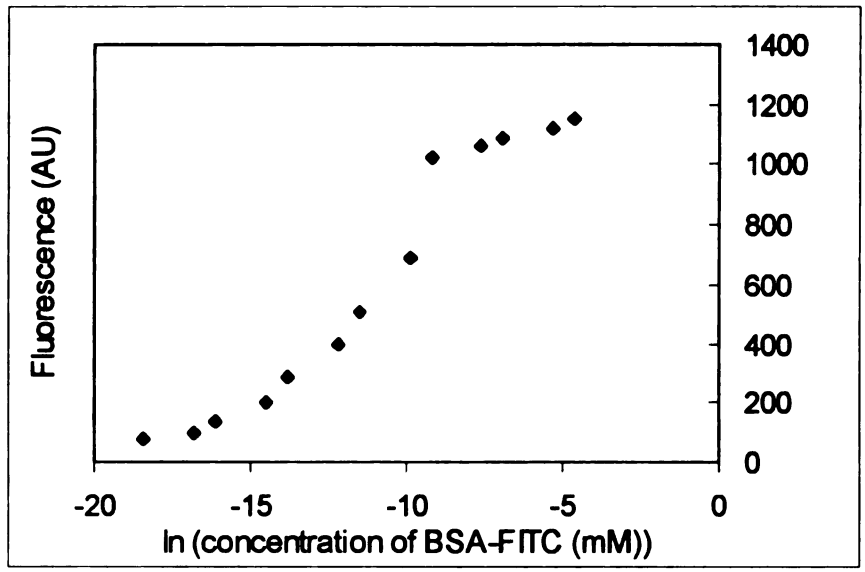

b.

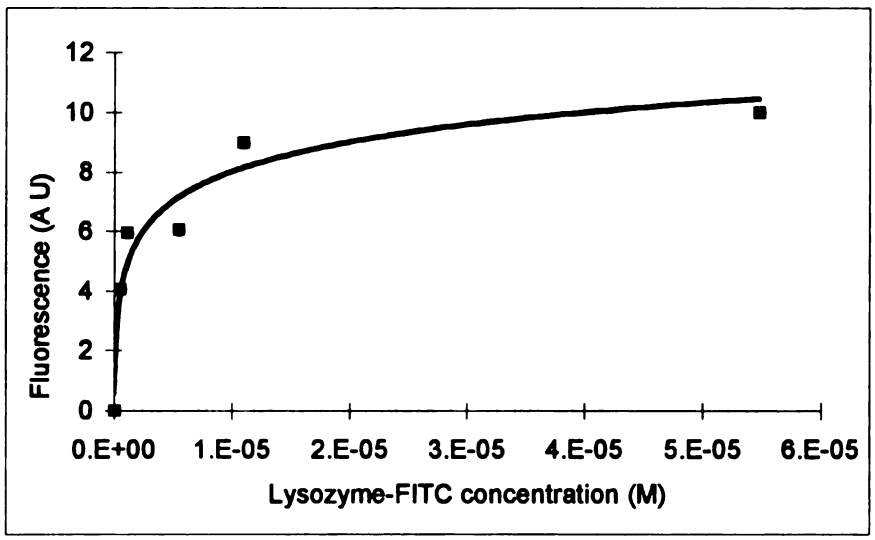

Figure 2.5. Equilibrium adsorption profiles for lysozyme and BSA conjugated with the FITC label. Plot a) for BSA is at a much higher concentration, and portrays a solution that has approached and exceeded interfacial saturation. The plot shows a clear break in profile at the cmc. Plot b) for lysozyme shows a gradual approach to interfacial saturation, with no indication of a cmc.

2.7.2.2 Equilibrium adsorption of lysozyme at the oil-water interface

The adsorption isotherm for lysozyme is plotted in Figure 2.5b. It shows a region where the fluorescence intensity initially rises linearly with concentration, as would be expected. As the concentration increases further and the interface becomes saturated with proteins, the fluorescence intensity levels off. This is a classical adsorption isotherm. We should note that there is no point of inflection or change of slope to indicate the formation of micelles in this system. Therefore, the profile is as expected, since lysozyme is a predominantly hydrophilic protein that does not form micelles in aqueous media (80).

2.8 Conclusions

We have developed a total internal reflection fluorescence microscopy (TIRFM) technique for quantitative molecular-level investigations of macromolecular adsorption and interactions at the oil-water interface. Due to the novel construction of the oil-water interface in our sample cell, we have circumvented the typical vibration-induced instability problems encountered with optical techniques at liquid-liquid interfaces of normal depth.

An important goal during our development was to put a thin oil layer in contact with a protein solution that is no more than 1000 μm deep. The thinness of the oil-water assembly makes it possible for us to achieve a diffusion time constant of no more than 3 minutes (see Table 1, chapter 3), and an equilibrium adsorption time on the order of minutes rather than hours. It also provides the possibility of using hydrodynamic shear to create a new interface.

In spite of the thinness of the resulting interface, it behaves as a true liquid-liquid interface, as evidenced by the classical adsorption data we obtained for lysozyme and BSA. To evaluate the interfacial integrity of our sample cell, we used the apparatus to estimate the critical micelle concentration (cmc) of BSA. A clear break in the adsorption isotherm, indicative of the cmc, occurred at approximately 0.1 mM, which is a typical value for this protein. On the other hand, the adsorption isotherm measured for lysozyme displayed a smooth curve without any breaks to indicate the formation of micelles, which is to be expected for a predominantly hydrophilic protein such as lysozyme.

The system is very flexible with respect to sample complexity. For example, by adding surfactant molecules and ions to this simple oil-water interface and/or controlling the pH, one can create more biologically relevant systems and interfaces. System flexibility also allows the study of macromolecular adsorption at different liquid-liquid interfaces, as long as both liquids are optically transparent.

3. EFFECT OF EXTRINSIC FLUORESCENT LABELS ON DIFFUSION AND ADSORPTION KINETICS OF BSA AT THE LIQUID-LIQUID INTERFACE.

3.1 Introduction and background

An important and widely-used technique in interfacial macromolecular adsorption experiments is the covalent attachment of an extrinsic fluorescent label. The purpose of labeling a macromolecule is to provide it with a "marker" that makes it readily trackable by optical means. Ideally, the marker emits a measurable fluorescence upon excitation at an appropriate wavelength. This fluorescence is an extremely sensitive optical technique for the detection of biological materials. This sensitivity, combined with the ease of use and the potential for multiparameter analysis, has resulted in widespread use of fluorescence in biology and medicine (81).

Extrinsic labels have been used to study a variety of macromolecular characteristics and behaviors. These include adsorbate enzyme activity (82), receptor-ligand binding (11, 12) and binding of proteins to specific membrane targets (18). They have also been used to model planar membranes (15, 20) and study conformational changes of proteins upon adsorption (83, 33, 84), as well as kinetics of protein adsorption (4, 12). Labels have also been used to study various aspects of protein adsorption at the solid-liquid (27, 32, 9, 78, 85) and liquid-liquid interfaces (86, 67, 87), and at biological membranes (88, 89, 90). Labeled proteins have also been very useful in such techniques as radioimmunoassays, enzyme immunoassay, fluorescent antibody staining and nucleic acid probes (91).

Ideally, labeling a macromolecule should not compromise the target properties or characteristics of interest in the native state. However, several researchers have discussed the possibility that extrinsic fluorophores do affect the biological phenomena being studied. For example, Axelrod et al. (62) and Burghardt and Axelrod (4) stated that, in principle, such labels probably affect the adsorption of proteins. Hoyland (92) has also reviewed the potential artifacts resulting from using fluorescence probes in membranes. Zimmerman et al. (14) showed that there were no differences in thermal denaturation (as measured by static light scattering) or enzymatic activity between labeled and unlabeled lysozyme. They concluded, however, that the labeled lysozyme, while being a functional protein, could have other altered properties that might be reflected in their adsorption behavior.

As early as 1978, Brynda et al. (93) evaluated alternatives to radioactive-labeling of proteins and concluded that BSA exhibited changes in its native electrophoretic properties when labeled with DANSI, fluorescamine or FITC. Sorption properties were also observed to be affected by conjugation with fluorescamine. However, no attempt was made to quantify the effects of the label. Crandall et al. (94) used electrophoretic mobility and ion-exchange chromatography, together with measurements of the degree of conjugation and sulfhydryl content, to study the effect of FITC, fluorescamine and radioiodine labels on BSA. The authors provided evidence of instability of protein conjugates and labeling-induced changes in their chromatographic and electrophoretic properties. They concluded that fluorescein conjugates should not be used for adsorption studies. In contrast, Robeson and Tilton (95) showed that FITC-Rnase A did not

preferentially adsorb in comparison to the native protein. However, due to possible complications arising from concentration quenching, the labeling ratios used were very low (~0.02). Therefore, this study may not provide conclusive evidence of the effect of labeling.

Lok et al. (27) used BSA doubly labeled with both tritium [^{3}H] and FITC to develop a calibration technique for adsorption of macromolecules at the solid-liquid interface. They investigated the influence of the label on protein adsorption by using mixtures of [^{3}H]FITC–BSA and unlabeled protein. They showed that mixtures containing 50 and 25% labeled proteins gave adsorption results with fluorescence intensities and tritium counts that were both 50 and 25%, respectively, of adsorption experiments with 100% labeled proteins. This study, performed in 1983, has since been widely cited to support the claim that there is no preferential adsorption of labeled protein over unlabeled protein or vice versa. However, we believe that the conclusions inferred in this study are unique and applicable only to the dual-labeled protein system used. We speculate that attaching a positively charged tritium molecule to the protein-label conjugate effectively nullifies the increase in electronegativity of the protein due to the addition of the fluorescence label. Hence, the surface hydrophobicity of the lysine group (to which both [^{3}H] and FITC are attached) remains unaltered, and therefore the sorption properties of the dual-labeled protein are unchanged in comparison to the native species.

Burghardt and Axelrod (4) measured the differences in equilibrium adsorption of unlabeled BSA and rhodamine-labeled BSA over various labeling ratios. Labeling ratios

were varied by either changing the molar rhodamine to BSA ratio or diluting labeled samples with unlabeled proteins. They concluded that the measured differences fall within the intrinsic error of the measuring system and could, therefore, not be totally attributed to labeling differences. However, they could not completely rule out the possibility that rhodamine-BSA sorption behavior was different from that of unlabeled BSA. Sacco et al. (96) showed that benzenehexacarboxylate (BHC) dextran-labeled haemoglobin exhibited a decreased oxygen affinity, rendering it suitable for use as a blood substitute.

With this uncertainty on the effect of labeling on protein dynamics, several studies have completely avoided using extrinsic labels by studying the intrinsic fluorescence of tryptophan or tyrosine residues in the protein (7, 9, 10, 8). Clearly, understanding the effect of fluorescence labeling on protein dynamics is important, and there is a need for further investigation into its effect on protein adsorption. However, a comprehensive search of the literature did not yield any studies that have specifically attempted to quantify this effect. This study aims to address this gap, by quantifying the changes in diffusive properties and adsorption kinetics that result from the conjugation of fluorescein-5-isothiocyanate (FITC) to bovine serum albumin (BSA).

3.2 Objectives

Our goal in this study was to quantify the effect of labeling BSA with FITC on the adsorption and diffusion of BSA. We have analyzed three different levels of BSA-FITC conjugations: BSA-1FITC (with exactly one conjugated FITC per BSA molecule), BSA-2FITC (with exactly two FITC per BSA molecule) and BSAm-FITC (with an average of

approximately 1.7 FITC per BSA molecule). We studied the three protein samples under two different concentration regimes:

1. The diffusion-limited (low concentration) regime, where we determined the mobile fraction and the apparent diffusion coefficient; and
2. The reaction-limited (high concentration) regime, where we determined the slow and rapid desorption rates and the fraction of slowly reversible and rapidly reversible proteins.

All studies were conducted at the oil-water interface.

3.3 Theory

3.3.1 Chemistry of the protein-labeling reaction

Fluorescein derivatives are the most common reagents for covalent labeling of proteins, because fluorescein has a relatively high absorptivity and an excellent quantum yield (~0.9). Additionally, it has an absorption maxima of about 490-494 nm that matches the spectral wavelength of an Arg-Ion laser (488 nm), and produces a fairly stable protein conjugate. The general labeling reaction is shown below for BSA.

$$\underset{\text{isothiocyanate (FITC)}}{R^1 - N = C = S} \quad + \quad \underset{\text{primary amine (BSA)}}{R^2 - NH_2} \quad \rightarrow \quad \underset{\text{thiourea conjugate (BSA - FITC)}}{R^1 - NH - CS - NHR^2} \qquad [4]$$

In most cases, fluorescent labeling utilizes the primary amino group on the target molecule. In the case of a polypeptide like BSA, the primary amino acid is usually in the

lysine group. The isothiocyanate group on the fluorophore provides efficient amino group labeling (81). A higher pH favors the $-NH_2$ group, which reacts well with the isothiocyanate over the unreactive $-NH_3^+$.

3.3.2 Diffusion of BSA-FITC

Fick's second law governs the lateral diffusion of a single non-interacting species of protein in the absence of convection.

$$\frac{dC(r,t)}{dt} = D\nabla^2 C(r,t) \qquad [5]$$

where $C(r, t)$ is the concentration of the diffusing species, D is the diffusion coefficient, t is the time of diffusion and r is the radial position of the species at the interface.

The concentration profile immediately after photobleaching is given by

$$C(r,0) = \bar{C}e^{-KI(r)} \qquad [6]$$

where $\bar{C}$ is the concentration before photobleaching, and K is the bleaching parameter, which is a function of the rate constant for photobleaching and the duration and intensity of the photobleaching pulse (29).

The fluorescence recovery profile following photobleaching is given by (29)

$$F(t) = \left(\frac{q}{A}\right)\int I(r)C(r,t)\,d^2r \qquad [7]$$

where $F(t)$ is the fluorescence at any time after the photobleaching flash (which occurs at $t = 0$ by definition). The quantum yield, q, is a product of the efficiencies of excitation light absorption and fluorescence emission and detection, $I(r)$ is the evanescent wave intensity profile at the interface, and A is the attenuation factor of the beam during the period of recovery.

The task now is to determine the functional form of $C(r, t)$ so that Eqn. [5] can be integrated. This problem has been resolved by Axelrod et al. (29), using the solution of the Fourier transform of Eqn. [5] (subject to the initial condition in Eqn. [6]) to yield a functional form of Eqn. [6]. Note that the initial condition depends on the bleaching parameter, K, which is a measure of the degree of bleaching in the system. For a Gaussian laser beam profile and for small values of the bleaching parameter K, the resulting equation is

$$F(t) = \bar{F}\left(1 - \frac{K}{2\left[1 + \frac{t}{\tau}\right]}\right) \qquad [9]$$

where $\overline{F}$ is the pre-bleach fluorescence, and τ is the characteristic diffusion time for spot photobleaching with a Gaussian laser beam. The detailed steps required to arrive at Eqn. [8], along with associated assumptions, are discussed in Appendix A.

3.3.3 Reaction kinetics of BSA-FITC at the interface

Given molecules of bulk concentration A(**r**, z, t) freely diffusing in solution and reacting with binding sites at an interface with a two-dimensional surface concentration B(**r**, t) to form fluorescent complexes of surface concentration C (**r**, t), we can write the reaction equilibrium as

$$A(\mathbf{r},z,t)+B(\mathbf{r},t)\underset{k_d}{\overset{k_a}{\rightleftharpoons}}C(\mathbf{r},t) \qquad [10]$$

where k_a and k_d are the adsorption and desorption rate constants, respectively. The vector **r** is the position at the interface from the center of the observation area, z is the perpendicular distance from the interface observation area to a point in the bulk solution, and t is time.

The equilibrium of the system is described by

$$\frac{\overline{C}}{\overline{A}\,\overline{B}}=\frac{k_a}{k_d} \qquad [11]$$

where $\overline{A}$, $\overline{B}$, and $\overline{C}$ are the equilibrium concentrations of the various species.

Thompson et al. (6) derived a mathematical model for use with TIRF/FPR experiments using the spot photobleaching technique. A brief summary of the model, as well as the final equations, is presented below.

The model is based on the monotonically decreasing function $G(t)$, which is defined as

$$G(t) = \overline{F} - F(t) \qquad [12]$$

where $F(t)$ is the fluorescence at any time t and $\overline{F}$ is the pre-bleach fluorescence. Combining Eqn. [12] with a form of Eqn. [42] (see Appendix A) that relates fluorescence intensity to interfacial concentration gives

$$G(t) = q\int I(\mathrm{r})C_P(\mathrm{r},t)\,\mathrm{d}^2r \qquad [13]$$

where $C_P = \overline{C} - C(\mathrm{r}, t)$ and q is the quantum efficiency discussed earlier.

The differential equations for A(**r**, z, t) and C(**r**, t) were solved by linear transformation theory. The initial conditions were derived from the intensity profile of the monitoring laser beam. The boundary conditions were based on the fact that only surface bound molecules within a finite surface area are photobleached. Away from the bleached region A(**r**, z, t) and C(**r**, t) do not depart from their equilibrium values.

Upon integration and application of these boundary conditions, and using a simplification valid for the reaction limited regime where the desorption rate is much smaller than the bulk normal diffusion rate, Eqn. [13] can be written as follows (6)

$$G(t) = G(0)e^{-k_d t} \qquad [14]$$

In our analysis, we have incorporated a modification, as recommended by Burghardt and Axelrod (4), to account for two different classes of adsorbing proteins. We have also included an additional modification, based on earlier work in our laboratory by Shukla et

al. (87), to account for the unintended photobleaching of fluorophores by the monitoring beam. These modifications are discussed later in this paper.

3.3.4 Concentration quenching: definition and concerns

Concentration quenching is a manifestation of the Forster non-radiative energy transfer phenomenon (97). This type of nonradiational deactivation of an excited fluorophore is called long-range quenching or Forster quenching. It is generally considered to be due to dipole-dipole coupling between a donor (the excited fluorophore) and an acceptor (the quencher) where the donor and the acceptor are different species. However, many fluorophores satisfy the requirement of self-energy transfer, namely that there is an overlap between the excitation and emission spectra. An inspection of the spectral profiles of fluorescein (appendix B) reveals a large overlap in the emission and excitation spectra.

Concentration quenching results in a drop in fluorescence emission upon increasing the fluorophore concentration. Understandably, this is to be avoided. The easiest way to do this is to keep the labeling ratio low, thus reducing the probability of two fluorophores coming into the close proximity required for quenching to occur. The reaction constant for energy transfer, k_T, is given by (98)

$$k_T = \tau_D^{-1}\left(\frac{R}{R_0}\right)^{-6} \qquad [15]$$

where R is the inter-fluorophore separation, τ_D is the luminescence lifetime of the donor fluorophore, and R_0 is the Forster distance. R_0 depends on the spectral overlap, the refractive index of the medium and the relative orientations of the donor and acceptor

fluorophores. Quenching may occur whenever fluorophores are within the Forster distance.

Previous research using conjugated BSA-FITC (33) has shown that there are no concentration quenching effects at a labeling ratio of 1.7. However, no preparative chromatography was performed on the protein conjugates used in that study. Therefore, the reported labeling ratio of 1.7 is actually an average molar ratio of bound FITC to BSA. In reality, the sample could potentially contain BSA with higher degrees of labeling, for instance BSA-3FITC or BSA-4FITC. It is our hypothesis that the concentration quenching artifacts suffered at average labeling ratios greater than 1.7 are due to BSA molecules in the sample that have higher labeling ratios. We speculate that, after preparative chromatography, a sample with a homogenous labeling ratio of 2 will not be subject to concentration quenching. This proposition was validated, as shown later in this chapter.

3.4 Materials and methods

3.4.1 Flowchart of strategy

The flowchart of the step by step procedure used to determine the effect of the extrinsic label is shown in Figure 3.1. The individual steps are discussed in detail later in this section.

The protein labeling reaction was carried out in 0.1 M, pH 9.2, borax buffer. An alkaline pH was required to ensure maximum conjugation of FITC to BSA. It was then necessary to separate out fractions of BSA-1FITC and BSA-2FITC from the polydispersed labeled

protein sample. This was performed using an ion-exchange chromatography column that was operated under isocratic elution conditions. Optimum operating pH for an anion exchange column is within 1 pH unit of the isoelectric point of the protein conjugate being fractionated. For BSA-FITC, the isoelectric point was measured at a pH of 4.6, hence the column was pre-equilibrated with a 0.01 M, pH 5.1 acetate buffer. To maintain isocratic elution conditions, it was necessary to reduce the pH of the protein solution to 5.1. This was accomplished in a two-stage stirred dialysis process. In the first stage the 0.1 M, pH 9.2, borax buffer was completely replaced by a 0.1 M, pH 5.1, acetate buffer. In the second stage the concentrated acetate buffer was exchanged with the 0.01 M, pH 5.1 acetate buffer, which was also used to pre-equilibrate the column.

The protein sample was then loaded onto the column and the elutant collected. The elutant from the ion-exchange column was analyzed using absorption versus concentration profiles developed for BSA and FITC in pH 5.1 acetate buffer, using a spectrophotometer. The absorbance values at 490 nm and 280 nm are used to determine the concentration of protein and the labeling ratio. However, at pH 5.1, the FITC label exists as a monoanion ($pk_a = 6.3$) which is four times less fluorescent than the dianion. The higher quantum yield of the fluorophore dianion makes it the preferred ionic state in subsequent TIRF/FPR experiments. The elutant was therefore dialyzed against a 0.03 M, pH = 7.4 PBS solution in order to completely replace the acetate buffer. While this process of dialysis does not affect the label ratio of the protein sample, it could alter the protein concentration. Therefore, the protein concentration was then measured again, using an absorbance versus protein concentration calibration curve developed in pH 7.4, PBS buffer.

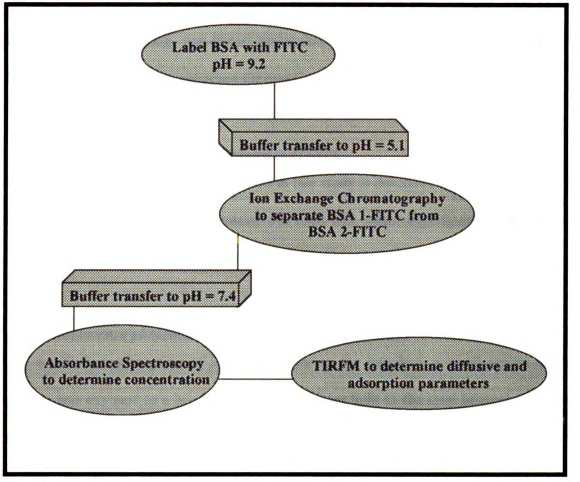

Figure 3.1. Flowchart of the experimental strategy used to determine the effect of extrinsic labeling on protein dynamics at and near the interface.

TIRF/FPR experiments were then performed to obtain the fluorescence recovery data after spot photobleaching of the interface. The data were then analyzed and fitted to the theoretical models, using non-linear regression algorithms, and the diffusion and adsorption parameters were extracted for protein samples with different labeling ratios.

3.4.2 Total internal reflection fluorescence (TIRF)

The total internal reflection technique used in this study is described in detail in Chapter 2 of this dissertation. The same equipment was used with minor experimental changes that are discussed later in this chapter.

3.4.3 Fluorescence photobleaching recovery (FPR)

After equilibrium adsorption of labeled proteins to the interface, a small region of the interface was exposed to a brief, intense flash of laser light in the total internal reflection geometry. Under ideal conditions, this results in the photobleaching of all the labels within the two-dimensional surface in the field of the evanescent wave. Photobleaching is the dynamic process in which fluorophore molecules undergo photo-induced chemical destruction and thus lose their ability to fluoresce. Several techniques based on this photobleaching phenomenon have been developed and successfully applied. The most widely used technique is fluorescence photobleaching recovery (FPR), first developed by Peters et al. (99).

After the photobleaching flash, the fluorescence intensity recovers towards the pre-bleach level by exchange of bleached interfacial species with unbleached fluorescent species in the

bulk. In FPR, this recovery is observed using a much-attenuated monitoring beam. Transport coefficients can be determined by measuring the rate of fluorescence recovery. Depending on the experimental conditions used, the recovery profile can be used to determine bulk diffusion and/or lateral diffusion of proteins, as well as the kinetics of adsorption and/or desorption. In this study, we have used FPR to determine bulk diffusion parameters and adsorption kinetics.

3.4.4 Protein labeling reaction

Bovine serum albumin (BSA), essentially fatty acid free, with greater than 97% albumin (A-7511) was obtained from Sigma Chemical Co. (St. Louis, MO) and used without further preparation. The proteins were labeled with fluorescein-5-isothiocyanate (FITC, F-1907, Molecular Probes, Eugene, OR) in our laboratory. The reaction was done in 0.10 M, pH 9.2 borax buffer for up to 6 hours at room temperature in the dark (27). Two different molar ratios of FITC to BSA were used to obtain the BSA-1FITC and BSA-2FITC samples. For BSA-1FITC, a molar ratio of 1.3:1 was used; for BSA-2FITC, a molar ratio of 3:1 was used. The average labeling ratio in the former sample was approximately 1 and in the latter was approximately 2.

The unreacted labels were removed by a two-stage dialysis process performed over a period of 48 hours. This length of time was found to be sufficient to completely remove any unreacted FITC. The protein solution (pH 9.2) was dialyzed with continuous stirring against a pH 5.1 acetate buffer, using a molecularporous regenerated cellulose dialysis membrane (Spectra/Por 1, molecular weight cutoff = 6,000, The Spectrum Companies,

Gardena, CA). Absorbance spectroscopy measurements with a diode array spectrophotometer (8452 A, Hewlett Packard, Brielle, NJ) at 280 nm and 500 nm were used to determine the protein and label concentrations, respectively. This is discussed in more detail in Chapter 4 and the absorption calibration curves for BSA and FITC are presented in appendix D.

3.4.5 Ion exchange chromatography

Ion exchange is probably the most frequently used chromatographic technique for the separation and purification of proteins. We selected this method because of its simplicity and high resolving power. Separation by ion exchange chromatography depends on the reversible adsorption of charged solute molecules to immobilized ion exchange groups of opposite charge. In this study, we exploited the anticipated differences in electronegativity created by the sequential addition of an extrinsic fluorophore to obtain separate fractions of unlabeled BSA, BSA-1FITC and BSA-2FITC.

Ion exchange chromatography was performed using DEAE sepharose CL-6B gel (17-0710-01, Pharmacia Biotech AB, Uppsala, Sweden). DEAE sepharose CL-6B, a macroporous bead-formed (mean particle size of 90 μm diameter) ion exchanger, is derived from the attachment of DEAE groups to a cross-linked agarose gel. The gel was packed into a SR 25/45 column fitted with SRA 25 flow adapters (19-0880-01 and 19-0867-01, Amersham Pharmacia Biotech, NJ). The DEAE column is flexible and can be run as an anion exchange or a cation exchange, depending on the working pH. In this study, the ion exchange chromatography was performed under isocratic conditions.

3.4.6 Determination of starting conditions: pH and molarity

The working buffer pH should be chosen such that substances to be bound to the ion exchange gel are charged. The isoelectric point (pI) of BSA, determined from several sources in the literature, was approximately 4.5. This means that, above a pH of 4.5, BSA is negatively charged; below this pH, BSA is positively charged. For an anion exchange, the starting pH should be at least 1 pH unit above the pI of the protein sample. Similarly, the pH should be at least one pH unit below the pI, for a cation exchange. We chose an anion exchange to protect the BSA-FTIC conjugation bond which might be endangered at a low, acidic pH.

To determine the pI for labeled BSA, the approach outlined in Amersham (100) was used. 1.5 ml of the gel was added to a series of ten 15 ml test tubes. The gel in each tube was equilibrated to a different pH by washing 10 times with 10 ml of 0.5 M of the selected starting acetate buffer (101). A pH range of 5 to 9 was chosen, with intervals of 0.5 pH units. The gel in each tube was then equilibrated to a lower ionic strength of 0.01 M, by washing 5 times with 10 ml of the buffer at the same pH but lower ionic strength. A known amount of sample was added to each tube and the contents were shaken for 10 minutes. After the gel settled, the supernatant was visually inspected and then assayed using absorption spectroscopy. A pH of 5.1 was selected. This would allow the protein to be bound to the gel, and still be sufficiently close to the isoelectric (or release) point. If the pH were too high (for example, more than 1.5 pH units away from the isoelectric point), the protein would be firmly bound to the gel, resulting in a difficult elution and necessitating the use of high salt concentrations.

A similar experiment was conducted to determine the molarity of the elution buffer. After equilibrium with buffer at the selected beginning pH, the gel samples were further equilibrated with solutions of varying ionic strength of the salt (NaCl) at a constant pH. A known amount of protein sample was added and the tubes were stirred for 10 minutes. The supernatant was then assayed to determine the highest ionic strength at which binding occurs and the lowest ionic strength at which elution occurs.

3.4.7 Elution of the protein

Elution of the protein was performed by increasing the ionic strength or lowering the pH of the elution buffer toward the isoelectric point. We used 5mM, 10mM, 15mM and 20 mM NaCl solutions to perform a stepwise elution procedure. Since the buffer used in the column is also an anionic buffer, care must be taken to ensure that equilibrium is attained in all stages of loading and elution. The column was connected to a double-syringe pump system (Model 551382, Harvard Apparatus, South Natick, MA) which served to introduce protein solutions and elution buffer via a T-valve. Once the elution was started, 2 ml samples of elutant were collected and analyzed for concentration and labeling ratio by absorption spectroscopy. Samples that fell within an acceptable range of labeling ratio and protein concentrations were pooled together to make up the final protein solutions of BSA-1FITC and BSA-2FITC. For example, samples with labeling ratios ranging from 0.98 to 1.02 were pooled together to make up BSA-1FITC.

3.4.8 Buffer exchange

The elutant from the chromatography column was at pH 5.1. At this pH, however, the FITC label exists as a monoanion ($pk_a = 6.3$) which is four times less fluorescent than the dianion (102) (please see appendix B for further details). It was thus necessary to perform a buffer exchange to replace the acetate buffer (pH = 5.1) with PBS buffer (pH = 7.4). This was performed by a two-stage, 36-hour, continuously stirred dialysis operation using a molecularporous regenerated cellulose dialysis membrane (Spectra/Por 1, molecular weight cutoff = 6,000, The Spectrum Companies, Gardena, CA). The completion of the buffer transfer was checked with a pH meter. Also, a spectroscopic check of the dialysis bath revealed no trace of FITC, indicating that the protein conjugation bond was not affected by the reduction in pH and subsequent ion-exchange chromatographic process.

3.4.9 TIRFM experiments

Earlier studies of the timescale of the adsorption of BSA-FITC (see chapter 2 of this dissertation) showed that BSA-FITC took minutes to equilibrate at the oil-water interface in our experimental cell. Typically the protein sample was introduced into the experimental cell and, after equilibration, the monitoring beam of 5 μW was switched on. Approximately 10 secs later, the shutter system was triggered. This caused a ~100 msec photobleaching flash of 15mW at the interface. All power readings were taken with a Newport detector (818-SL, Newport Corporation, Irvine, CA) and measured with a Newport power meter (1815-c, Newport Corporation, Irvine, CA). The shutter system closes and protects the PMT for the duration of the bleach. Immediately after the bleach, the PMT was opened to record the fluorescence recovery. The microscope stage was then

slowly moved via the modular automation control from the computer, to allow another location on the interface to be photobleached and studied. After three different locations were studied, the cell was flushed for 20 minutes with protein solution at the rate of 0.1ml/min. Since the volume of the experimental cell was 960 μL, this completely replaces the bulk solution.

A detailed description of the computer software used to collect data, the RS-232 interface with the MAC 2000 (modular automation controller), the sample rate and averaging techniques of data collection, as well as the photomultiplier tube (PMT) settings can be found in appendix E.

3.5 **Data analyses**

The data were analyzed with the PROC NLIN (NonLINear regression) program in SAS. Two iterative algorithms, the modified Gauss-Newton method and the Marquardt method, were used. Both methods regress the residuals onto the partial derivatives of the model with respect to the parameters until the estimates converge. The complete SAS code written for the two algorithms is given in appendix C.

3.5.1 Processes contributing to fluorescence recovery.

Following photobleaching, four processes contribute to the redistribution of bleached and unbleached fluorophores and combine to affect the speed of recovery and the shape of the recovery curve (14):

1. Diffusion-controlled motion of free bulk molecules within the 'cylinder' of the evanescent wave;
2. bulk diffusion-controlled refilling of the depletion layer of fluorescent molecules built up during the bleaching pulse;
3. exchange of surface-bound bleached molecules with the unbleached bulk molecules, as governed by the adsorption and desorption rate constants; and
4. lateral diffusion of surface-bound molecules into the monitoring beam.

In addition to these, one might theoretically consider rotational diffusion of the fluorophores, orientation and conformational changes of the irreversibly adsorbed proteins and possibly spontaneous recovery of photobleaching (dark recovery). However, these processes do not affect measurements in our system, as discussed below.

Previous studies (103, 104) have shown that for FPR experiments involving one non-interacting protein species, rotational and translational contributions to the fluorescence recovery are naturally separated, because they occur on different time scales. However, it is possible, for a sufficiently short photobleaching pulse, that only those fluorophores with transition moments parallel to the electric field of the excitation beam will be bleached. Then a fluorescence recovery would be observed as the rotational diffusion of unbleached fluorophores cause their transition moments to align with the electric field vector of the monitoring beam and emit fluorescence. This recovery is independent of the translational motion of the protein and would compromise the validity of our theory. However, rotational diffusion as measured by time-resolved phosphorescence anisotropy decay

(Edidin 1987) takes place over very short timescales (10-100 μ seconds). Typical bleach pulse durations in our experiments are 100 ms; therefore, we assume that fluorophores are bleached isotropically.

This ensures that rotational diffusion effects do not compromise the qualitative nature of the crucial early stage of our fluorescence recovery curves. Additionally, steady-state TIR fluorescence polarization (36) and polarized fluorescence recovery after photobleaching (PFRAP) studies (105) have shown that the rotational diffusion of interfacially adsorbed molecules is restricted. Since our apparatus is designed to be extremely interfacially sensitive, we believe that this renders the effects of rotational diffusion negligible in our studies.

Orientational and conformational changes in an adsorbed protein layer are due to changes in the tertiary structure of the protein, which typically occur over a period of several hours. This has been seen in interfacial tension experiments conducted in our laboratory (106) by a slow gradual decrease of interfacial tension over a period of several hours, following a quick initial drop. However, the entire timescale of our adsorption experiments in this study is only 60 seconds. Hence the effects of orientational and conformational changes in the adsorbed BSA layer can be ignored.

Stout and Axlerod (107) first identified possible complications arising from dark recovery or reversible photobleaching. However, the study also showed that, for a non-deoxygenated, air-equilibrated system, photobleaching is totally irreversible. For this

study, we did not deoxygenate our protein samples. It could potentially be argued that this could result in artifacts caused by photochemical crosslinking of proteins at the interface. However, this is a slow phenomenon that is seen after equilibrium adsorption of the protein. Over the timescale of our experiments, reversible photobleaching is a more potentially significant factor.

Processes (2) and (4) are essentially absent in our experiments. The size of the photobleaching beam in relation to the monitoring beam (3:1) prevents any contributions from lateral diffusion over the time scale of our fluorescence recovery curve. Jauhari (108) calculated an approximate time of 900 seconds for the lateral diffusion of unbleached proteins into the monitoring beam. Similarly, due to the relatively large bulk diffusion coefficient of BSA (calculated in an earlier experiment to be 10^{-7} cm^2/s), the bulk exchange takes place too quickly (2 ms) to be captured during the timescale of our experiments. Thus, the fluorescence recovery depends mainly on the bulk diffusion of desorbed molecules away from the interface, and the kinetics of the exchange between surface-adsorbed and bulk free proteins.

At lower concentrations when bulk diffusion is slow, reversibly adsorbed bleached molecules diffuse very slowly from the vicinity of the interface. Sometimes they even readsorb onto the interface, thereby slowing the recovery. In this case, the rate of recovery, governed by the slowest step, depends on the bulk diffusion coefficient and not on the adsorption reaction kinetics. This is the bulk-diffusion regime, and for BSA in our experimental set-up, it has been shown to exist at concentrations less than 0.015mM (1

mg/ml) (87). At higher protein concentrations, the bleached solute rapidly disperses into the bulk after desorption, and the probability of readsorption is very low. In this reaction-limited regime, the region close to the interface has a high concentration of unbleached protein molecules and serves as an infinite reservoir to exchange with desorbing proteins. Here, the desorption rate constant, k_D, controls the recovery of fluorescence.

Experiments were conducted in both diffusion-limited and reaction-limited regimes. They provide information about the effect of conjugation on diffusion and adsorption kinetics, respectively.

3.5.2 The diffusion-limited regime

The equation for analysis of bulk diffusion was modified to account for possible photobleaching of fluorescent moieties by the monitoring beam (87). The resulting equation is

$$F(t) = \overline{F}.e^{(-k_{PB}.t)}\left(1-\frac{K}{2\left[1+\frac{t}{\tau}\right]}\right) \qquad [16]$$

where $\overline{F}$ is the pre-bleach fluorescence and τ is the characteristic diffusion time for spot photobleaching with a Gaussian laser beam:

$$\tau = \frac{w^2}{4D} \qquad [17]$$

Here, w is the half-width at e^{-2} of the height of the Gaussian intensity profile of the laser beam. Since this is difficult to estimate in practice, and the non-ideality of the beam leads to further complications, absolute values of D are not reported.

Monitoring beam photobleaching is essentially negligible in our current set-up, which is an improved version of the one used by Shukla (87) for diffusion-limited experiments. Further evidence of this may be discerned from the low values obtained for k_{PB}.

The mobile fraction, f, defined as the fraction of proteins reversibly adsorbed, is given by

$$f = \frac{F_0 - F(\infty)}{F_0 - \bar{F}} \qquad [18]$$

where $F(\infty)$ is the asymptote of the fluorescence recovery curve and F_0 is the post-bleach fluorescence.

It must be noted that the term 'reversibly adsorbed' is always subject to both the timescale and environment of the experiment. In this case, the proteins are reversibly adsorbed over the timescale of our experiments (60 seconds) at pH 7.4.

The prebleach value, $\bar{F}$, is determined directly from the data by inspection. The parameters, τ, K and k_{PB}, are obtained by curve fitting, after initial guesses are provided to the non-linear regression program. The iterative process fits the recovery data to Eqn. [16] and returns the fitted parameters.

3.5.3 Reaction-limited regime

A visual inspection of the fluorescence recovery curves of BSA-FITC in the reaction-limited regime reveals three qualitative features: a fast initial recovery, followed by a slower recovery manifested by a less steep upward slope, and a prolonged period of fluorescence recovery towards the prebleach level (Figure 4.5). To characterize the recovery curve quantitatively, Burghardt and Axelrod (4) approximated the recovery as a sum of exponentials.

$$g(t) = r_0 + r_1 e^{-k_{d1} t} + r_2 e^{-k_{d2} t} \qquad [19]$$

In an attempt to ascribe a physical significance to the fitted parameters, they classified the adsorbing proteins into two classes, a slowly desorbing fraction (r_1 at a rate k_{d1}), and a more rapidly desorbing fraction (r_2 at a rate k_{d2}).

Later studies of proteins at various interfaces have confirmed that fluorescence recovery curves in the reaction-limited regime are best described by two exponential desorption terms (21, 17). Further, an additional term to account for unintended photobleaching of fluorophores by the monitoring beam has been suggested by Shukla (87)

The final modeling equation, using $G(t) = \overline{F} - F(t)$ is then

$$F(-) - F(t) = \left[F(-) - F(0) e^{-k_{pb} t}\right]\left(r_0 + r_1 e^{-k_{d1} t} + r_2 e^{-k_{d2} t}\right) \qquad [20]$$

The mobile fraction, f, is given by

$$f = 1 - r_0 = r_1 + r_2 \qquad [21]$$

The prebleach value is determined directly from the data. $F(0)$, r_0, r_1, r_2, k_{d1}, k_{d2}, and k_{pb} are obtained by non-linear curve-fitting, after initial guesses are provided to the PROC NLIN program.

3.6 Results and discussion

3.6.1 The diffusion limited regime

Table 1 gives final values for the time constant (τ), the mobile fraction (f), the photobleaching rate constant (k_{PB}) and the bleaching parameter (K) for labeled BSA at a concentration of 0.01 mM (0.7 mg/ml). We obtained the values by non-linear regression (Gauss-Newton method) of the data to Eqn.[16] using the Statistical Analysis Software (SAS). We report the average and standard deviation of 10 runs performed in the dark at room temperature (20 °C) for protein samples with L = 1, L = 2 and L ~ 1.7.

Figure 3.2a shows the dependence of τ, the characteristic diffusion time, on labeling ratio measured in the diffusion-limited regime. The characteristic diffusion time for spot photobleaching with a Gaussian beam, τ, for BSA-1FITC was nearly 60 seconds longer than for BSA-2FITC. Based on Eqn.[16], which was used to calculate the diffusion coefficient, this translates into an apparent diffusion coefficient for BSA-2FITC that is 41% greater than that calculated for BSA-1FITC. The primary driving force for the diffusion of a protein in an aqueous solution toward an interface is the hydrophobicity of the molecule. Upon conjugation with BSA, the FITC molecule attacks the highly polar (and hence hydrophilic) side chain of the lysine group. This results in a loss of lysine

groups and the acquisition of carboxyl groups, thus increasing the overall negative charge of the protein. The characteristic diffusion time obtained for BSA-mFITC, with an average labeling ratio of 1.7, was approximately between the value for BSA-1FITC and BSA-2FITC.

It has been previously reported (91) that the formation of an ε-fluorescein thiocarbamyl-lysyl bond lowers the isoelectric point of the protein, rendering it more electronegative at a given pH. The net effect of the loss of the hydrophilic lysine groups and hence the increase in the electronegativity of the protein is an increase in the hydrophobic nature of the protein surface. There is very good correlation between the Nakai surface hydrophobicity (a measure of protein hydrophobicity introduced by Nakai et al. (109)) and the surface activity of a protein (53). We believe that the increased hydrophobicity of BSA-2FITC leads to greater surface activity, which results in a higher apparent diffusion coefficient. Note that the diffusion coefficient measured here is an apparent diffusion coefficient which reflects a combination of bulk diffusion and lateral mobility of proteins associated with (but not adsorbed at) the interface. The increased surface hydrophobicity results in a greater driving force for proteins seeking to remove themselves from the aqueous bulk environment (by adsorption at the interface), thus resulting in a faster diffusion rate. It may be argued that an increase in surface activity should result in slower exchange kinetics, due to larger residence times for proteins at the interface. This should slow the rate of recovery of fluorescence and reduce the apparent diffusion coefficient. However, in the diffusion-limited regime, the rate-limiting step is the diffusive process, and thus

increased surface hydrophobicity is manifested in this step, resulting in a higher apparent diffusion coefficient.

The fraction of mobile proteins *f*, does not show a dependence on labeling ratio within experimental error (Figure 3.2b). During equilibrium adsorption at lower concentrations, there is sufficient time for the protein molecules to unfold and fully exploit the hydrophobic residues buried within the globular structure of the native protein. This is because, at lower concentrations, during the finite time required for unfolding of a protein, it is not affected by steric hindrances from the adsorption of another protein molecule. In this situation, the increased surface hydrophobicity caused by the presence of extrinsic fluorophores has a negligible effect on the total surface activity that governs the degree of irreversibility of protein adsorption. Therefore, the measured mobile fractions *f*, do not show a dependence on the labeling ratio.

In our apparatus, it is difficult to precisely determine *w*, the half-width at e^{-2} of the height of the Gaussian intensity profile of the monitoring beam. This makes it difficult to determine the absolute diffusion coefficient; hence we do not report absolute values in this study. However, using rough estimates of *w* based on Jauhari (108), we calculated diffusion coefficients comparable to values reported in the literature (on the order of 10^{-6} cm^2/s) for BSA-FITC under similar conditions. The apparent diffusion coefficients calculated in this study should not be confused with bulk diffusion coefficients. Physically, the apparent diffusion coefficient reported here can be thought of as a parameter that

characterizes a combination of bulk diffusion and lateral mobility of proteins near or loosely associated with the interface.

To ensure that the two sets of experiments were comparable, we examined the bleaching parameter K, expressed as shown in Eqn. [22].

$$K = \alpha I(0)T \qquad [22]$$

Physically, K denotes the amount of bleaching induced in time T, and $\alpha I(0)$ is the rate constant of the simple irreversible first order photobleaching reaction at the interface. K was constant throughout all our experiments, indicating that the bleaching conditions, as well as the beam profile, were identical for both sets of experiments.

a.

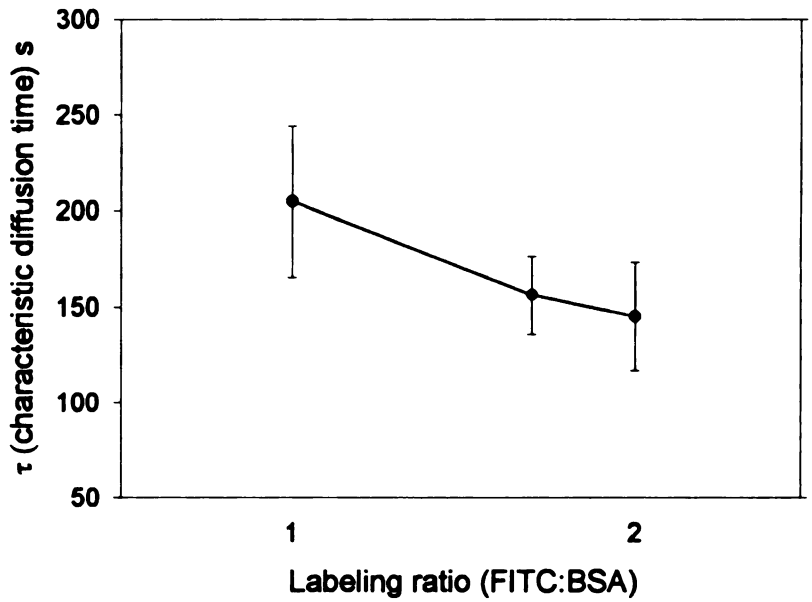

b.

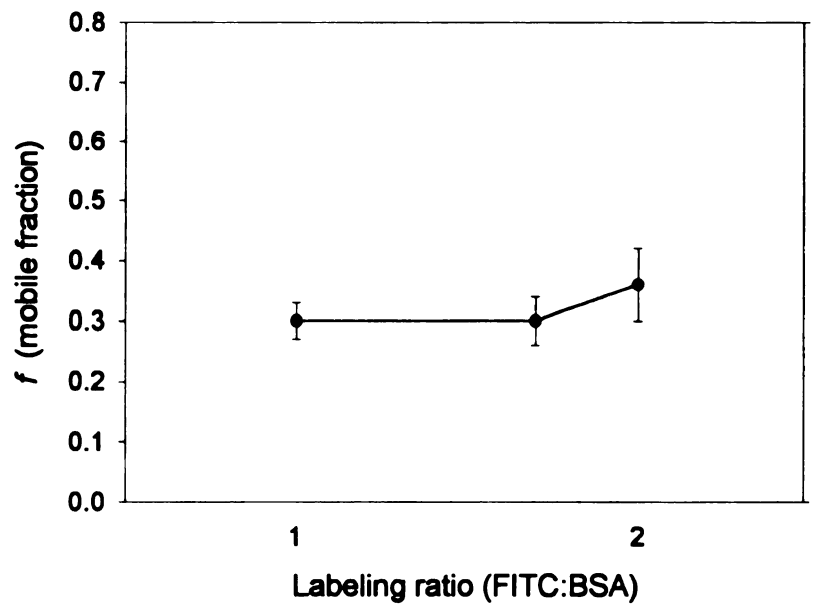

Figure 3.2. Dependence of a) τ (characteristic time of diffusion) and b) f (mobile fraction) on labeling ratio in the diffusion-limited regime for BSA at the oil-water interface. The bulk protein concentration was 0.01 mM.

Table 1. Summary of results for BSA-FITC in the diffusion-limited regime. The bulk protein concentration was 0.01 mM

Protein Conc. = 0.01 mM	**L = 1**	**L ~ 1.7**	**L = 2**
$\tau(s)$ Time constant	204.8 ± 39.4	156.1 ± 20.3	145.0 ± 28.1
f Mobile fraction	0.30 ± 0.03	0.30 ± 0.04	0.36 ± 0.06
k_{PB} (s^{-1}) Rate of photobleaching	0.0013 ± 0.0002	0.0015 ± 0.0002	0.0013 ± 0.0003
K Bleaching parameter	0.69 ± 0.08	0.65 ± 0.08	0.70 ± 0.14

3.6.2 The reaction-limited regime

Table 2 shows a summary of the results of experiments conducted in the reaction-limited regime, at a protein concentration of 0.025 mM (1.7 mg/ml). The fluorescence recovery data were non-linearly regressed (Marquardt method) to fit Eqn. [20] using SAS. Again, we report the average and standard deviation of 10 runs performed in the dark at room temperature (20 °C), for L = 1, L = 2 and L ~ 1.7.

Three parallel non-interacting classes of proteins account for the shape of the fluorescence recovery curves (4): an irreversible protein fraction (r_0) called the immobile fraction, a slowly reversible fraction r_1 with a slow desorption rate of k_{d1} (s^{-1}) and a rapidly reversible fraction (r_2) with a rapid desorption rate of k_{d2} (s^{-1}). Physically, the simplest model that appears to be consistent with the data is as follows.

The three classes of adsorbed proteins may be thought of as representing different bound layers. The irreversible bound layer is the layer closest to the oil-water interface and is in intimate contact with the oil. After this layer come the reversible classes with the slowly reversible class closest to the adsorbed layer. The rapidly desorbing class constitutes proteins that are loosely attached to the adsorbed layers in a surface-associated state. A more realistic model might include several classes of binding proteins that interact with each other. However, adding adjustable parameters to the non-linear regression algorithms increases the dependencies between/of the fitted parameters to unacceptable levels. This decreases the reliability of the regression, and makes it increasingly difficult to attribute physical significance to the experimental results.

a.

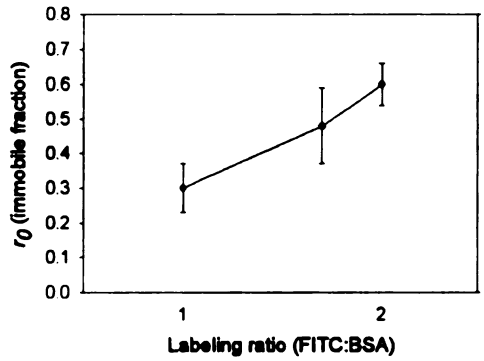

b.

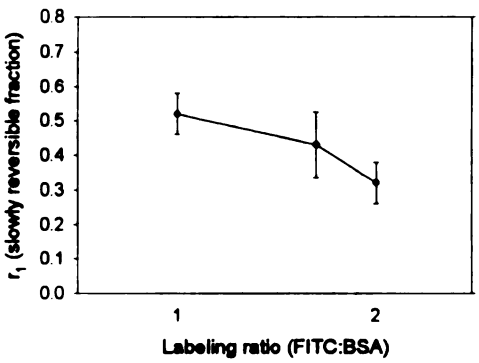

c.

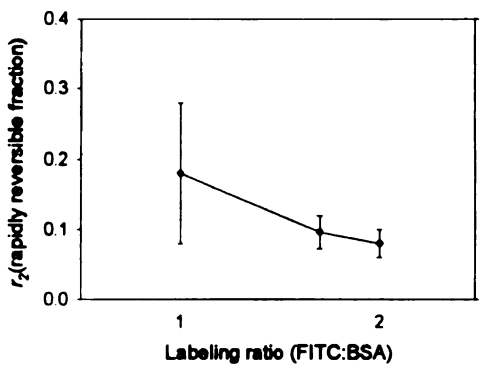

Figure 3.3. Dependence of a) r_0 (immobile fraction), b) r_1 (slowly reversible fraction) and c) r_2 (rapidly reversible fraction) on labeling ratio in the reaction-limited regime for BSA at the oil-water interface. The bulk protein concentration was 0.025 mM.

a.

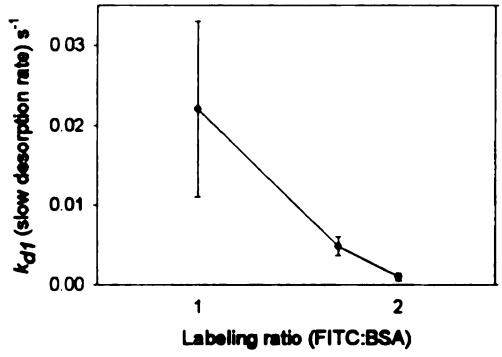

b.

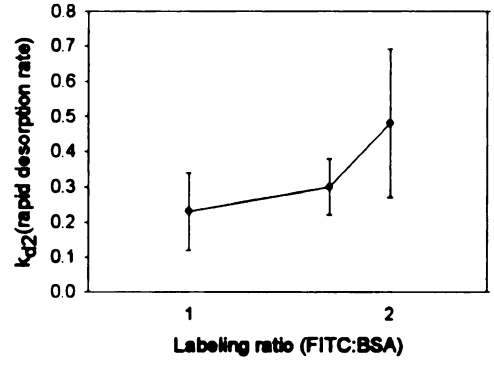

c.

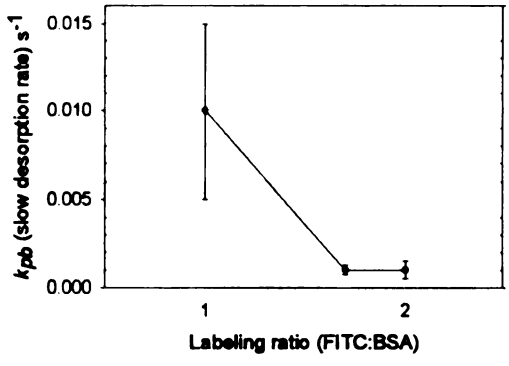

Figure 3.4. Dependence of a) k_{d1} (rate of slow desorption), b) k_{d2} (rate of rapid desorption) and c) k_{pb} (rate of photobleaching) on labeling ratio in the reaction-limited regime for BSA at the oil-water interface. The bulk protein concentration was 0.025 mM.

3.6.2.1 The immobile fraction r_0

Figure 3.3a illustrates the dependence of the immobile fraction on the labeling ratio. The immobile fraction increases nearly linearly with labeling ratio. For BSA-2FITC, the fraction of proteins classified as irreversible is 0.61 ± 0.06 which is almost double the value computed for BSA-1FITC, 0.30 ± 0.07. This can be attributed to the increased hydrophobic nature of BSA-2FITC, which increases r_0, the fraction of irreversibly adsorbed proteins in two ways. First, since it is more surface-active, BSA-2FITC is more irreversibly adsorbed at the interface. Secondly, the higher diffusion coefficient of BSA-2FITC enables it to saturate the interface at a faster rate. Since the time allowed for equilibrium adsorption is identical in all experiments, this provides a longer period of time for the adsorbed protein layer to 'settle' into the interface, thus increasing the fraction of irreversibly adsorbed proteins.

3.6.2.2 The reversible fractions, r_1 and r_2

Figure 3.3b shows the values of r_1, the slowly reversible protein fraction plotted against the labeling ratio. The graph is fairly linear, with a negative slope. For BSA-1FITC, r_1 = 0.52 ± 0.06 which is greater than the corresponding value of 0.32 ± 0.06 reported for BSA-2FITC. This might seem to be contrary to the hypothesis expounded earlier, as it seems to indicate that BSA-1FITC is more firmly adsorbed. However, if one examines the rates of desorption, plotted against labeling ratio in Figure 3.4a, one sees that k_{d1} for BSA-1FITC is 0.022 ± 0.011 s^{-1} which is much faster than the corresponding rate of 0.001 ± 0.0005 s^{-1} reported for BSA-2FITC. In other words, even though there is a larger fraction

of BSA-1FITC in the slowly desorbing class, the rate of desorption is much faster than that of the corresponding BSA-2FITC class.

To get a clearer picture of the effect of the label, we can consider the ratio r_1: r_2, a measure of the distribution of the protein population amongst the rapidly and slowly desorbing classes. For BSA-1FITC this ratio is approximately 3 and for BSA-2FITC it is approximately 4. We can thus conclude that a larger percentage of BSA-2FITC is in the slowly desorbing class of proteins and, in addition, desorbs at a slower rate. This is in agreement with the increased hydrophobicity of BSA-2FITC discussed earlier.

Figure 3.4b shows the dependence of k_{d2} on labeling ratio. We observed that BSA-2FITC desorbs with a faster k_{d2} (the rapid desorption rate constant) than BSA-1FITC, 0.48 ± 0.21 compared to 0.23 ± 0.11. This is presumably due to the fact that, since this class of proteins is loosely associated with the interface, lateral diffusion plays a more important role in the desorption process. The higher rate constant of BSA-2FITC then simply reflects the higher diffusion coefficient, which we measured in the diffusion-limited regime (discussed earlier).

The dependence of the photobleaching rate constant k_{pb} is shown in Figure 3.4c. The salient feature of the graph is that the rate constant of photobleaching is much larger at a labeling ratio of 1. The random statistical probability of photobleaching a fluorophore has been estimated between 1:1000 and 1:5000 (110). In other words, a fluorophore will go through the excitation-emission cycle between 1000 and 5000 times before being

Table 2. Summary of results for BSA-FITC in the reaction-limited regime. The bulk protein concentration was 0.025 mM

Protein Conc. = 0.025 mM	**L = 1**	**L ~ 1.7**	**L = 2**
r_0 Immobile fraction	0.30 ± 0.07	0.48 ± 0.11	0.61 ± 0.06
r_1 Slowly reversible fraction	0.52 ± 0.06	0.43 ± 0.095	0.32 ± 0.06
r_2 Rapidly reversible fraction	0.18 ± 0.10	0.096 ± 0.024	0.08 ± 0.02
k_{d1} (s^{-1}) Rate of slow desorption	0.022 ± 0.011	0.0048 ± 0.0012	0.001 ± 0.0005
k_{d2} (s^{-1}) Rate of rapid desorption	0.23 ± 0.11	0.30 ± 0.08	0.48 ± 0.21
k_{PB} (s^{-1}) Rate of photobleaching	0.01 ± 0.005	0.001 ± 0.0003	0.001 ± 0.0005

photochemically destroyed. At a lower labeling ratio of 1, there are fewer fluorophores at the interface that are undergoing the excitation-emission cycle for the same laser intensity. This results in a higher rate of destruction of these fluorophores since they go through the excitation-emission cycles more often.

Concentration quenching can be detected by observing the qualitative shape of the fluorescence signal during the adsorption process. Concentration quenching is present when the fluorescence signal passes through a maximum and then decreases, as the concentration of labeled proteins at the interface increases, as shown in the theoretical curve in Figure 3.5. This overshoot in the fluorescence is due to the competition between an increase in the number of fluorophores at the interface with adsorption and the decrease in the quantum yield of these fluorophores as the average interfluorophore separation falls within the concentration quenching range (within the Forster distance). Larger labeling ratios therefore produce more dramatic signal maxima that occur at earlier times (33).

We conducted checks for concentration quenching in a sample of 0.025 mM protein with a monodisperse labeling ratio of 2. The data, shown in Figure 3.5, clearly do not portray a maximum in the TIRF signal. This proves our earlier hypothesis that preparative chromatography eliminates concentration quenching by removing the higher labeled proteins from the sample. Concentration quenching can also be manifested in the early phase of fluorescence photobleaching recovery. Again, the effect of concentration quenching is to produce an overshoot in the recovery.

Figure 3.7a shows a typical recovery curve for 0.025 mM protein concentration at a labeling ratio of 2. One can see a smooth increase in post-bleach fluorescence, typical of a system free from the effects of concentration quenching. Figure 3.7 b, shows a recovery curve for 0.025 mM protein concentration with an average labeling ratio of 2.5. This sample was prepared without preparative chromatography. The plot shows the distortion of the initial stages of the recovery curve, due to the effects of concentration quenching.

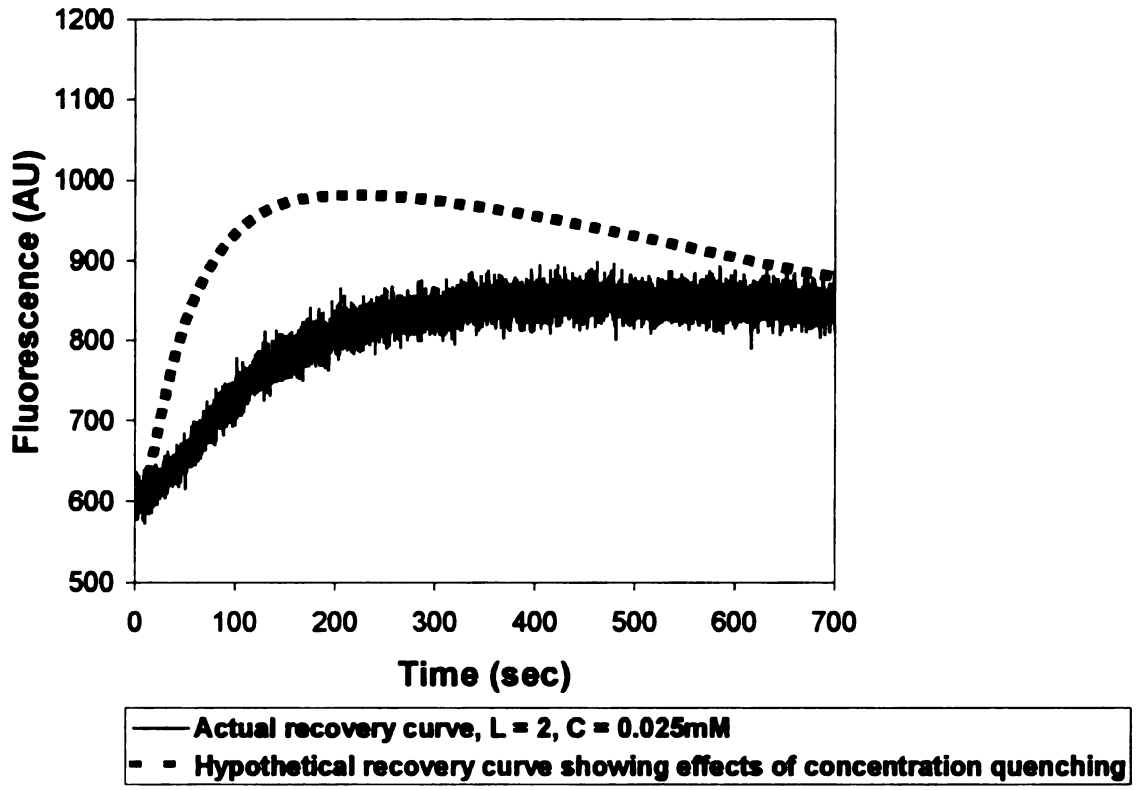

Figure 3.5. Check for concentration quenching effects in the equilibrium adsorption of L = 2, 0.025 mM BSA at the oil-water interface.

a.

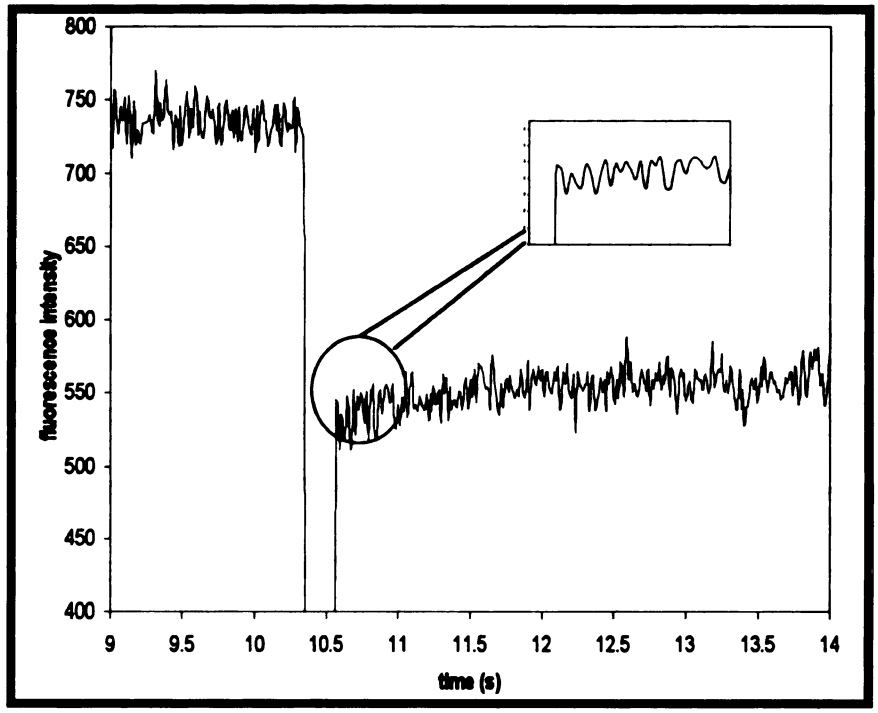

b.

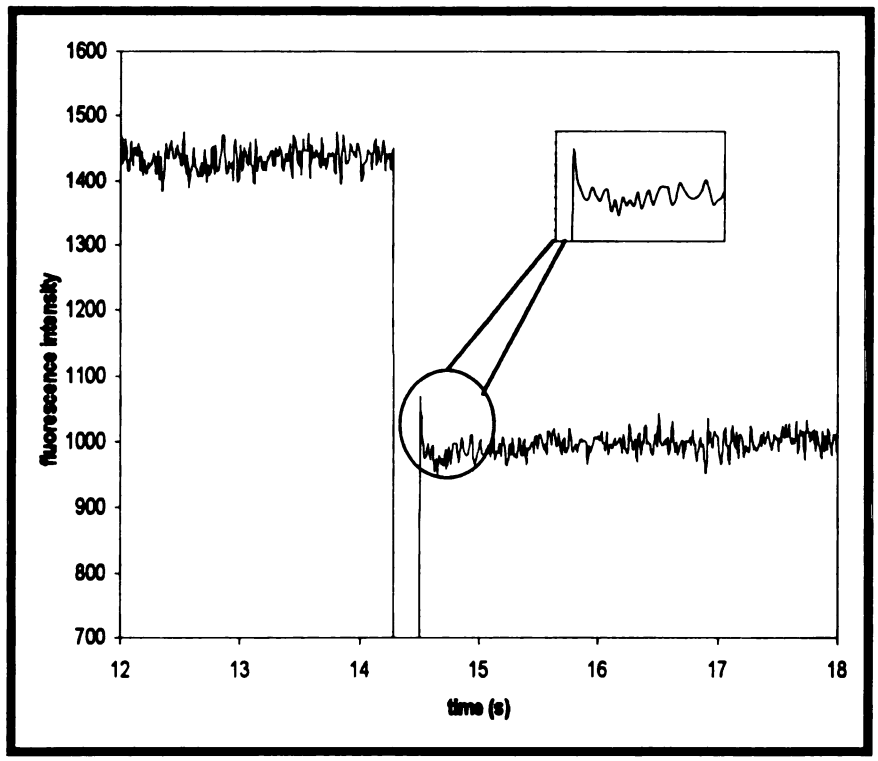

Figure 3.6 a. Normal (quenching free) fluorescence recovery of L = 2, 0.025 mM BSA after preparative chromatography. b. Fluorescence recovery of L ~ 2.5. 0.025 mM BSA showing the effects of concentration quenching

3.7 Conclusions

Preparative (ion exchange) chromatography was used to separate BSA conjugated with FITC into two samples with labeling ratios (L = number of FITC molecules attached to a single BSA molecule) of 1 and 2. Experiments were conducted by total internal reflection fluorescence microscopy (TIRFM) along with fluorescence photobleaching recovery (FPR), using proteins labeled with 1, 2 and approximately 1.7 FITC molecules. The diffusion and adsorption kinetics of BSA-FITC were investigated under two different concentration regimes at each labeling ratio.

In the diffusion-limited regime (protein concentration of 0.01 mM or 0.7 mg/ml), BSA-2FITC has a diffusion coefficient that is 40% larger than BSA-1FITC. We attributed this to an increase in surface hydrophobicity caused by the presence of the additional fluorophore molecule. If we assume a simple linear relationship for the effect of the fluorophore on the surface hydrophobicity of the macromolecule, this would imply that previous studies of this nature have overestimated the lateral mobility of labeled proteins by up to 40%.

In the reaction-limited regime (protein concentration of 0.025 mM or 1.7 mg/ml), the additional label led to an increase in surface hydrophobicity and hence a more irreversible adsorption of BSA-2FITC. The result was that BSA-2FITC has:

1. An immobile fraction of 0.6 ± 0.06 which is larger than the r_0 for BSA-1FITC, which was 0.30 ± 0.07

2. A smaller rate constant k_{d1} of 0.001 ± 0.0005 s^{-1} for the slowly desorbing proteins than for BSA-1FITC for which we measured a k_{d1} of 0.022 ± 0.0011 s^{-1}; and
3. a higher r_2:r_1 ratio (the ratio of the slowly desorbing protein class to the rapidly desorbing protein class) of 4:1 compared to a similar ratio of 2.9:1 for BSA-1FITC.

We have shown that the attachment of an extrinsic label does have a pronounced effect on the adsorption properties and the diffusion of proteins near the interface. Intuitively, one would expect that the addition of a planar fluorescein label to a globular protein (BSA) would increase the characteristic timescale of diffusion, due to viscous drag. This is most likely true for pure bulk diffusion of BSA in solution. However, for diffusion measured near the interface in these studies, our experiments show that the addition of the label significantly decreased the timescale of the diffusion process.

Experiments performed in the reaction limited concentration regime conclusively prove that the adsorption kinetics of proteins are affected by the presence of the fluorophore label. Due to an increased surface hydrophobicity, the protein-label conjugate is more surface-active and tends to adsorb more irreversibly than the native protein. This leads to a slower desorption rate for labeled proteins and hence effectively a preferential adsorption of labeled proteins over unlabeled proteins.

Based on the results presented in this study, we recommend that the covalent labeling of proteins to quantitatively investigate interfacial phenomena be undertaken with caution. Preparative chromatography can be used to separate proteins into fractions with different monodisperse labeling ratios. Experiments can be performed on protein samples with different labeling ratios to quantify the effect of the label unique to the characteristic property being investigated. The results can then be carefully extrapolated to determine the properties of the native unlabeled protein.

4. A CALIBRATION PROTOCOL FOR QUANTITATION OF INTERFACIAL CONCENTRATIONS OF MACROMOLECULES AT THE LIQUID-LIQUID INTERFACE.

4.1 Introduction

We have successfully used total internal reflection fluorescence microscopy to study protein adsorption at the liquid-liquid interface (86, 111, 87). So far in these studies, it has not been necessary to precisely calculate the interfacial concentrations of proteins. However, in studying many other adsorption phenomena, it is important to know the concentrations of macromolecules at the interface. In these types of situations, it would be particularly beneficial to be able to directly calculate the concentration of adsorbed interfacial species from fluorescence emission intensity data.

In general, devising a reliable calibration technique to enable quantification of interfacial amphiphilic concentrations on the basis of fluorescence emission intensity is a very difficult problem at the liquid-liquid interface, at least in comparison to the solid-liquid interface. Techniques that have been routinely used to determine interfacial concentrations at the solid-liquid interface have been made possible by the fact that a) protein adsorption is essentially irreversible at this interface, b) the interface is very stable, and c) the interface can be easily disassembled to enable adsorption on the solid surface to be quantified. Common techniques include assessment of depletion of adsorbates in the bulk phase (4), use of non-adsorbing species (such as polystyrene spheres) as standards, use of

scintillation counting in combination with TIRF (27, 2), and combination of reflectometry with TIRF (33).

Unfortunately, none of these techniques will work at the liquid-liquid interface, because of two primary limitations. Even if adsorption at this interface were irreversible, there is no reliable technique that can be used to drain the bulk solution from the sample cell without incorporating adsorbed species as well as some of the oil layer into the aqueous effluent. Quantitation methods that combine reflectometry or scintillation counting with TIRF rely on the immobilization of proteins on one of the surfaces that make up the interface. For example, adsorbed species at the solid-liquid interface can be isolated on the solid surface. The solid can then be separated from the sample cell and the quantity of adsorbed species determined reasonably accurately by any one of several methods. Such an operation is obviously impossible at the liquid-liquid interface. Therefore, a very different approach is required for this interface.

In this study, we propose a calibration technique that uses fluorescence photobleaching recovery to determine the interfacial concentration of adsorbed species *in situ*, without destabilizing the oil-water interface. In addition, no external measuring devices are required in this protocol.

4.2 Theory

4.2.1 The evanescent wave

A general overview of the theory of total internal reflection is described in Chapter 2 of this dissertation. Here, we present a detailed analysis of the development of the equation characterizing the evanescent wave. This exponentially decaying wave is the partial emergence of the electromagnetic field into the rarer medium at the point of total internal reflection. The success of TIRF as an interfacial tool is due to the unique properties of the evanescent wave.

A thorough mathematical development of Maxwell's wave equations under conditions of total internal reflection has been presented by Reichert et al. (112). They showed that the perpendicularly polarized component of the transmitted electric field could be expressed by the following equation

$$\overline{E}_s^t = \hat{y}t_s\overline{E}_{0S}^t \exp\left[-j\frac{2\pi x}{\lambda_2}\left(\frac{n_1}{n_2}\right)\sin\theta_1 - \frac{2\pi z}{\lambda_2}\left(\left(\frac{n_1}{n_2}\right)^2 \sin^2\theta_1 - 1\right)^{\frac{1}{2}}\right] \qquad [23]$$

where $\overline{E}_{0S}^t$ is the amplitude of the electric field at the interface in the optically rarer medium 2, n_1 and n_2 are the refractive indices of media 1 and 2, respectively, λ_2 is the wavelength of incident light in medium 2, and θ_1 is the incident angle of the excitation beam measured normal to the interface. The variables, x, y, and z, are three mutually perpendicular coordinates, with the interface lying in the x-y plane. The superscript, t, indicates that the equation describes the transmitted electric field.

For an incident beam of finite width, Eqn. [23] represents the surface wave that propagates along the interface as demonstrated by Goos and Hanschen (please see Harrick (75)). The first term in the equation accounts for the longitudinal displacement (in the y direction) between the incident and reflected beams at the interface, and is called the Goos Hanschen shift. The second term accounts for the penetration of the surface wave into the rarer medium (in the z direction); this is a standing wave of exponentially decaying intensity, and is referred to as the evanescent wave.

We can relate the second term to the penetration depth, d_P, of the evanescent wave as follows:

$$\frac{1}{d_p} = \frac{4\pi}{\lambda_2}\left(\left(\frac{n_1}{n_2}\right)^2 \sin^2\theta_1 - 1\right)^{\frac{1}{2}} \qquad [24]$$

and write Eqn. [23] as

$$\overline{E}_S^t = \overline{E}_S^{t'} \exp\left[-\frac{z}{2d_p}\right] \qquad [25]$$

where $\overline{E}_S^{t'} = \hat{y}t_s\overline{E}_{0S}^t \exp\left[-j\frac{2\pi x}{\lambda_2}\left(\frac{n_1}{n_2}\right)\sin\theta_1\right]$

The effective depth of penetration, d_p, is defined for mathematical convenience to be the distance z required for the electric field to decay to e^{-1} of its original value. If we note that λ_1, the wavelength of the excitation wave in the medium 1, can be given by $\lambda_1 = \lambda_0/n_1$, where λ_0 is the free space wavelength of the incident beam, then Eqn. [24] reduces to the expression for the penetration depth presented in Chapter 2 of this thesis:

$$d_p = \frac{\lambda_o}{4\pi n_1 \sqrt{\sin^2 \theta - n_{21}^{\ 2}}} \qquad [26]$$

where $n_{21} = n_2 / n_1$ is the relative refractive index.

Given randomly oriented dipoles on the fluorophores, the probability of absorption of energy from the evanescent wave is proportional to the intensity; as such, $I \equiv |E_s^t|^2$ (62). Thus, Eqn. [25] reduces to the more familiar expression for the evanescent wave:

$$I(z) = I_o e^{-z/d_p} \qquad [27]$$

It is important to note that I_0 in the above equation refers to the incident beam intensity in the optically rarer medium. Experimentally, it is easier to measure the intensity of the incident beam in medium 1, the optically denser medium. However, I_0, for incident angles within 10° of the critical angle, can be up to five times larger than the intensity of the incident wave. This is of particular concern since underestimating I_0 could potentially cause unintended photobleaching of fluorophores by the monitoring beam since, in this situation, the monitoring beam would be more intense than would be anticipated. The calculation of I_0 and its relation to the monitoring beam intensity will be discussed later in this chapter.

4.2.2 Interfacial selectivity of TIRF

The major challenge in studying the interfacial adsorption of any macromolecule is the need to exclude the properties of the bulk molecules from those at the interface. In TIRF,

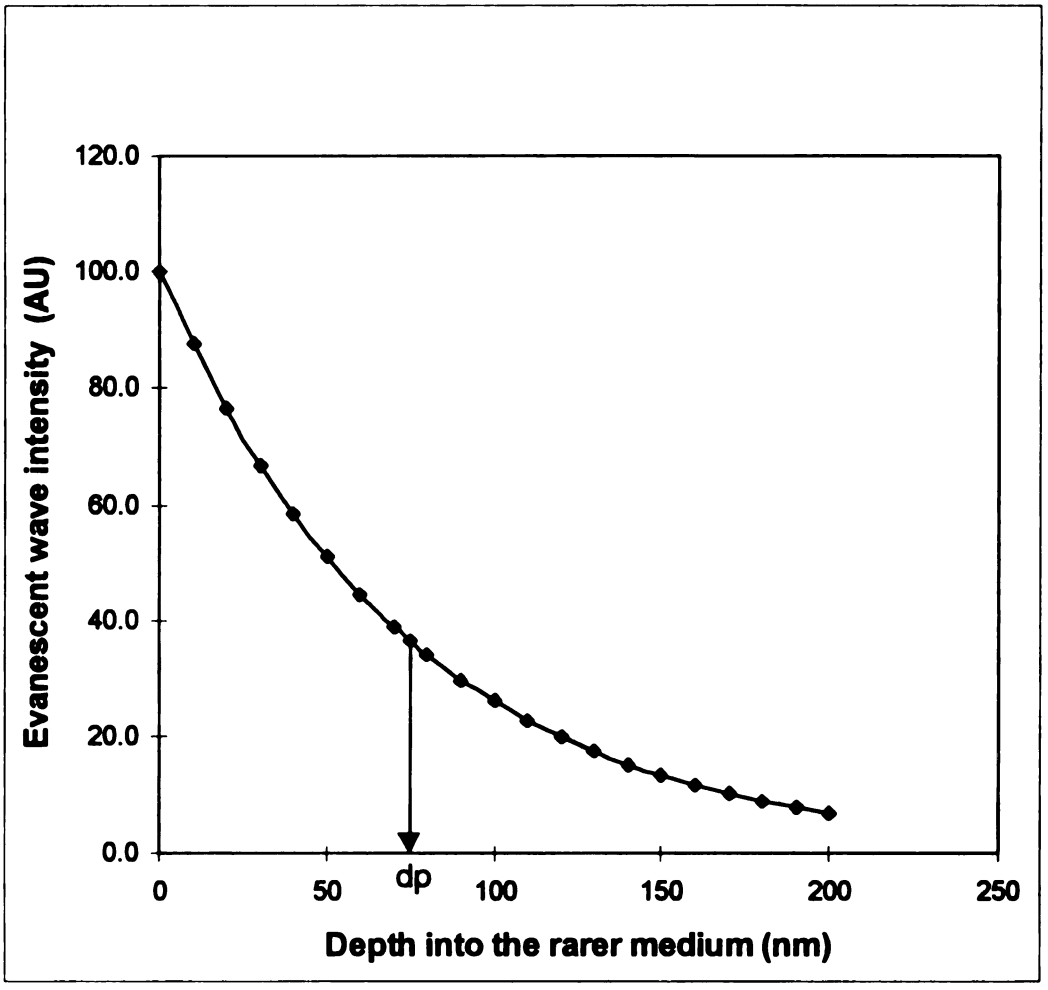

Figure 4.1. Evanescent wave intensity as a function of depth of penetration into the rarer medium. The penetration depth, d_p, is 75 nm in our setup, for an interface between oil (n_1 = 1.52), and water (n_2 = 1.33) for an incident light of wavelength λ = 488 nm, at an angle of incidence θ = 70°.

the exponential nature and shallow penetration depth (d_p) of the evanescent wave help to effectively accomplish this. The d_p for most TIR systems ranges from 75 to 150 nm. This allows preferential and selective illumination of a very thin layer closest to the interface.

Figure 4.1 shows a plot of the evanescent wave intensity with distance into the rarer medium for our system (d_p = 75 nm). From the graph, it can be seen that the evanescent wave intensity drops to about 25% of its initial value within the first 100 nm of the interface.

In addition, microscope optics allow reasonably precise focussing at the interface, further contributing to better interfacial selectivity by rejecting out of focus fluorescence from the bulk. A microscope objective with a high numerical aperture gives a small depth of focus d_f according to the relation (Technical support, Melles Griot, personal communication):

$$d_f \sim \frac{\lambda_{em}}{4.NA^2} \qquad [28]$$

where λ_{em} is the wavelength of the light and NA is the numerical aperture of the objective.

The depth of focus refers to a region where all objects are simultaneously in focus, determined by just meeting the Rayleigh criteria of resolution (which is +/- $\lambda_{em}/4$). It should be noted that, in our system, the light collected by the microscope objective is the emitted fluorescence for which λ is 519 nm. With NA = 0.75 and λ_{em} = 519 nm, Eqn. [28] gives a depth of focus of approximately 200 nm. Therefore, careful focusing of the

microscope leads to the rejection of bulk fluorescence emissions more than 200 nm away from the interface.

Despite these precautions, there is still a sizable contribution of fluorescence from fluorophores in the bulk in most practical situations. However, by reducing the incident light intensities in our experiments to 1-5 μW and using an extremely sensitive detection system, we are able to minimize these unwanted contributions. For an accurate, absolute quantitation of interfacial proteins, it is necessary to completely account for emissions from the bulk and subtract this contribution from the total fluorescence signal. This is accomplished by using a photobleaching pulse to eliminate fluorescence emission from proteins adsorbed at the interface and thus enable the calculation of the bulk fluorescence. The details and theory are presented below.

4.2.3 The calibration protocol

The calibration protocol presented here was adapted from Zimmerman et al. (14), who applied the technique to measure the adsorption of BSA at the quartz/water interface. The method is self-contained, in that it does not require any other external measuring techniques such as ellipsometry, γ-detection of radiolabeled proteins or spectrofluorimetry. The method is based on the fact that the total fluorescence detected by the PMT is a combination of contributions from the bulk and the interface (29):

$$F_T = F_{ads} + F_{bulk} = q_I \int_0^\infty I(z)C(z)q_f(z)dz \qquad [29]$$

where q_I is the overall instrument constant which accounts for the collection efficiency of the optical system as well as the fraction of labeled proteins, and q_f is the quantum yield of the fluorophore.

Incorporating the expression for the evanescent wave from Eqn. [27] gives

$$F_T = F_{ads} + F_{bulk} = q_I I_0 \int_0^l e^{-\left(\frac{z}{d_p}\right)} C(z) q_f(z) dz \qquad [30]$$

where $C(z)$ is the concentration of proteins, and is a function of the z direction perpendicular to the interface.

Note that the upper limit of the integration is l, the depth of the aqueous phase in our experimental cell. We assume a simple model of protein adsorption, whereby there is a layer of adsorbed protein molecules at the interface of thickness s and two-dimensional concentration C_S, in equilibrium with a bulk concentration of C_B. We can now split up the definite integral into two terms, the first representing F_{ads}, the surface fluorescence, and the second F_{bulk}, the bulk fluorescence:

$$F_T = F_{ads} + F_{bulk} = q_I I_0 \left(C_S q_{fS} + C_B q_{fB} \int_S^l e^{-\left(\frac{z-s}{d_p}\right)} dz \right) \qquad [31]$$

where q_{fS} and q_{fB} are quantum efficiencies of the fluorophore in the adsorbed layer and in the bulk, respectively.

In this analysis, we have assumed that q_{fS} is equal to q_{fB} (this and other assumptions are discussed in the next section). We can therefore combine the fluorophore quantum efficiency with q_I, the overall instrument constant to get q, the overall system constant. Note that we have assumed here that total internal reflection occurs on a plane parallel to the interface and at a depth of $z = s$. This is a valid assumption for a dense adsorbed layer of proteins, since the index of refraction of proteins is approximately 1.5 (113), which is approximately the same as the refractive index of the oil phase in our system.

Based on the shape and dimensions of a BSA molecule, we can make a rough estimate of the magnitude of s in our system. BSA has been well described hydrodynamically as a prolate ellipsoid. Wright and Thompson (114) have used transient electric birefringence to calculate dimensions of 14.1 nm for the major axis and 4.1 nm for the minor axis. For a multilayer adsorption model, with at least three different classes of proteins (discussed in more detail in Chapter 3), this means that s lies somewhere in the range of 10 nm to 50 nm. Therefore, s is clearly much smaller than l ($s<<l$), the depth of the aqueous phase (which is approximately 0.9 mm). Therefore, we can simplify the expression for F_{bulk}, the bulk fluorescence as follows:

$$F_{bulk} = qC_b \int_s^l e^{-\frac{(z-s)}{d_p}}\, dz = qC_b \left[-d_p e^{-\frac{(z-s)}{d_p}} \right]_s^l = qC_b \left(-d_p e^{-\frac{(l-s)}{d_p}} + d_p \right) \approx qC_b d_p \qquad [32]$$

Incorporating Eqn. [32], we can rewrite Eqn. [31] as

$$F_T = F_{ads} + F_{bulk} = qI_0 \left(C_S + C_B d_p \right) \qquad [33]$$

where the factor qI_0 is called the instrument constant.

Since the bulk concentration is known, we need only to measure its fractional contribution to the total fluorescence to calculate both the unknown instrument constant and the interfacial concentration. In fact, according to Axelrod et al. (62), one can easily deduce this fractional contribution by two simple techniques. The first is to abolish the fluorescence from the interface with a strong photobleaching pulse of incident light, so the bulk fluorescence emission can be measured. The second is to replace the bulk solution with a fluorescence-free rinse, so the measured fluorescence will only come from the interface. Of course, this second technique is only appropriate if adsorption is irreversible at the interface of interest.

Previous work in our laboratory (87) has demonstrated that protein adsorption at the oil-water interface is not entirely irreversible. Therefore, the introduction of a fluorescent-free rinse (by either an equivalent solution of unlabelled proteins or a buffer solution free of proteins) into the flow cell will affect the determination of the concentration of adsorbed proteins. In the case of introducing an unlabelled protein rinse, there is the possibility of exchange of the reversibly adsorbed labeled proteins with bulk unlabeled proteins, which will reduce the fluorescence intensity detected at the interface. The result is that the measured concentration will be less than the actual prevailing surface concentration. On the other hand, the introduction of a buffer solution into the flow cell will, at the least, change the microenvironment of the fluorescent tag on the protein. This will induce changes in the quantum yield of the fluorophore (2) that could potentially lead to erroneous estimates of the interfacial concentration.

Fortunately, photobleaching interfacially adsorbed species allows us to circumvent these potential problems. Using controlled photobleaching experiments, the difference in mobilities between surface-adsorbed and free bulk proteins can be exploited to separate the surface and the bulk components of the fluorescence signal. The proteins in the bulk are mobile with a diffusion coefficient on the order of 10^{-7} cm^2/s (115). The time taken for exchange of unbleached fluorophores with bleached fluorophores in the bulk can be calculated by the following simple equation:

$$t = \frac{x^2}{D} \qquad [34]$$

where x is the distance traveled to effect the exchange, and D is the bulk diffusion coefficient.

For an evanescent wave penetration depth of 75 nm, this corresponds to an average exchange time on the order of milliseconds. This is less than the time resolution of our experiments (10-12 ms) and results in an apparent unbleachability of the bulk fluorophores. In other words, even though the photobleaching beam bleaches proteins in the bulk, the fast diffusion coefficient causes the recovery to occur before the detection system can record it. Experimentally then, F_{bulk}, can be determined by measuring the fluorescence intensity after complete bleaching of the adsorbate layer and can be expressed as

$$F_{bulk} = qI_0C_Bd_p \qquad [35]$$

If we make the reasonable assumption that the concentration of proteins in the bulk is not affected by adsorption at the interface (the so-called "infinite well" assumption), then C_B is

essentially the protein concentration injected into the experimental cell and is thus known. Combining Eqn. [33] and Eqn. [35], we can express the concentration of interface-associated proteins, C_S, as

$$C_S = C_B d_p \left(\frac{F_T}{F_{bulk}} - 1 \right) \qquad [36]$$

Therefore, C_S can be calculated by measuring F_T and F_{bulk}, for a given bulk concentration C_B.

4.2.4 Relation between evanescent intensity (I_0) and monitoring beam intensity

The light intensity at the interface (I_0 in Eqn. [42]) is a function of the angle of incidence and the polarization of the incident laser beam. The incident light can either be p-polarized (transverse magnetic field) with the electric field vector parallel to the plane of incidence, or s-polarized (transverse electric field) with the electric field vector perpendicular to the plane of incidence. The intensity of the evanescent wave at z = 0, for unit incident intensities, are given by Harrick (75):

$$I_p(0) = \frac{(4\cos^2\theta)(\sin^2\theta)}{n^4\cos^2\theta + \sin^2\theta - n^2} \qquad [37]$$

$$I_s(0) = \frac{(4\cos^2\theta)}{1 - n^2} \qquad [38]$$

where θ is the angle of incidence and $n = n_{21} = n_2 / n_1$ is the relative refractive index.

For incident angles less than the critical angle (θ_C = 61° for our system), the intensity of the transmitted electromagnetic waves can be calculated from the Fresnel equations:

$$I_p(0) = E^2{}_p(0) = \left(\frac{(2n\cos\theta)}{n^2\cos\theta + \sqrt{n^2 - \sin^2\theta}} \right)^2 \quad [39]$$

$$I_s(0) = E^2{}_s(0) = \left(\frac{(2\cos\theta)}{\cos\theta + \sqrt{n^2 - \sin^2\theta}} \right)^2 \quad [40]$$

The transmitted light intensities in our system for incidence angles ranging from subcritical to supercritical are plotted in Figure 4.2 using Eqns. [37]-[40]. Note that the evanescent intensities near the interface and within 10° of the critical angle are up to five times larger than the intensities of the incident plane waves.

The incident angle of the laser beam in our system was fixed at 70° by the geometry of the TIR prism. For p-polarized incident light, this gives a relative intensity of 2.5. In other words, the evanescent intensity at $z = 0$ is 2.5 times greater than the intensity of light striking the oil-water interface. This is approximately equivalent to the monitoring beam intensity. However, the monitoring beam intensity is measured outside the experimental cell, i.e. before the laser beam is incident on the prism. To relate the intensity of the monitoring beam to the evanescent wave intensity, it is necessary to estimate losses due to reflection at the prism surface and absorption by the prism and the slide.

In a separate experiment, we used a Newport detector (818-SL, Newport Corporation, Irvine, CA) and a Newport power meter (1815-c, Newport Corporation, Irvine, CA) to measure laser light intensities before and after passing through the prism and slide. An average transmission efficiency of 0.85 was measured which, when coupled with the

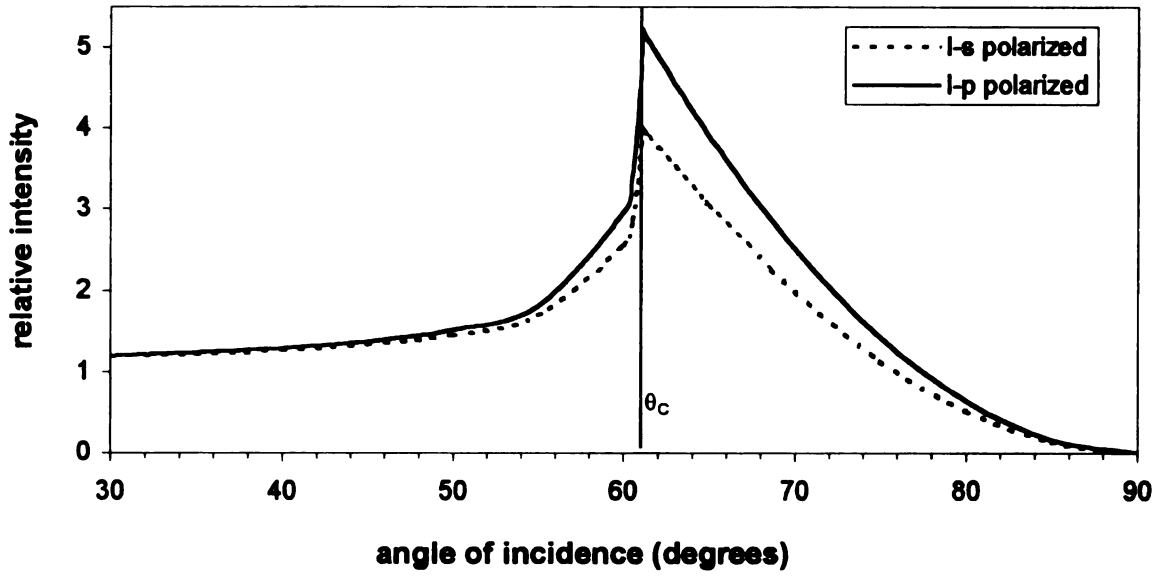

Figure 4.2. Evanescent intensities I-s and I-p for perpendicular and polarized incident light (λ = 488 nm) at the oil-water interface (z = 0) as a function of angle of incidence. The critical angle, θ_C, in our experiments is 61° for oil (n_1 = 1.52) and water (n_2 = 1.33).

relative intensity factor (2.5), resulted in an evanescent wave intensity that was a factor of 2.1 times greater than the monitoring beam intensity. Thus, in our system, typical monitoring beam intensities of 1-5 μW resulted in evanescent wave intensities of 2-10 μW.

4.3 Materials and methods

The experimental apparatus used is discussed in detail in Chapter 2 of this dissertation. Protein solutions of concentrations ranging from 10^{-4} mM to 0.3 mM were injected into the experimental cell. An FITC:BSA molar labeling ratio of 1:1 was used for all experiments. Absorption spectroscopy was used to measure protein concentrations and labeling ratios, as discussed later in this chapter.

4.3.1 TIRFM calibration experiments

A description of the experimental used in general TIRFM experiments can be found in Chapter 2. Here we present the procedures specific to experiments conducted to develop the calibration protocol.

All calibration experiments were performed in the dark at room temperature, with protein concentrations ranging from 10^{-3} mM to 0.15 mM at a monodisperse labeling ratio of 1. The experimental cell was first flushed with pure PBS buffer at a pH of 7.4, for a period of 25 minutes. This served to remove the air bubbles in the tubing and the experimental cell. The proteins were then injected into the cell using a reciprocating syringe pump that

simultaneously withdrew PBS buffer solution. All flowrates in and out of the cell were held constant at 0.5 ml/min. At this flowrate, it took approximately 20 minutes to completely replace the bulk solution in the experimental cell, assuming that the flow regime in the cell could be modeled as plug-flow. However, to ensure equilibrium, the proteins were injected into the cell for 45 minutes, after which the syringe pump was turned off and another 20 minutes was allowed to ensure equilibrium adsorption.

The interface was then bleached for 150 ms with a 15 mW laser beam and the subsequent drop in fluorescence was recorded by the PMT. The microscope stage, on which the experimental cell rests, was then slowly moved to a new position. The exact destination, coordinates and speed of motion were controlled from the computer via the RS-232 interface. By doing this, a new location on the interface was brought into focus to be bleached by the photobleaching beam. This procedure was repeated for 10 different locations on the interface. The average F_T to F_{bulk} ratio was used to estimate the surface concentration.

4.3.2 Calculation of C_B by absorption spectroscopy

A diode array spectrophotometer (8452 A, Hewlett Packard) was used to determine the bulk concentration of proteins in the aqueous phase. The absorbance of the protein sample was measured at 280 nm and compared with previously developed calibration curves of absorbance versus unlabelled protein concentration. These calculations were complicated by the fact that FITC absorbs at both 280 nm and 490 nm. Thus, the absorbance of the labeled protein sample at 280 nm has contributions from FITC as well as BSA. To obtain

an accurate value for the absorbance of BSA alone, it was necessary to subtract the absorbance of FITC at 280 nm from the total absorbance at 280 nm. To this end, a calibration chart of absorbance at 490 nm versus concentration of pure FITC was prepared. From this, we could calculate the concentration of FITC in the protein sample. Another absorbance calibration chart for pure FITC at 280 nm was then used to calculate the absorbance of FITC at 280 nm. This was then subtracted from the total absorbance of the protein sample at 280 nm to obtain the actual absorbance attributable to protein alone. The protein concentration corresponding to this absorbance could then be calculated from the unlabeled protein calibration chart. The calibration graphs along with sample spectra for BSA and FITC are given in Appendix B and D.

4.3.3 Prevention of protein adsorption on the bottom slide

In the calibration protocol discussed earlier, we made the assumption that the bulk concentration of proteins is not affected by adsorption (this assumption is discussed in detail in the Discussion section). In order to ensure that this assumption is valid at even the lowest concentrations of proteins (10^{-8} M), it is necessary to prevent adsorption of proteins from the bulk on to the waterwhite glass slide that serves as the bottom of the flowcell.

Coating of a glass surface with polyethylene glycol, also called polyethylene oxide (PEO), has been shown to effectively prevent adsorption of BSA (78). PEO-based protein resistant surfaces function primarily by a steric exclusion mechanism involving very high

surface mobility and surface dynamics of the PEO chains. Andrade et al. (116) have shown that, for a PEO-coated surface, protein resistance depends on several factors, including protein size, surface density and chain length of PEO, as well as the degree of polymerization. PEO polymers with the longest chain lengths at the optimum surface density were shown to give maximum resistance to protein adsorption. To this end, we used PEO with a molecular weight (M_v) of approximately $8x10^6$ (No. 37,283-8, Aldrich Chemical Company, Milwaukee, WI). Deionized water was used to make a 600-ppm PEO solution. A bottom glass slide, which had previously been cleaned using the procedure described by Cheng et al. (78), was immersed in the PEO solution for two hours to form a coating on the slide. Before the slide was used, it was rinsed with water to remove excess PEO.

4.4 Data analyses

The magnitude and quality of the output signal from the PMT depends on several factors besides the actual fluorescence emission. These factors include dark current, background light and flicker noise. In order to reliably interpret PMT data, it is necessary to examine and account for these factors. Typical PMT outputs showing levels of dark current, background light and concentration-dependent flicker noise are superimposed on a single diagram in Figure 4.3

Dark current is the small amount of current that flows in a photomultiplier tube even when operated in a completely dark environment. It is primarily due to thermionic emissions from the photocathode and dynodes, leakage current (between the anode and the other

electrodes in the tube head) and ionization of residual gases in the tube. The level of dark current in our system depends on the high voltage applied to the PMT and the set point of the PMT cooling system. We measured a dark current of 50 counts at a high voltage of 800 V at a temperature of –22°C. These settings were maintained throughout all our calibration experiments, and the dark current value was subtracted from all PMT readings.

Even with the utmost precautions, stray light from various sources can enter the PMT tube. For example, fluorescence from the immersion oil used to optically couple the prism and the top microscope slide, scattered evanescent energy that bypasses the interference filter or reflected laser light that enters the PMT tube from outside the microscope light path. Together, these constitute the background noise in the PMT signal and can be measured in the system at the pure buffer/oil interface. In, Figure 4.3 the fluorescence signal jumps from the dark current level to the background noise level upon opening the PMT shutter. Note that this is prior to the injection of proteins into the system. Background light levels of 40 counts were typical in our calibration experiments, and were subtracted from all PMT readings.

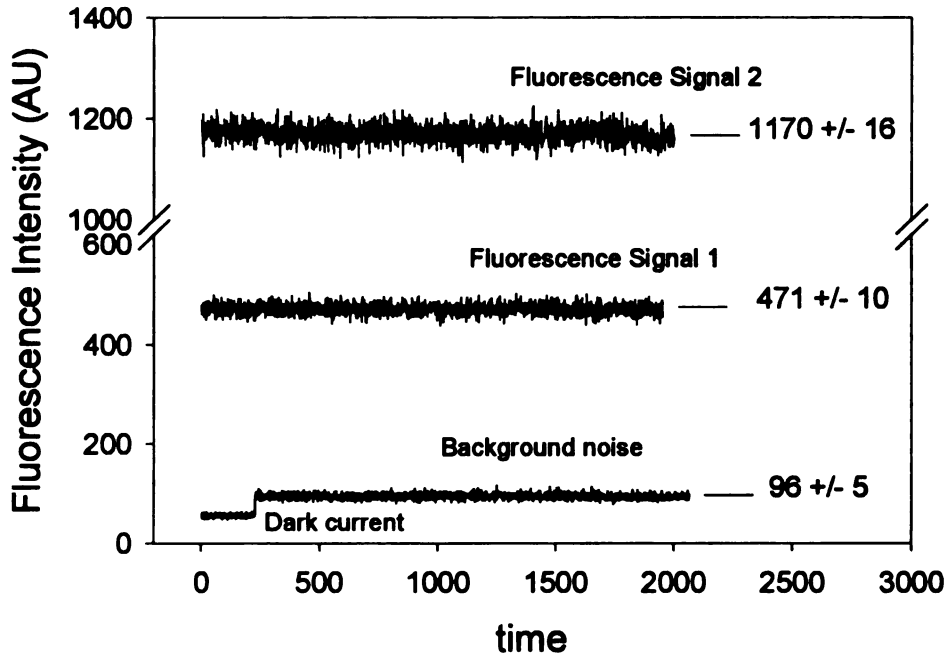

Figure 4.3. PMT signal outputs showing typical levels of dark current, background noise and shot noise proportional to fluorescence signals. The PMT is operated at 800 V and –22°C.

The output from the PMT has an AC component noise that can be categorized by origin as follows:

1. Shot noise from signal light (flicker and quantum noise);
2. Shot noise from background light; and
3. Shot noise from dark current

The first kind of noise can come either from the inherent randomness of the fluorescence excitation process (quantum noise) or from non-ideal experimental conditions (flicker noise). For example, scattering of light by components of the experimental cell (prism, microscope slide, oil etc) can excite fluorophores in the bulk, causing flicker noise. The magnitude of the shot noise in the signal is usually expressed as the root mean square value of the signal. The shot noise calculated for several different levels of PMT signals is plotted in Figure 4.4. The rms value of the shot noise varies linearly with the signal and is approximately 0.5 % of the magnitude of the signal.

In our calibration experiments, the PMT records data at a rate of 82 readings per second. Each reading is the average of 256 samples of the detector by the photometer device. The process of sampling the data 256 times takes approximately 4-6 msecs.

A typical fluorescence recovery curve is shown in Figure 4.5. After equilibrium adsorption, the PMT was switched on at t = 0 seconds. For the first ten seconds of the experiment, we measured the total fluorescence from the interface and the bulk. After ten seconds, the shutter system was triggered causing the interface to be bleached while

simultaneously shuttering the PMT. This is manifested as a brief drop of approximately 100 ms in the fluorescence signal. The fluorescence signal immediately after photobleaching is the bulk fluorescence (F_{bulk}). A simple arithmetic average of the first 10 seconds of the fluorescence data gives F_T, the total fluorescence.

Estimating the bulk fluorescence is however a more complicated task. Taking a simple time average, as in the case of F_T is unacceptable since the fluorescence signal increases with time during the recovery process. Additionally, the first data point after opening the shutter is not a valid reading since it can be artificially low. This is because the opening of the PMT shutter is not always precisely synchronized with the start of the sampling process. Hence, for a part of the sampling duration of 4-6 msecs, the PMT shutter might have been closed, and thus some of the 256 samples of the detector that make up the first reading could be only a measure of the dark current levels. Therefore the second data point after photobleaching is used as the bulk fluorescence signal. The error in estimating the bulk fluorescence signal in this fashion is approximately 0.5 %, which is the rms value of the shot noise of the signal as discussed earlier.

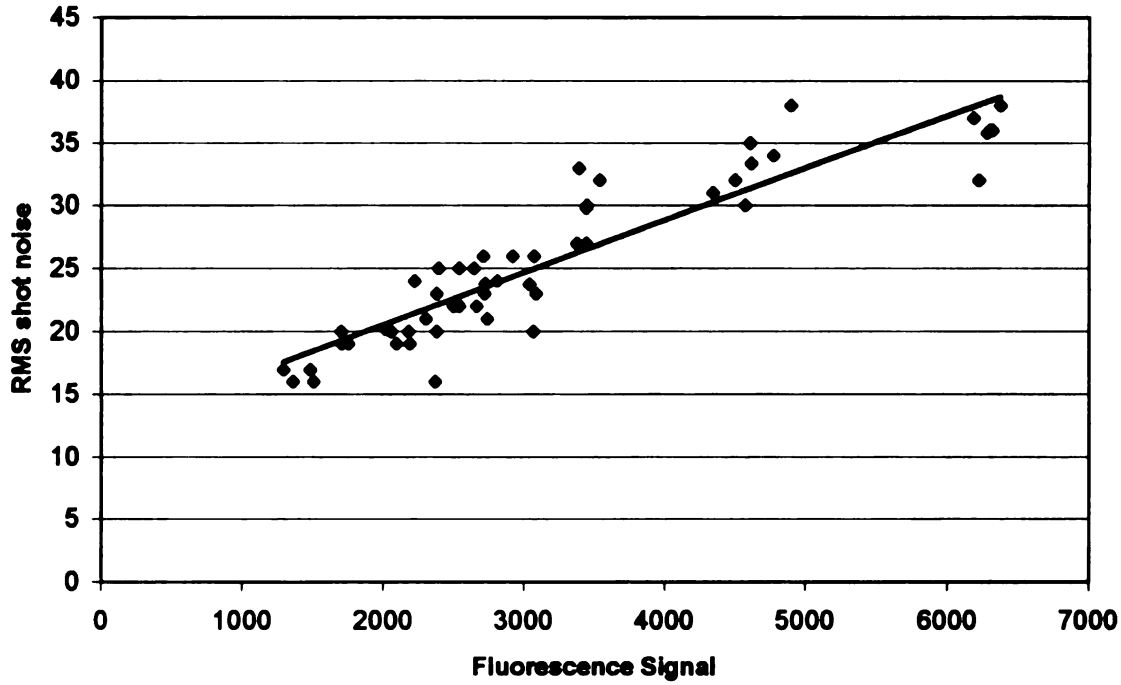

Figure 4.4. RMS shot noise as a function of the magnitude of the fluorescence signal.

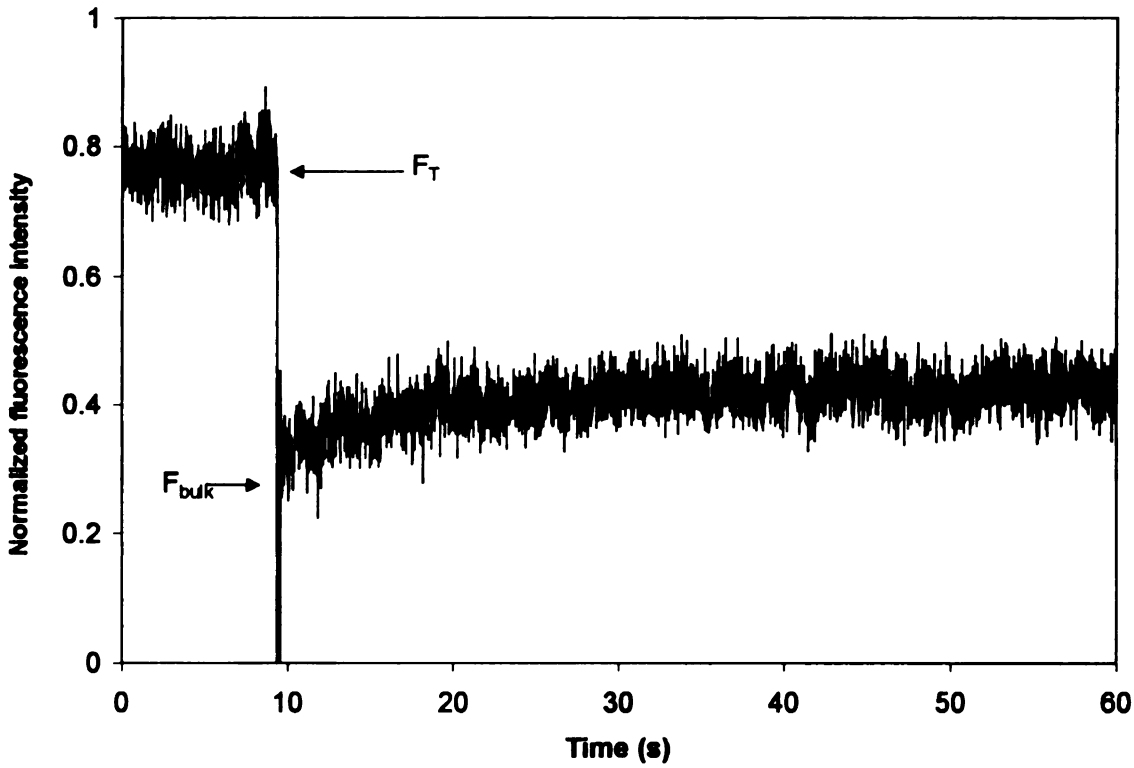

Figure 4.5. A typical fluorescence recovery curve for TIRF/FPR experiments. F_T is the equilibrium fluorescence emission prior to photobleaching, and F_{bulk} is the fluorescence emission immediately following a 15 mW, 100 ms photobleaching pulse.

4.5 Results

The concentration of adsorbed BSA calculated by the calibration protocol at different bulk protein concentrations is shown in Figure 4.6. The interfacial concentration increases linearly with bulk concentration up to 0.025 mM, after which the slope of the curve levels off as the proteins begin to saturate the interface. The interface is saturated with BSA at a surface coverage of approximately 0.07 mg/m^2 at a bulk concentration of approximately 0.1 mM. Saturation at this bulk concentration is expected, since the critical micelle concentration (cmc) of BSA, estimated in chapter 2 of this dissertation, is approximately 0.1 mM.

The adsorbed quantities of BSA reported here are lower than the saturation adsorption concentrations typically reported for the solid-liquid interface. Previous estimates of the surface coverage of BSA using TIRF on various polymeric surfaces ranged from 0.1-1 mg/m^2. However, these studies were performed at a bulk concentration above the cmc of BSA (78). On the other hand, lower estimates of surface saturation have been reported at the oil-water interface. For example, Beaglehole et al. (117) used ellipsometry to estimate the adsorption of BSA at the water-oleyl alcohol interface. They measured an adsorption of 0.45 mg/m^2 at a concentration of 0.05 mM.

Two factors can potentially contribute to the low estimates of interfacial protein concentration reported in this work. First, it is possible that the high intensity laser beam flash is not completely bleaching the interfacially adsorbed proteins. In this case, the post-photobleach fluorescence will have a contribution from the interface, leading to an

overestimation of the bulk emission at the expense of the interfacial emission. This will result in an erroneously low calculation of the interfacial protein concentration. However, previous experiments in our laboratory have shown that increasing the duration of the bleach pulse above 150 ms has a negligible effect on the post-bleach fluorescence. Secondly, as discussed earlier, the assumption that the quantum yields of fluorophores do not change on adsorption can lead to an artificially low estimate of interfacial protein concentration. Since, upon conjugation to BSA, the quantum yield of a fluorophore drops by about 60% (92), it is unlikely that adsorption will cause a further reduction of similar magnitude. However, even correcting for a 60% reduction in the quantum yield of a fluorophore on adsorption will only increase the interfacial protein concentration by a factor of 2.5. This, for the improbable and extreme case, is not large enough to account for differences between the surface coverages reported for the solid-liquid interface, and those measured at our liquid-liquid interface.

We believe that the smaller interfacial concentrations measured in our system are due to the fluid nature of the liquid-liquid interface. According to Dickinson 'the greater mobility at a fluid interface (e.g. liquid-oil) allows greater opportunity for protein unfolding than at a solid surface' (53). Given the dilute concentrations used in this study, one can postulate that proteins arriving first at the fresh interface have the time and space to unfold and denature, occupying a greater surface area per molecule and preventing further adsorption. This leads to a lower surface coverage at the liquid-liquid interface. Additionally, at the higher concentrations typically used in the solid-liquid experiments cited earlier, the finite time required for unfolding is very limited. Therefore a molecule is

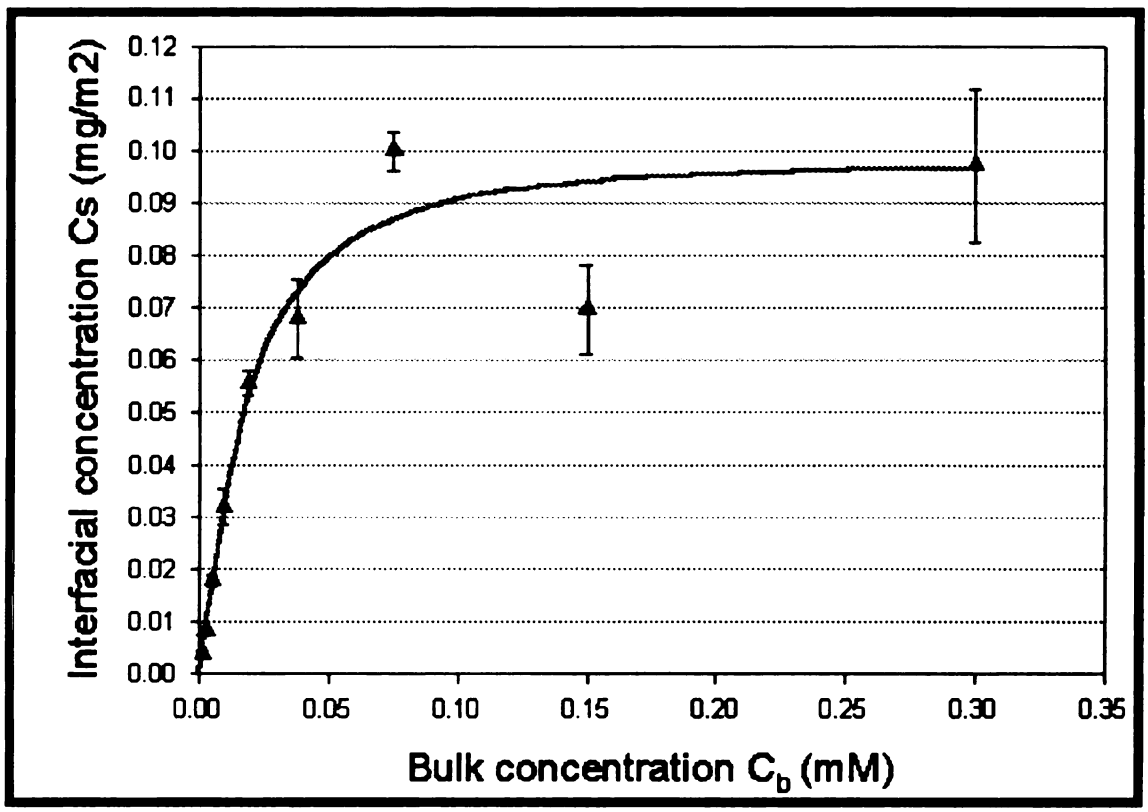

Figure 4.6. Interfacial concentration of BSA, at the oil-water interface, as a function of bulk concentration estimated by the calibration protocol.

rapidly surrounded by others, producing a close-packed state in which any configurational readjustment is severely restricted. The rigid nature of the solid-liquid interface further

restricts the relaxation of the protein and thus encourages closer packing of the unfolded globular proteins, leading to higher surface coverages.

4.6 Scope and application of the calibration protocol

The interfacial protein concentration estimated by the calibration protocol is dependent on the accuracy with which the microscope is focussed at the interface. Improper focusing could lead to a large bulk contribution to the total fluorescence signal and hence an underestimation of the interfacial concentration. This is because, even though the evanescent wave is naturally only formed at the interface, the absolute distance between the microscope objective and the origin of the evanescent wave changes due to bumps and ridges at the interface. For a fixed beam alignment and objective position, the accuracy of the focus will then vary with these surface irregularities at the liquid-liquid interface. This variance makes it impossible to compare data from different interfaces or even different locations on the same interface. It is therefore necessary to refocus the microscope at every new location on the interface to maximize the PMT signal, thereby ensuring an optimum focus. After the microscope stage is moved to examine a new location, minute changes in the focus of the microscope can be performed to maximize the 'live' PMT signal (read directly off the MAC terminal). Now, even though the absolute PMT signal may change at different locations on the interface, the ratio of total to bulk fluorescence is constant. Thus a ratio of F_T/F_{bulk} obtained by bleaching one location on the interface will yield the surface concentration (C_s) at any other point on the interface. In our calibration experiments, at a given interface the standard deviation of the F_T/F_{bulk} ratio at various locations was less than 3%.

In theory, it is possible that the F_T/F_{bulk} ratio at a given bulk concentration will be the same at different oil-water interfaces. By meticulously maintaining the experimental conditions observed in the calibration experiments, this was shown to be true within an experimental error of 5%. The variances between two oil-water interfaces are no larger than the variances between different locations on the same interface. However, precisely duplicating the laser beam intensity, the PMT voltage and operating conditions, the beam alignment, and the quality of the top slide and its optical coupling to the prism is not easy in practice.

4.7 Discussion

Calibration of the TIRF apparatus to enable direct estimation of interfacial concentration of proteins from fluorescence emission data is a difficult endeavor. Several experimental precautions needed to be rigorously observed to ensure that the integrity of the TIRF instrumentation is not compromised. These are discussed below.

4.7.1 The detection system

A photomultiplier tube (PMT) is at the heart of our current TIRF system. The fluorescence emission from the interfacial species is focussed on to the photocathode of the PMT, causing the ejection of photoelectrons. A system of dynodes (the electron multiplier) uses high voltages to multiply and amplify the photoelectrons eventually reaching the anode, after which they are converted into an intensity signal. With current

amplifications as large as 10^8, it is important to ensure that the PMT electronics do not drift. Drift usually occurs only during initial operation, as the signal tends to stabilize as operating time elapses. We used a combination of aging and warm-up techniques (118) to effectively eliminate drifting. Before an experiment, the PMT was run at the desired operating voltage and exposed to light levels anticipated during the experiment for a period ranging from 45 minutes to an hour. This was judged to be a sufficient enough duration to stabilize the signal. Additionally, the laser was also run for a period of one hour at the desired intensity prior to initiating experiments, as recommended by the manufacturer.

An additional source of concern was the thermionic emission of photoelectrons. Due to the extremely low work function of the multi alkali (Na-K-Sb-Cs) photocathode material, thermally induced ejection of photoelectrons can occur even at room temperature. To prevent this, we jacketed the PMT in a thermoelectrically cooled system, maintaining a temperature of -25°C throughout the course of data collection.

4.7.2 Heating effects of the laser beam

A source of concern in fluorescence photobleaching experiments is the possibility of temperature variations due to the intense bleach pulse and the subsequent attenuated monitoring laser beam. Potentially, this could cause several unwanted results, including the following:

1. Distortion of the fluorescence recovery curves by convectional currents in the experimental cell, thus interfering with the calculation of protein diffusion;
2. Photodestruction of the protein molecule or alteration of its native properties upon bleaching; and
3. Apparent photochemically induced cross-linking of proteins at the interface by the monitoring beam.

Axelrod (77) has shown that, for a system with similar laser intensities, the local temperature rise from the bleach pulse is approximately 0.03°C, and thus essentially negligible. Also, since proteins predominantly absorb in the ultraviolet region of the spectrum, the laser beam (which is at a wavelength of 488 nm, the excitation wavelength of the fluorophore) is not expected to have any effect on protein structure or function.

The apparent photochemically-induced crosslinking of proteins adsorbed at the interface is typically manifested by a very slow illumination-dependent increase in the observed fluorescence. This is difficult to observe with our equipment, since bleaching of fluorophores by the monitoring beam could possibly mask this effect. For experiments on a short timescale (< 90 seconds), this effect is negligible and can be ignored. For longer experiments, we use a spinning disc beam chopper that only allows periodic sampling of the interface by the monitoring beam, so it is not always incident on the interface.

4.7.3 The quantum yield problem

In the calibration protocol discussed earlier, we assumed that there was no difference in the quantum yield of a fluorophore whether it is in the adsorbed layer (q_{fS}) or in the bulk (q_{fB}). This enabled us to directly equate fluorescence from the bulk and the surface, eliminating the need to explicitly calculate either the quantum yield or the instrument constant. We now discuss what we believe to be the validity of this assumption.

Fluorescence is a radiational transition between electronic states of the same multiplicity. After an electron is excited to the first electronic state, it can return to the ground state by two possible routes: emission or radiationless decay (including intersystem crossing). The fraction of excited photons that decay through emission is called the quantum yield. Thus, the quantum yield can also be defined as the ratio of the number of photons emitted to the number absorbed. Environmental factors such as temperature, pH, and the presence of other species can affect the quantum yield of any given molecule (98). These factors can affect the rate constant of the luminescence and radiationless deactivation processes or the nature of the lowest-lying excitation state.

Since fluorophores attached to surface-adsorbed proteins and bulk free proteins are exposed to different microenvironments, we expect differences in their quantum yields. In our experiments, we have eliminated changes in quantum yield due to fluorophore-fluorophore interactions at the interface, which is caused by the close proximity of

adsorbed proteins. This is the phenomenon of concentration quenching, and was avoided by using low labeling ratios and preparative chromatography, as discussed in chapter 3.

Additionally, the effective quantum yield, a factor included in the overall instrument constant, can differ between bulk and surface-associated fluorophores, due to the variance of the collection efficiency of the microscope objective with distance from the interface. In general, the dipole emission of the fluorophore has angular characteristics that depend on the distance from the surface of TIR. However, for an isotropic angular orientation of transition moments excited by p-polarized light and given a high detection aperture, the integral quantum yield was shown to be independent of the distance from the interface, with a maximum difference of 5% (62).

However, the presence of quenchers, such as molecular oxygen in the bulk, and the effects of surface properties like charge and hydrophobicity may have an effect on the quantum yield. With our experimental set-up, it is not possible to determine the importance of these effects, or quantify them, and so we have neglected them in our analysis. At the present time, the approach we have taken is widely used in the literature, although further investigation into the quantum yield problem is clearly warranted. Lok et al. (2) reported that exposing adsorbed BSA to a PBS solution caused an increase in extrinsic fluorescence over that seen when unlabeled protein (in PBS) contacted the adsorbed protein, but no attempt was made to quantify this effect.

It is possible, however, to qualitatively state that the quantum yield of the fluorophore at the surface is less than that in the bulk. Physicochemical processes occurring as a result of protein adsorption probably tend to decrease the quantum yield of an extrinsic label such as fluorescein because its quantum yield is initially high. Further conformational changes of the protein at the interface cannot increase the fluorescence quantum yield (119). Therefore, the result of equating q_{fS} to q_{bS} is to potentially overestimate the quantum yield of the fluorophores in the surface adsorbed layer. This causes the calibration protocol to underestimate the concentration of interfacially adsorbed protein species.

4.7.4 Does adsorption change the bulk concentration?

In our calibration protocol, we have assumed that the bulk concentration of proteins in the aqueous phase of the experimental cell is unaltered by adsorption at the interface. This enabled us to determine the bulk concentration by simply measuring the protein concentration injected into the experimental cell. Since the experimental cell is flushed with approximately three times its volume of protein solution before the cell is allowed to achieve equilibrium, this would appear to be a valid assumption. Even at the lowest bulk protein concentration (10^{-8} M), we calculated an aqueous phase bulk protein content that was at least two orders of magnitude greater than the total surface excess of protein at the interface. The total surface excess was estimated by multiplying the total interfacial area of our cell with the unit surface excess measured by the calibration protocol.

As an additional check, we used absorption spectroscopy to determine the protein concentrations entering and leaving the experimental cell. These were sampled from the infusion and withdrawal syringes of the syringe pump respectively, and were equal within experimental error. Hence, even with the low volume of our bulk aqueous phase (~ 1 ml), we are confident that the bulk concentration remains unchanged following interfacial adsorption.

4.7.5 Elimination of PMT light hysteresis: the shutter system

When the incident light or the supply voltage is changed in a step function, a photomultiplier tube may not produce an output comparable with the same step function. This phenomenon is known as PMT hysteresis and can be classified into either light hysteresis or voltage hysteresis. Since we maintain a stabilized, constant high voltage supply to the PMT, voltage hysteresis is not a problem in our experiments. However, at the end of the bleach pulse, there is a drastic step change in the incident intensity as the light level drops from the photobleaching level (20 mW) to the monitoring beam level (1 – 5 μW). At constant voltage, such a step change across nearly the entire measuring range of the PMT will result in a temporary variation in the anode output. This variation is highly undesirable, since it compromises the shape of the initial recovery curve and the accuracy of the bulk fluorescence measurement.

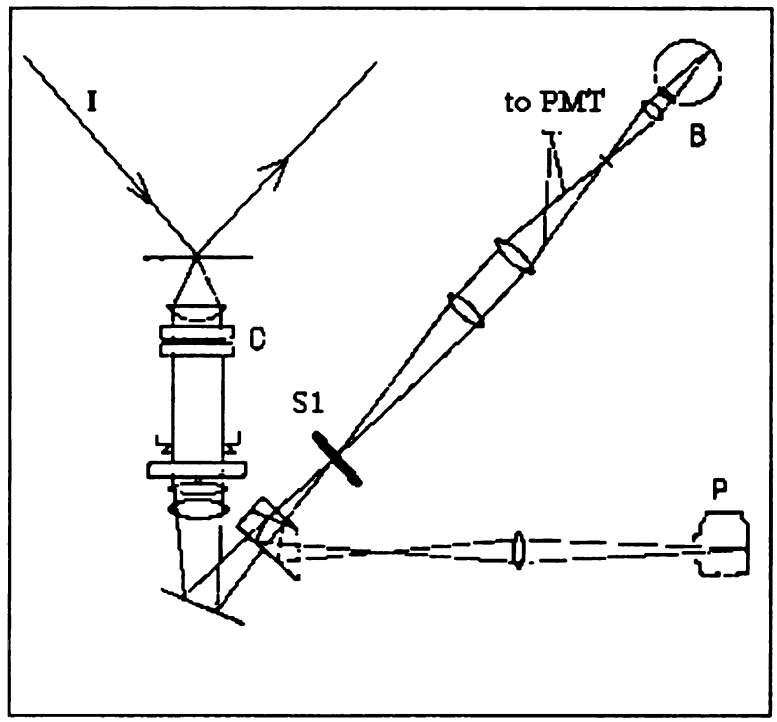

I	Incident laser light
B	Observation beam path
P	Photo beam path
K	Condenser
O	Objective
S1	PMT shutter

Figure 4.7. Beam path of Axiovert 135 microscope showing placement of the PMT shutter (S1).

To prevent hysteresis, we shuttered the PMT for the duration of the photobleaching pulse using a fast-acting, electro-programmable shutter (LS6Z2, Vincent Associates, Rochester, NY). The microscope was modified to allow the shutter to be placed in the path of the observation beam inside the microscope cavity as depicted in Figure 4.7. The PMT shutter (S_1) has to be perfectly synchronized with the shutter blocking the photobleaching beam (S_2), such that when S_2 is open S_1 is closed, and when S_2 is closed, S_1 is open. However, the exact synchronization of the shutter system is complicated by the fact that the two shutters have different response and transfer times on opening and closing. Each shutter is driven by a model T-132 shutter driver (Uniblitz, Vincent Associates, Rochester, NY) that allows the control of delay and exposure times. A remote footswitch (44-610D, Radio Shack, Fort Worth, TX) was used to simultaneously trigger the two shutter drivers. Separate experiments were performed to determine the optimum settings of the shutter drivers to enable synchronization of the shutters.

4.8 Conclusions

We have developed a calibration protocol for quantitation of interfacial protein species based on the intensity of fluorescence emission. The method exploits the fact that the total fluorescence detected by the PMT is a combination of contributions from the bulk and the interface. We used photobleaching techniques to eliminate the interfacial fluorescence, to enable determination of the fluorescence emission from a known bulk concentration. From this data, we deduced the instrument constant, which subsequently allows the calculation of the interfacial protein concentrations from fluorescence emission data.

The technique is instantaneous and self-contained, in that it does not require the use of external standards or additional equipment. Also, since the protocol automatically accounts for irregularities in the oil-water interface, the interfacial protein concentration in a given situation can be determined by bleaching any random location at the interface. This is highly desirable as it allows non-invasive sampling of the interface. In other words, by bleaching in a corner of the interface, the adsorbed protein concentration can be determined without compromising the nature of the macromolecular phenomena being investigated at any other location on the interface.

We have measured a saturation surface coverage for BSA at the oil-water interface of approximately 0.07 mg/m^2, at a bulk concentration of 0.1mM. This is in agreement with previously reported values of 0.1 mM for the critical micelle concentration (cmc) of BSA. However, the values we calculated for the interfacial concentration of BSA are lower than corresponding values reported for the solid-liquid interface. While this could be partially attributable to experimental error and simplifications inherent in the theory of the calibration protocol, we believe that it primarily reflects the increased mobility afforded to proteins at a liquid-liquid interface in comparison to those at the solid-liquid interface.

A source of concern in the development of the theory for the calibration protocol is the assumption that the quantum yield of fluorophores does not change on adsorption. We have discussed the validity of this assumption and its effect on various aspects of the measuring system.

5. SUMMARY AND CONCLUSIONS

Protein adsorption dynamics at liquid-liquid (and liquid-like) interfaces play an important role in several biological, pharmaceutical and food-related processes. For example, the action of hormones in the body is mediated by the binding of a ligand protein to a receptor protein adsorbed at the cell membrane. Also, the pharmacological activity of drugs is governed by their behavior at bio-membranes, which can be modeled to a first approximation by liquid-liquid interfaces. In food systems, protein adsorption at the oil-water interface plays an important role in the stability of food colloids such as mayonnaise, margarine, ice cream, etc., thus affecting their appearance and shelf life, as well as storage and processing conditions. Thus, understanding and accurately characterizing the adsorption and dynamics of amphiphiles at the liquid-liquid interface is of both scientific and technological interest.

The overall goal of this dissertation was to investigate, develop and verify a novel quantitative and *in-situ* technique for investigating macromolecular adsorption and interactions at the liquid-liquid interface. The interfacial selectivity of the total internal reflection geometry was exploited to enable extraction of molecular level information about the dynamics of protein adsorption at the oil-water interface. An important component of the apparatus is the development of a novel oil-water interface, which is constructed from a thin film of oil coated on a microscope slide in contact with water approximately 1 mm deep. This innovation has circumvented the typical vibration-induced

instability problems encountered with optical techniques at liquid-liquid interfaces of normal depth.

As a means of verifying the accuracy of the apparatus, the equilibrium adsorption of two proteins, bovine serum albumin (BSA) and lysozyme, was investigated. The two proteins were labeled with fluoresceine isothiocyanate (FITC), and were selected for evaluating the equipment because they are of different sizes, and are contrasts in nature. BSA is a large globular protein that tends to unfold upon adsorption, whereas lysozyme is a smaller, compact enzyme that undergoes very little structural change upon adsorption. The adsorption profiles obtained correlated quite well with independently developed estimates using the traditional method of interfacial tensiometry, and accurately reflected the nature of the two proteins. In particular, the equilibrium adsorption profile of BSA showed a pronounced break in the slope at a bulk aqueous concentration of approximately 0.1 mM, indicating the onset of micellization. In contrast, lysozyme, which is a predominantly hydrophilic protein and is thus not expected to form micelles, did not portray any evidence of aggregate formation.

The effect of attaching an extrinsic fluorophore on the adsorption and diffusion of proteins was also investigated in this work. Ion-exchange chromatography was used to separate proteins into samples with different monodisperse labeling ratios. This process helped to ensure that we do not simply use a sample of an appropriate average labeling ratio which, in reality, may contain many species with very high degrees of fluorophore conjugation. Therefore, concentration quenching effects, which may be normally present in samples at

an equivalent average labeling ratio, were avoided. Near interface diffusion coefficients measured for proteins conjugated with two FITC molecules were 40% larger than the coefficients for proteins labeled with a single FITC molecule. This difference was attributed to an increase in surface hydrophobicity caused by the presence of the additional fluorophore. These results indicate that previous studies of this nature most likely overestimated the lateral mobility of proteins by as much as 40%.

Fluorescence photobleaching recovery (FPR) was combined with TIRF to develop a calibration protocol for the quantitation of proteins adsorbed at the interface. The method is instantaneous, self-contained and non-invasive. Bulk BSA concentrations required to produce interfacial saturation were measured, and were in very good agreement with information available in the technical literature. However, surface coverages of BSA measured at the oil-water interface were lower than those typically reported for the solid-liquid interface. This difference was attributed to greater fluidity at the oil-water interface, which allowed proteins to unfold to a greater extent. This, in turn, increased the surface area per protein molecule and thus decreased the surface coverage.

As a result of the work presented here, a new tool is now available for investigating molecular-level protein dynamics at the oil-water interface. For situations where it is necessary to calculate the concentration of interfacial moieties, a calibration procedure has been developed and tested to enable absolute quantitation of adsorbed species. The effect of attaching an extrinsic label to a protein has been of long-standing interest, since it is generally believed that labeling affects the dynamics of the protein relative to its native

behavior. This work has clearly demonstrated that this is indeed the case, and that accurate determination of native protein characteristics must account for the effect of any extrinsic labels. It is expected that this apparatus will make it possible to study several important phenomena relating to the dynamics of macromolecules at liquid-liquid interfaces, including the study of receptor-ligand interactions at the oil-water interface.

6. RECOMMENDATIONS FOR FUTURE WORK

The work presented in this dissertation has resulted in the development of a total internal reflection fluorescence microscopy (TIRFM) tool to study macromolecular interactions at the liquid-liquid interface. So far, the study has verified the integrity of the novel thin liquid-liquid interface, and produced a calibration protocol for quantitation of the concentration of interfacially adsorbed species. The stage is thus set for investigation of a wide variety of more complex and application-oriented interfacial phenomena.

Receptor-ligand interactions are of great importance in understanding cell behavior in terms of molecular properties, which is a goal of molecular cell biologists and bioengineers. Most of the efforts of the pharmaceutical industry are aimed at formulating drugs that mimic, replace or interfere with natural compounds which regulate cell function. Thus, understanding cell behavior at the molecular level is vital for work of this nature. Additionally, the initial step in viral penetration of cells is binding to cell receptors. Hence, this research would also provide a valuable insight into viral targeting. The TIRFM tool developed in this work can be used to study various aspects of receptor-ligand interactions, including, determination of the number of ligands bound by a given receptor and the molecular mechanism and/or kinetics of receptor-ligand complexation. Initial adsorption of the receptor onto the oil-water interface can be followed by introduction of the appropriate ligand into the system. An experimental protocol developed to differentiate between free and bound ligands, can then be used to study

receptor-ligand binding. For instance, 1-anilino-8-naphthalene sulfonic acid (ANS), which is practically nonfluorescent in aqueous solution, shows markedly increased fluorescence with a blue shift in emission wavelength upon binding to BSA. Thus, this property can be exploited to monitor the binding of ANS too BSA. Additionally, varying the solvent conditions of the aqueous phase can provide valuable information on the dependence of biological reactions on pH, ionic strength, temperature, etc.

In food colloids, as well as in *in vivo* biological systems, there is rarely a lone protein species involved in the adsorption process at the interface. Typically, the adsorbed layer in a food product is a mixture of several different kinds of proteins, surfactants, as well as small molecules and ions. The food technologist/scientist would ideally like to be able to predict the behavior of a mixture of proteins over a range of processing and storing conditions (53). Similarly, in biological systems, ligands can be multivalent, crosslinked or coupled to other molecules. Thus, any studies beyond the most fundamental would need to consider the competitive adsorption and interaction between different adsorbing species. Up to the present time, most competitive adsorption studies of proteins at liquid-liquid interfaces have been performed by interfacial tensiometry. These studies lack molecular detail and are limited in scope. Our TIRF technique is admirably suited to examining the molecular aspects of competitive adsorption. Different proteins can be introduced sequentially or simultaneously to compare surface efficiency, surface activity and replacement kinetics. Also, the addition of ions and small molecule surfactants to the aqueous phase of the interface can be used to improve the membrane mimetic chemistry of the interface. Additionally, excitation with a tunable laser will allow the use of several

extrinsic fluorophores so that each protein species can be monitored at a different wavelength.

An interesting idea is the use of a two-laser excitation system to study simultaneous competitive adsorption. An Arg-ion laser can be used to monitor the FITC labeled protein at 488 nm, and a tunable laser can monitor another protein-label conjugate at a different wavelength. A suitable emission filter can be chosen to block both the laser wavelengths while allowing the fluorescence emissions to reach the PMT. The contributions to the PMT signals from the two different fluorophores can be distinguished by:

1. laser excitation on different timescales, i.e. one laser in a continuous mode while the other is either optically chopped or in a pulsed mode; and/or
2. differences in laser monitoring intensities coupled with inherent differences in quantum yields of the two fluorophores.

The TIRF apparatus can also be adapted to study the behavior of proteins at the interface between natural hydrocarbons and water. The refractive index of natural hydrocarbons is typically lower than the oil currently used in our system. Therefore, this will necessitate a change in the angle of incidence of the laser beam and possibly the use of a prism of lower refractive index. For example, the interface between crown glass (n = 1.46) and water has a critical angle of 68°. However, one should proceed with caution since it has been reported that certain protein solutions have refractive indices quite different from pure

water. In fact, the development of an auxiliary technique to measure the refractive indices of protein solutions would be very helpful.

Estimation of the intensity profile and exact dimensions of the photobleaching and monitoring beam would be useful in the determination of absolute diffusion coefficients and development of more accurate models of interfacial phenomena. Conventional methods of translation against a knife edge or use of a light sensitive diode are tedious and subject to experimental error. An immobilized fluorophore system (FITC in gelatin), developed by Robeson et al (33) to measure the amplitude of interference fringes, can be used to elegantly accomplish this as described below.

FITC is reacted with the gelatin and the resulting solution is spin cast onto the top microscope slide prior to gelation. This three-dimensional system is free of concentration quenching artifacts (Forster 1959), and using a gel with a high water content preserves the conditions necessary for total internal reflection at the substrate/water interface. The immobilized fluorophore system is photobleached either with a flash of the photobleaching beam or for a longer duration by the monitoring beam. Since the fluorophores are immobile, there is no recovery of fluorescence over time. Therefore, the degree of bleaching and the size of the bleached spot will accurately reflect the beam properties. Then, the beam geometry and size can be deduced from the PMT signal obtained by subsequent translation of the monitoring beam across the interface. In our system, the monitoring beam can be translated across the interface by moving the microscope stage.

The velocity and distance of the microscope stage can be accurately controlled from the computer via an RS-232 interface.

The second study in this dissertation investigated the effect of an extrinsic fluorophore on the functionality of proteins. This research compared the behavior of protein samples with monodisperse labeling ratios of 1 and 2. In a related experiment, we also showed that the effects of concentration quenching were not manifested in a sample with a monodisperse labeling ratio of 2. It would be of interest to study samples with progressively higher yet monodisperse labeling ratios to determine when the effects of concentration quenching are first manifested. Subsequent investigation of quenching in protein samples with average labeling ratios equivalent to the monodisperse samples which are free of concentration quenching can be performed. These experiments would provide information on the efficacy of monodisperse labeling as a technique to avoid concentration quenching.

7. BIBLIOGRAPHY

[1] Stryer, L.,"Protein Structure and Function, "*Protein Structure and Function*, W. H. Freeman and Company, New York, 1995.

[2] Lok, B. K.; Cheng, Y.-L.; Robertson, C. R. , "Protein adsorption on crosslinked polydimethylsiloxane using total internal reflection fluorescence, "*J. Colloid Interface Sci.* **1983b,** 91, 104-116.

[3] Axelrod, D. , "Cell-substrate contacts illuminated by total internal reflection fluorescence, "*J. Cell Biology* **1981,** 89, 141-145.

[4] Burghardt, T. P.; Axelrod, D. , "Total internal reflection/fluorescence photobleaching recovery study of serum albumin adsorption dynamics, "*Biophys. J.* **1981,** 33, 455-468.

[5] Burghardt, T. P.; Axelrod, D. , "Total internal reflection fluorescence study of energy transfer in surface-bound and dissolved bovine serum albumin, "*Biochemistry* **1983,** 22, 979-985.

[6] Thompson, N. L.; Burghardt, T. P.; Axelrod, D. , "Measuring surface dynamics of biomolecules by total internal reflection fluorescence with photobleaching recovery or correlation spectroscopy, "*Biophys. J.* **1981,** 33, 435-454.

[7] Iwamoto, G. K.; Winterton, L. C.; Soker, R. S.; VanWagenen, R. A.; Andrade, J. D.; Mosher, D. F. , "Fibronectin adsorption detected by interfacial fluorescence, "*J. Colloid Interface Sci.* **1985,** 106, 459-463.

[8] Lowe, R.; Hlady, V.; Andrade, J. D.; VanWagenen, R. A. , "Human haptoglobin adsorption by a total internal reflection fluorescence method Biomaterials, "*7:* **1986,** 41-44, 1986.

[9] Horsely, D.; Herron, J.; V., H.; Andrade, J. D., "Human and hen lysozyme adsorption: a comparitive study using total internal reflection fluorescence spectroscopy and molecular graphics, " In *Proteins at Interfaces: Physicochemical and Biochemical Studies*, Brash, J. L., Horbett, T. A. Eds., 1987.

[10] Hlady, V.; Rickel, J.; Andrade, J. D. , "Fluorescence of adsorbed protein layers II Adsorption of human lipoproteins studies by total internal reflection intrinsic fluorescence, "*Colloids Surf.* **1988,** 34, 171-183.

[11] Hlady, V.; Andrade, J. D. , "Fluorescence emission from adsorbed bovine albumin and albumin-bound 1-anilinonaphthalene-8-sulfonate studied by TIRF, "*Colloids Surf.* **1988,** 32, 359-368.

[12] Hlady, V.; Andrade, J. D. , "A TIRF titration study of 1-anilinonaphthalene-8-sulfonate binding to silica-adsorbed bovine serum albumin, "*Colloids Surf.* **1989,** 42, 85-96.

[13] Schmidt, C. F.; Zimmerman, R. M.; Gaub, H. E. , "Multilayer adsorption of lysozyme on a hydrophobic substrate, "*Biophys J.* **1990,** 57, 577-588.

[14] Zimmerman, R. M.; Schmidt, C. F.; Gaub, H. E. , "Absolute quantities and equilibrium kinetics of macromolecular adsorption measured by fluorescence photobleaching in total internal reflection, "*J. Colloid Interface Sci.* **1990,** 139, 268-280.

[15] Pisarchick, M. L.; Thompson, N. L. , "Binding of a monoclonal antibody and its Fab fragment to supported phospholipid monolayers measured by total internal reflection microscopy, "*Biophys. J.* **1990,** 58, 1235-1249.

[16] Pisarchick, M. L.; Thompson, N. L. , "Surface binding kinetics of a monoclonal Fab fragment on supported phospholipid monolayers measured by total internal reflection/fluorescence photobleaching recovery, "*Biophys. J.* **1991,** 59, 350a.

[17] Pisarchick, M. L.; Gesty, D.; Thompson, N. L. , "Binding kinetics of an anti-dinitrophenyl monoclonal Fab on supported phospholipid monolayers measured by total internal reflection with fluorescence photobleaching recovery, "*Biophys. J.* **1992,** 63, 215-223.

[18] Kalb, E.; Engel, J.; Tamm, L. K. , "Binding proteins to specific target sites in membranes measured by total internal reflection fluorescence microscopy, "*Biochemistry.* **1990,** 29, 1607-1613.

[19] Hellen, E. H.; Axelrod, D. J. , "Kinetics of epidermal growth factor/receptor binding on cells measured by total internal reflection/fluorescence recovery after photobleaching, " *J. Fluor.* **1991,** 1, 113-128.

[20] Pearce, K. H.; Hiskey, R. G.; Thompson, N. L. , "Binding kinetics of fluorescently labeled bovine prothrombin fragment 1 at planar model membranes measured by total internal reflection fluorescence microscopy, "*Biophys. J.* **1991,** 59, 622a.

[21] Pearce, K. H.; Hiskey, R. G.; Thompson, N. L. , "Surface binding kinetics of prothrombin fragment 1 on planar membranes measured by total internal reflection fluorescence microscopy, "*Biochemistry* **1992,** 31, 5983-5995.

[22] Poglitsch, C. L.; Sumner, M. T.; Thompson, N. L. , "Binding of IgG to MoFc*RII purified and reconstituted into supported planar membranes as measured by total internal reflection fluorescence microscopy, "*Biochemistry* **1991,** 30, 6662-6671.

[23] Shibata, C. T.; Lenhoff, A. M. , "TIRF of salt and surface effects on protein adsorption, I Equilibrium, "*J. Colloid and Interface Sci.* **1992,** 148, 469-484.

[24] Shibata, C. T.; Lenhoff, A. M. , "TIRF of salt and surface effects on protein adsorption, II Kinetics, "*J. Colloid and Interface Sci.* **1992,** 148, 485-507.

[25] Harrick, N. J.; Loeb, G. I. , "Internal-reflection techniques in fluorescence spectroscopy, "*Modern Fluorescence Spectroscopy* **1973,** 1, 211-225.

[26] Watkins, R. W.; Robertson, C. R. , "A total internal-reflection technique for the examination of protein adsorption, "*J. Biomed. Mater. Res.* **1977,** 11, 915-938.

[27] Lok, B. K.; Cheng, Y.-L.; Robertson, C. R. , "Total internal reflection fluorescence: A technique for examining interactions of macromolecules with solid surfaces, "*J. Colloid Interface Sci.* **1983a,** 91, 87-103.

[28] Kronick, M. N.; Little, W. A. , "A new immunoassay based on fluorescence excitation by internal reflection spectroscopy, "*J. Immunol. Methods* **1975,** 8, 235-240.

[29] Axelrod, D.; Koppel, D. E.; Schlessinger, J.; Elson, E.; Webb, W. W. , "Mobility measurement by analysis of fluorescence photobleaching recovery kinetics, "*Biophy. J.* **1976,** 16, 1055-1069.

[30] Axelrod, D.; Thompson, N. L.; Burghardt, T. P. , "Total internal reflection fluorescent microscopy, "*J. Microscopy* **1983,** 129 (Pt. 1), 19-28.

[31] Weis, R. M.; Balakrishnan, K.; A., S. B.; McConnel, H. M. , "Stimulation of fluorescence in a small contact region between rat basophil leukemia cell and planar lipid membrane targets by coherent evanescent radiation, "*J. Biol. Chem* **1982,** 257, 6440-6445.

[32] Tilton, R. D.; Gast, A. P.; Robertson, C. R. , "Surface diffusion of interacting proteins: Effect of concentration on the lateral mobility of adsorbed bovine serum albumin, "*Biophys. J.* **1990,** 58, 1321-1326.

[33] Robeson, J. L., "Application of TIRF to probe surface diffusion and orientation of adsorbed proteins, " Ph.D. dissertation. Carnegie Mellon University, 1995,

[34] Lauffenburger, D. A.; Linderman, J. J.,"Receptors: Models for binding, trafficking and signaling., "*Receptors: Models for binding, trafficking and signaling.*, Oxford University Press, New York, 1996.

[35] Arai, K.; Kusu, F.; Takamura, K., "Electrochemical behaviour of drugs at the oil/water interfaces, " In *Liquid-liquid interfaces: Theory and Methods*, Volkov, A. G., Deamer, D. W. Eds.; CRC Press, 1996, p. 375-400.

[36] Morrison, L. E.; Weber, G. , "Biological membrane modeling with a liquid/liquid interface, "*Biophys. J.* **1987,** 52, 367-379.

[37] Arai, K.; Ohsawa, M.; Kusu, F.; Takamura, K. , "Drug ion transfer across an oil-water interface and pharmacological activity, "*Bioelectrochem. Bioenerg.* **1993,** 31, 65.

[38] Provost, C.; Herbots, H.; Kinget, R. , "Transparent oil water gels. study of some physicochemical and biopharmaceutical characteristics. Part IV: the in vitro release of hydrophilic and lipophilic drugs,, "*Acta. Pharma. technol.* **1989,** 35, 143.

[39] Yoshikawa, K.; Shoji, M.; Nakata, S.; Maeda, S.; Kawakami, H. , "An excitable liquid membrane possibly mimicking the sensation of tase., "*Langmuir* **1988,** 4, 759.

[40] Deamer, D. W.; Volkov, A. G., "Oil/water interfaces and the origin of life, " In *Liquid-liquid interfaces: Theory and Methods*, Volkov, A. G., Deamer, D. W. Eds.; CRC Press, 1996.

[41] Nakanaga, T.; Takenaka, T. , "Resonance Raman spectra of monolayers of a surface-active dye adsorbed at the oil-water interface, "*J. Phys. Chem.* **1977,** 81, 645-649.

[42] Takenaka, T.; Nakanaga, T. , "Resonance Raman spectra of monolayers adsorbed at the interface between carbon tetrachloride and an aqueous solution of a surfactant and a dye, "*J. Phys. Chem.* **1976,** 80, 475-480.

[43] Takenaka, T. , "Effect of electrolyte on the molecular orientation in monolayers adsorbed at the liquid-liquid interface: Studies by resonance Raman spectra, "*Chem. Phys. Lett.* **1978,** 55, 515-518.

[44] Conboy, J. C.; Messmer, M. C.; Richmond, G. L. , "Investigation of surfactant conformation and order at the liquid-liquid interface by total internal reflection sum-frequency Vibrational Spectroscopy, "*J. Phys. Chem.* **1996,** 100, 7617-7622.

[45] Perera, J. M.; McCulloch, J. K.; Murray, B. S.; Grieser, F.; Stevens, G. W. , "An attenuated total internal reflection spectrometer study of the kinetics of metal ion extraction at the decane aqueous solution interface., "*Langmuir* **1992,** 8, 336.

[46] Grubb, S. G.; Kim, M. W.; Rasing, T.; Shen, Y. R. , "Orientation of molecular monolayers at the liquid-liquid interface as studied by optical second harmonic generation, "*Langmuir* **1988,** 4, 452-454.

[47] Sauer, B. B.; Chen, Y.; Zografi, G.; Yu, H. , "Static and dynamic interfacial tensions of a phospholipid monolayer at the oil/water interface: Dipalmitoylphosphatidylcholine at heptane/water, "*Langmuir* **1986,** 2, 683-685.

[48] Dickinson, E.; Euston, S. R.; Woskett, C. M. , "Competitive adsorption of food macromolecules and surfactants at the oil-water interface, " *Progr. Colloid Polym. Sci.* **1990,** 82, 65-75.

[49] Plucinski, P.; Nitsch, W. , "Kinetics of interfacial phenylalanine solubilization in a liquid-liquid microemulsion system, "*J. Phys. Chem.* **1993,** 97, 8983-8988.

[50] Graham, D. E.; Chatergoon, L.; Phillips, M. C. , "A technique for measuring interfacial concentrations of surfactants at the oil-water interface, "*J. Phys. E: Scientific Instruments* **1975,** 8, 696-699.

[51] Kakiuchi, T., "Equilibirum electric potential between two immiscible electrolyte solutions, " In *Liquid-liquid interfaces: Theory and methods*, Volkov, G. A., Deamer, D. W. Eds.; CRC Press: New York, 1996.

[52] Dickinson, E.; Stainsby, G.,"Colloids in Foods, "*Colloids in Foods*, Applied Science Publishers, Barking, UK, 1982.

[53] Dickinson, E.,"Food Colloids, "*Food Colloids*, 1982.

[54] Markin, V. S.; Volkov, A. G., "Adsorption isotherms and the structure of oil-water interface., " In *Liquid-liquid interfaces: Theory and methods*, Deamer, D. W., Volkov, A. G. Eds.; CRC Press: New York, 1996.

[55] Leaver, J.; Dalgleish, D. G. , "Variations in the binding of b-casein to oil-water interfaces detected by trypsin-catalyzed hydrolysis, "*J. Coll. Interface. Sci.* **1992,** 149, 49-55.

[56] Ando, J.; Albeda, S. M.; Levine, E. M. , "Culture of human adult endothelial cells on liquid-liquid interfaces- A new approach to the study of cell-matrix interactions, "*In Vitro Cell. Dev. Bio* **1991,** 27, 525-532.

[57] Murray, B. S.; Nelson, P. V. , "A novel langmuir trough for equilibrium and dynamic measurements oil air-water and oil-water monolayers, "*Langmuir* **1996,** 12, 5973-5976.

[58] Malmsten, M. , "Ellipsometry and TIRF studies of adsorption processes in parenteral drug delivery, "*Interface Sci.* **1997,** 5, 159-167.

[59] Aoyama, K.; Ogawa, K.; Kimura, Y.; Fujiyoshi, Y. , "A method for 2D crystallization of soluble-proteins at liquid-liquid interface., "*Ultramicroscopy* **1995,** 57, 345-354.

[60] Shiba, Y.; Ohshima, T.; Sato, M. , "Growth and morphology of anchorage-dependent animal cells in a liquid-liquid interface system, "*Biotech. Bioeng.* **1998,** 57, 583-589.

[61] Andrade, J. D.; Smith, L. M.; Gregonis, D. E., "The Contact Angle and Interface Energetics Surface and Interfacial Aspects of Biomedical Polymers Vol 1:, " In *Surface Chemistry and Physics*, Andrade, J. D. Ed.; Plenum Press: NY, 1985.

[62] Axelrod, D.; Hellen, E. H.; Fulbright, R. M., "Biochemical Applications, " In *Topics in Fluorescence Spectroscopy, Vol. 3*, Lakowicz, J. R. Ed., 1992, p. 289-343.

[63] Tweet, A. G.; Gaines, G. L.; Bellamy, W. D. , "Fluorescence of chlorophyll * in monolayers, "*J. Chem. Phys.* **1964,** 40, 2596-2600.

[64] Wirth, M. J.; Burbage, J. D. , "Adsorbate reorientation at a water/(octadecylsilyl)silica interface, "*Anal. Chem.* **1991,** 63, 1311.

[65] Bessho, K.; Uchida, T.; Yamauchi, A.; T., S.; Teramae, N. , "Microenvironments of 8-anilino-1-naphthalenesulfonate at the heptane-water interface: Time-resolved total internal reflection fluorescence spectroscopy, " *Chem. Phys. Lett.* **1997,** 264, 381.

[66] Watarai, H.; Saitoh, Y. , "Total internal reflection fluorescence measurements of ion-association adsorption of water-soluble porphyrins at liquid/liquid interface, "*Chem. Lett.* **1995,** 283, 4.

[67] Tupy, M. J.; Blanch, W. H.; Radke, J. C. , "Total internal reflection fluorescence spectrometer to study dynammic adsorption phenomena at liquid/liquid interfaces, "*Ind. Eng. Chem. Res.* **1998,** 37, 3159-3168.

[68] Cheesman, D. F.; Davies, J. T. , "Physicochemical and biological aspects of proteins at interfaces, "*Adv. Protein Chem.* **1954,** 9, 439-501.

[69] Aveyard, R.; Vincent, B. , "Liquid-liquid interfaces: In isolation and in interaction, "*Prog. Surface Sci.* **1977,** 8, 59-102.

[70] MacRitchie, F. , "Proteins at interfaces, "*Adv. Protein Chem.* **1978,** 32, 283-326.

[71] Davies, J. T.; Mayers, G. R. , "Studies on the interfacial viscosities of monolayers, "*Trans. Faraday Soc.* **1960,** 59, 691-696.

[72] Fisher, L. R.; Mitchell, E. E., "Effect of adsorbed proteins on interactions between emulsion droplets, " In *Food Colloids*, Bee, R. D., Richmond, P., Mingins, J. Eds., 1989, p. 123-137.

[73] Yonese, M.; Hioki, Y.; Yano, M.; Kishimoto, H. , "Isooctane/water interfacial adsorption of chondroitin sulfates having hydrophobic counterions, "*J. Colloid Interface Sci.* **1992,** 149, 314-321.

[74] Castle, J.; Dickinson, E.; Murray, B. S.; Stainsby, G. , "Mixed-protein films adsorbed at the oil-water interface, "*ACS Symposium Series,* **1987,** 343, 118-134.

[75] Harrick, N. J.," Internal Reflection Spectroscopy, " *Internal Reflection Spectroscopy*, Interscience Publishers, New York, NY, 1967.

[76] Prieve, D. C.; Frej, N. A. , "Total internal reflection microscopy: A quantitative tool for the measurement of colloidal forces, "*Langmuir* **1990,** 6, 396-403.

[77] Axelrod, D. , "Cell surface heating during fluorescence photobleaching recovery experiments, "*Biophys. J.* **1977,** 18, 129-131.

[78] Cheng, Y. L.; Darst, S. A.; Robertson, C. R. , "Bovine serum albumin adsorption and desorption rates on solid surfaces with varying surface properties, "*J. Colloid Interface Sci.* **1987,** 118, 212.

[79] Edidin, M., "Fluorescent labeling of cell surfaces, " In *Methods in Cell Biology*, Wang, Y.-L., Taylor, D. L. Eds., 1989, p. 87-102.

[80] Canfield, E. R. , "The amino acid sequence of egg white lysozyme, "*J. Biol. Chem.* **1963,** 238, 2698-2707.

[81] Waggoner, A. , "Covalent labeling of proteins and nucleic asids with fluorophores, "*Methods in Enzymology* **1995,** 246, 363-373.

[82] Gölander, C.-G.; Hlady, V.; Caldwell, K.; Andrade, J. D. , "Absorption of human lysozyme and adsorbate enzyme activity as quantified by means of total internal reflection fluorescence, 125I labelling and ESCA, "*Colloids Surf.* **1990,** 50, 113-130.

[83] Robeson, J. L.; Tilton, R. D. , "Spontaneous reconfiguration of adsorbed lysozyme layers observed by total internal reflection fluorescence with a pH=sensitive fluorophore, "*Langmuir* **1996,** 12, 6104-6113.

[84] Britt, D. W.; Buijs, J.; Hlady, V. , "Tobacco mosaic virus adsorption on self-assembled and Langmuir-Blodgett monolayers studied by TIRF and SFM, "*Thin Solid Films* **1998,** 327, 824-824.

[85] Tilton, R. D.; Robertson, C. R.; Gast, A. P. , "Lateral diffusion of bovine serum albumin adsorbed at the solid-liquid interface, "*J. Coll. Interfacial Sci.* **1990,** 137, 192-203.

[86] Gajraj, A.; Ofoli, R. , "A quantitative technique for investigating macromolecular adsorption and interactions at the liquid-liquid interface, "*submitted to Langmuir* **1999**.

[87] Shukla, B. A., "Kinetics of desorption of BSA at the oil-water interface using total internal reflection fluorescence photobleaching recovery, " Ph.D. dissertation. Michigan State University, 1999,

[88] Johns, L. M.; Shelden, E. A.; Levitan, E. S.; Holz, R. W.; Axelrod, D. , "Motion of chromaffin granules near the plasma membrane as visualized with total internal reflection fluorescence microscopy, "*Biophys. J.* **1999,** 76, A70-A70.

[89] Sund, S. E.; Swanson, J.; Dzakpasu, R.; Axelrod, D. , "Cell membrane curvature visualized by polarized total internal reflection fluorescence, "*Biophys. J.* **1999,** 76, A75-A75.

[90] Fulbright, M. R.; Axelrod, D. , "Dynamics of nonspecific adsorption of insulin to erythrocyte membranes, "*J. Fluorescence* **1993,** 3, 1-16.

[91] Anderson, A. J. , "Covalent labeling of a protein, "*J. Chem. Edu.* **1991,** 68, 521-522.

[92] Hoyland, J., "Fluorescent probes in practice - potential artifacts, " In *Fluorescent and luminescent probes for biological activity*, Mason, W. T. Ed.; Academic Press: Cambridge, UK, 1993.

[93] Brynda, E.; Drobnik, J.; Vacik, J.; Kalal, J. , "Protein sorption on polymer surfaces measured by fluorescence labels, "*J. Biomed. Mat. Res.* **1978,** 12, 55-65.

[94] Crandall, R. E.; Janatova, J.; Andrade, J. D. , "The effects of radioiodination and fluorescent labelling on albumin, "*Preparative Biochemistry* **1981,** 11, 111-138.

[95] Robeson, J. L.; Tilton, R. D. , "Effect of concentration quenching of fluorescence recovery after photobleaching measurements, "*Biophys. J.* **1995,** 68, 2145-2155.

[96] Sacco, D.; Dellacherie, E.; Prochayret, F. , "Effect of covalent labeling of dextran-benzenehexacarbosylate on haemoglobin, "*J. Protein Chem.* **1994,** 13, 1-8.

[97] Stryer, L. , "*Ann. Rev. Biochem.* **1978,** 47.

[98] Ingle, J. D.; Crouch, S. R.,"Spectrochemical Analysis, "*Spectrochemical Analysis*, Prentice Hall, NJ, 1988.

[99] Peters, R.; Peters, J.; Tews, K. H.; Bahr, W. , "Microfluorimetric study of translational diffusion of proteins in erythrocyte-membrane, "*Biochim. Biophys. Acta.* **1974,** 367, 282-294.

[100] Amersham, P.-B.,"Ion Exhange Chromatography: Principles and Methods, "*Ion Exhange Chromatography: Principles and Methods*, Amersham Pharmacia Biotech, Upsala, Sweden, 1996.

[101] Lange, N. A.,"Lange's Handbook of Chemistry, "*Lange's Handbook of Chemistry*; vol. 13th edition, McGraw-Hill, 1985.

[102] Ygueribide, J. E.; Talavera, E.; Alvarez, J. M.; Quintero, B. , "*Photochem. Photobiol.* **1994,** 60, 435.

[103] Wegener, W. A.; Rigler, R. , "Separation of translational and rotational contributions in solution studies using fluorescence photobleaching recovery, "*Biophys. J.* **1984,** 46, 787-793.

[104] Wegener, W. A. , "Fluorescence recovery spectroscopy as a probe of slow rotational motions, "*Biophys. J.* **1984,** 46, 795-803.

[105] Axelrod, D.; Rubinstein, J. L.; Yuan, Y. , "Fast rotational diffusion measured by fluorescence recovery after photobleaching, "*Abstr. Pap. Amer. Chem. Soc.* **1992,** 203.

[106] Ofoli, R. Y.; Patel, A. , "*to be submitted to Langmuir* **1999**.

[107] Stout, A. L.; Axelrod, D. , "Spontaneous recovery of fluorescence by photobleached surface-adsorbed proteins, "*Photochem. photobiol.* **1995,** 62, 239-244.

[108] Jauhari, P., "A study of the diffusion of bovine serum albumin at the oil-water interface using total internal reflection fluorescence and fluorescence photobleaching recovery, " Ph.D. dissertation. Michigan State University, 1997,

[109] Nakai, S.; Lichan, E.; Hayakawa, S. , "Contribution of protein hydrophobicity to its functionality, "*Nahrung-Food* **1986,** 30, 327-336.

[110] Thomas, J.; Webb, W. W., "Fluorescence photobleaching recovery: A probe of membrane dynamics, " In *Non-invasive techniques in cell biology*; Wiley-Liss Inc, 1990.

[111] Ofoli, R. Y.; Gajraj, A.; Jauhari, P. , "Bulk and lateral diffusion of bovine serum albumin at the oil-water interface, "*Colloids and Surfaces (to be submitted)* **1999**.

[112] Reichert, M.; Rockhold, S.; Van Wagenen, R. A.; Andrade, J. D.,"Interfacial aspects of biomedical polymers, "*Interfacial aspects of biomedical polymers*; vol. 2, Plenum Press, New York, 1984.

[113] Norde, W. , "Adv. Colloid. Interface Sci., "*Adv. Colloid. Interface Sci.* **1986,** 25, 267.

[114] Wright, A. K.; Thompson, M. R. , "Hydrodynamic structure of bovine serum albumin determined by transient electric birefringence, "*Biophys. J.* **1975,** 15, 137-141.

[115] Cha, W. N.; Beissinger, R. L. , "Macromolecular mass transport to a surface: Effects of shear rate, pH and ionic strength, "*J. Coll. Interface. Sci* **1996,** 177, 666-674.

[116] Andrade, J. D.; Hlady, V.; Jeon, S. I. , "Poly(ethylene oxide) and protein resistance - principles, problems, and possibilities, "*Advan. Chem. Ser.* **1996,** 248, 51-59.

[117] Beaglehole, D.; Lawson, F.; Harper, G. , "Tryptophan, tryptophan-leucine, and BSA adsorption at an oil-water interface, "*J. Colloid Interf. Sci.* **1997,** 192, 266-268.

[118] Hamatsu,"Photomultiplier tyubes: Principle to application, "*Photomultiplier tyubes: Principle to application*, Hamamatsu Photonics, 1994.

[119] Rockhold, S. A.; Quinn, R. D.; VanWagenen, R. A.; Andrade, J. D.; Reichert, M. , "Total internal-reflectionfluorescence (TIRF) as a quantitative probe of protein adsorption, "*J. Electroanal Chem.* **1983,** 150, 261-275.

8. APPENDICES

8.1 Appendix A: Development of mathematical model for TIRF/FPR experiments in the diffusion-limited regime.

The following steps present the details of the development of a model of fluorescence recovery for pure-two-dimensional diffusion monitored by a laser beam with a Gaussian intensity profile. For simplicity, we approximate the photobleaching of fluorescent species as a simple, irreversible first order reaction with a rate constant proportional to the intensity profile.

Then the concentration of unbleached fluorophore, C (r, t), at a point r on the interface and at time t is given by

$$\frac{dC(r,t)}{dt} = -\alpha\, I(r)\, C(r,t) \qquad [41]$$

where $I(r)$ is the bleaching intensity profile and α is a proportionality constant. For a bleaching pulse that lasts a time interval T that is small compared with the characteristic time for transport, the post-photobleaching fluorophore concentration at $t = 0$ is given by

$$C(r,0) = C_0\, e^{-[\alpha T I(r)]} \qquad [42]$$

where C_0 is the uniform pre-bleach fluorophore concentration.

The amount of bleaching in time T is expressed by k, where

$$k = \alpha I(0)T$$

For a Gaussian intensity profile, $I(r)$ is given by

$$I(r) = \frac{2P}{\pi w^2}\exp\left(-\frac{2r^2}{w^2}\right) \qquad [43]$$

where w is the half-width at e^{-2} height, and P is the total laser power.

The differential equation for lateral transport of a single non-interacting species of protein in the absence of convection is given by Fick's law

$$\frac{dC(r,t)}{dt} = D\nabla^2 C(r,t) \qquad [44]$$

where D is the two dimensional diffusion coefficient. The boundary condition is $C(\infty, t) = C_0$, and the initial condition is given by Eqn. [42]

The fluorescence $F(t)$ observed at time $t \geq 0$ is given by

$$F(t) = \left(\frac{q}{A}\right)\int I(r)C(r,t)\,d^2r \qquad [45]$$

where $C(r, t)$ is the solution to Eqn. [44], subject to the boundary condition and k dependant initial condition described earlier. q is the product of all the quantum efficiencies of the fluorophore emission, absorption and detection, and A is the attenuation factor of the beam during observation of the recovery.

The pre-bleach fluorescence $\overline{F}$ can be written as

$$\overline{F} = \frac{qp\overline{C}}{A} \qquad [46]$$

The Fourier transform of [44] yields

$$\frac{d\tilde{C}(\mu, t)}{dt} = -\left[\mu^2 D\right]\tilde{C}(\mu, t) \qquad [47]$$

where $\mu^2 = \mu_x{}^2 + \mu_y{}^2$. The solution of Eqn. [47] is

$$\tilde{C}(\mu, t) = \tilde{C}(\mu, 0)\exp\left[-\mu^2 Dt\right] \qquad [47]$$

Since,

$$\tilde{C}(\mu, 0) = (2\pi)^{-1}\int d^2 r e^{i\mu.r} C(r, 0) \qquad [48]$$

with C $(r, 0)$ given by initial conditions and

$$C(r, t) = (2\pi)^{-1}\int e^{-i\mu.r}\tilde{C}(\mu, t)d^2\mu \qquad [49]$$

We obtain from Eqn. [45]

$$F(t) = \left(\frac{q\overline{C}}{4\pi^2 A}\right)\int d^2\mu.\phi(\mu).e^{-i\mu^2 D.t} \qquad [50]$$

where $\phi(\mu)$ is a function which depends on the laser intensity profile but not on the mechanism of transport. On expanding $\phi(\mu)$ and performing the integrations explicitly for a general term in the series we obtain a series solution applicable for all values of k and t.

$$F(t) = \bar{F}\sum_{n=0}^{\infty}\left[\frac{(-k)^n}{n!}\right]\left(1+n\left(1+\frac{2t}{\tau}\right)\right)^{-1} \qquad [51]$$

For k values smaller than 1 this reduces to the simple form

$$F(t) = \bar{F}\left(1-\frac{k}{2\left[1+\frac{t}{\tau}\right]}\right) \qquad [52]$$

8.2 Appendix B: FITC

8.2.1 Structure

Fluorescein isothiocyanate (FITC) is a derivative of fluorescein, an amine-reactive fluorescent molecule that is widely used in covalent labeling of proteins. The FITC molecule shown in Figure 8.1 is identical to the fluorescein molecule except for the presence of the isothiocyanate group at the 5- or the 6- position of the "bottom" ring of the fluorescein structure. The 5-isomer is the more common form because it is easier to isolate and is used in all experiments.

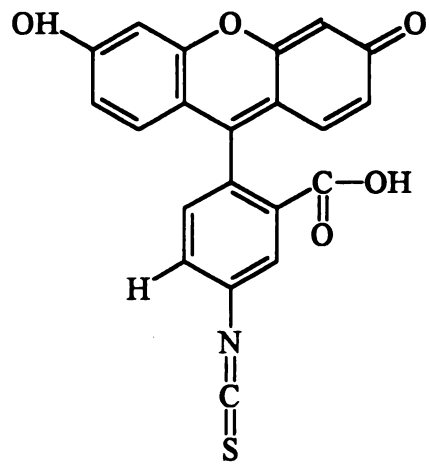

Figure 8.1. Structure of fluorescein isothiocyanate (5-isomer)

8.2.2 Prototropic forms

The fluorescence efficiency of FITC is closely dependent on the ionic state of the molecule, which in turn is affected by environmental factors. Figure 8.2 shows the various prototropic states of fluorescein at different pH values. An excellent source of information on the different states of protonation of fluorescein can be found in Ygueribide et al. (102). At low pH, the cationic form of fluorescein predominates and the molecule is slightly fluorescent. In the range 2.2 <pH< 4.4 the neutral prototropic form dominates and the molecule is non-fluorescent. At pH greater than 4.4 but less than 6, the slightly fluorescent monoanion is present and this converts to the dianion at pH greater than 6. The dianion shows a drastic, four-fold increase in fluorescence efficiency over the anion. All our experiments were run at a pH of 7.4, to ensure maximum fluorescence efficiency of FITC.

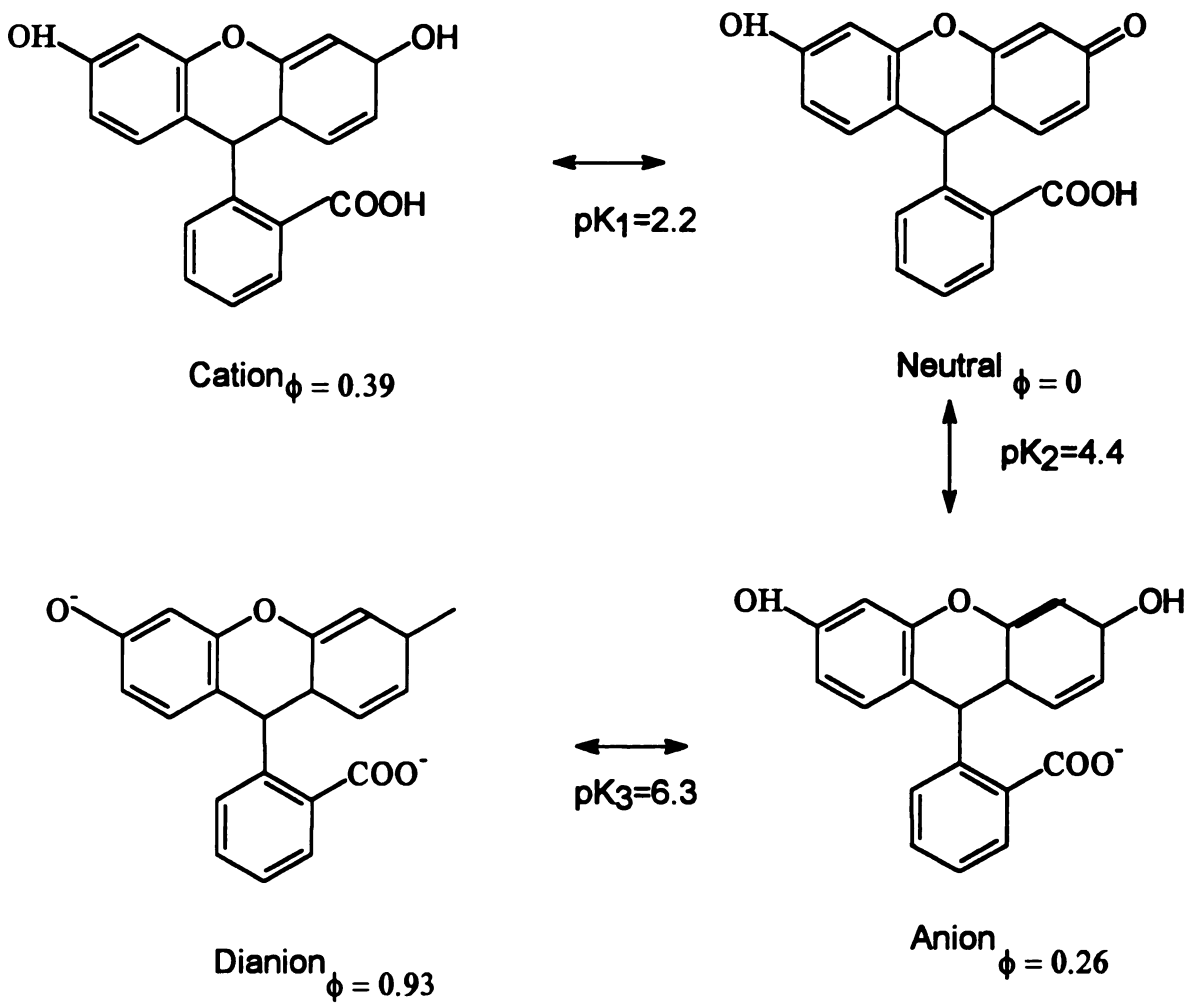

Figure 8.2. Prototropic forms of fluorescein at different pH with fluorescence efficiencies.

8.2.3 Absorption and emission spectra

The absorption and emission spectra for pure FITC in a pH 7.4 PBS buffer are shown in Figure 8.3 below. Fluorescein displays a Stokes' shift of about 20-25 nm between emission and excitation maxima. This is due to vibrational decay of excited molecules. The dotted straight line at 500 nm denotes the 500nm EFLP (emission frequency long pass) filter. This filter was placed after the microscope objective in the light path (from the interface to the PMT), and blocks all light of wavelength below 500 nm. This excludes excitation laser light, thus ensuring that the light impinging on the PMT is only from the emission of fluorescence.

The region of overlap between the emission and excitation spectra can also be seen in the figure. In this region, it is possible for a fluorophore to undergo a self-quenching process, in which emission energy is lost in a radiationless transfer.

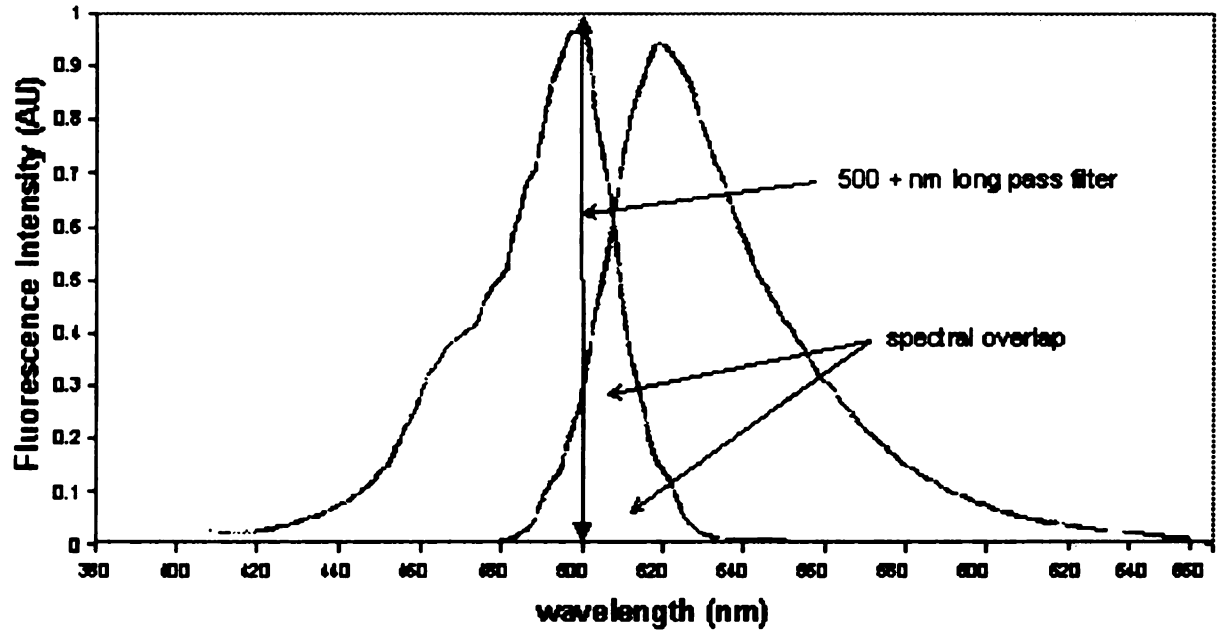

Figure 8.3. Absorption and emission spectra (excitation at 488 nm) for FITC in pH = 7.4 PBS buffer, showing spectral overlap and Stokes' shift

8.3 Appendix C: SAS programs for data analysis

Diffusion-limited regime

The Statistical Analysis Software (SAS) code used to perform non-linear regression of fluorescence recovery data in the diffusive regime model is given below. The maximum number of iterations allowed was 250, after which the data was abandoned as non-convergent. On an average, each regression program took 30 seconds to return the fitted parameters, depending on the size of the matrix of initial values provided. Comments describing the code are provided in italics immediately after the relevant line.

```
libname client 'c:\data';
filename adsas8 dde "excel|new8!r1009c3:r8000c4";
import of data from excel spreadsheet
data client.adsas8;
      infile adsas8;
      input ft time;
proc nlin method=gauss;
identification of non-linear regression algorithm
      parameters
            p=0.0004
            k=0.8
            tau=1000
            f=786;
     declaration of initial parameters
      bounds k>0;
      bounds tau>0;
```

```
    declaration of constraints
    temp=time/tau;
    pb = exp(-p*time);
    model ft= pb*(f+f*(-k*(2+2*temp)**(-1)+k**2/2*(3+4*temp)**(-1)-
              k**3/6*(4+6*temp)**(-1)));
    description of diffusion-limited model
    der.k=f*pb*(-(2+2*temp)**(-1)+k*(3+4*temp)**(-1)-k**2/2*(4+6*temp)**(-1));
    partial derivative with respect to bleaching parameter
    der.tau=f*pb*(-k*time/2*(tau+time)**(-2)+2*k**2*time*(3*tau+4*time)**(-2)
            -k**3*time*(4*tau+6*time)**(-2));
    partial derivative with respect to characteristic time of diffusion
    der.p=-time*pb*(f+f*(-k*(2+2*temp)**(-1)+k**2/2*(3+4*temp)**(-1)-
          k**3/6*(4+6*temp)**(-1)));
    partial derivative with respect to photobleaching rate constant
run;
```

Reaction-limited regime

The Statistical Analysis Software (SAS) code used to perform non-linear regression of fluorescence recovery data in the reaction regime model is given below. The maximum number of iterations allowed was 250, after which the data was abandoned as non-convergent. On an average, each regression program took 40 seconds to return the fitted parameters, depending on the size of the matrix of initial values provided. Comments describing the code are provided in italics immediately after the relevant line.

```
libname client 'c:\data';
filename br1 dde "excel|br1!r1029c3:r8001c4";
import of data from excel spreadsheet
data client.br1;
    infile br1;
    input ft time;
proc nlin method=marquardt maxiter = 250 g4singular;
identification of non-linear regression algorithm
    parameters
        f0=400
        kpb=0.001
        r0=0.64
        r1=0.05
        k1=0.5
        k2=0.01
        f=596;
    declaration of initial parameters
    bounds f0>0;
    bounds 0<r0<1;
    bounds 0<r1<1;
```

```
bounds k1>0;
bounds k2>0;
bounds kpb>0;
declaration of constraints
temp=exp(-time*kpb);
temp1=exp(-time*k1);
temp2=exp(-time*k2);
model ft=f-(f-f0*temp)*(r0+r1*temp1+(1-r0-r1)*temp2);
description of reaction-limited model
der.f0=temp*(r0+r1*temp1+(1-r0-r1)*temp2);
partial derivative with respect to post-bleach fluorescence
der.kpb=-f0*time*temp*(r0+r1*temp1+(1-r0-r1)*temp2);
 partial derivative with respect to bleaching rate constant
der.r0=-(f-f0*temp)*(1-temp2);
der.r1=-(f-f0*temp)*(temp1-temp2);
partial derivatives  with respect to protein fractions
der.k1=(f-f0*temp)*(time*r1*temp1);
der.k2=(f-f0*temp)*(time*(1-r0-r1)*temp2);
partial derivatives  with respect to desorption rate constants
run;
```

8.4 Appendix D: Absorbance calibration experiments

8.4.1 BSA at pH 7.4, PBS buffer

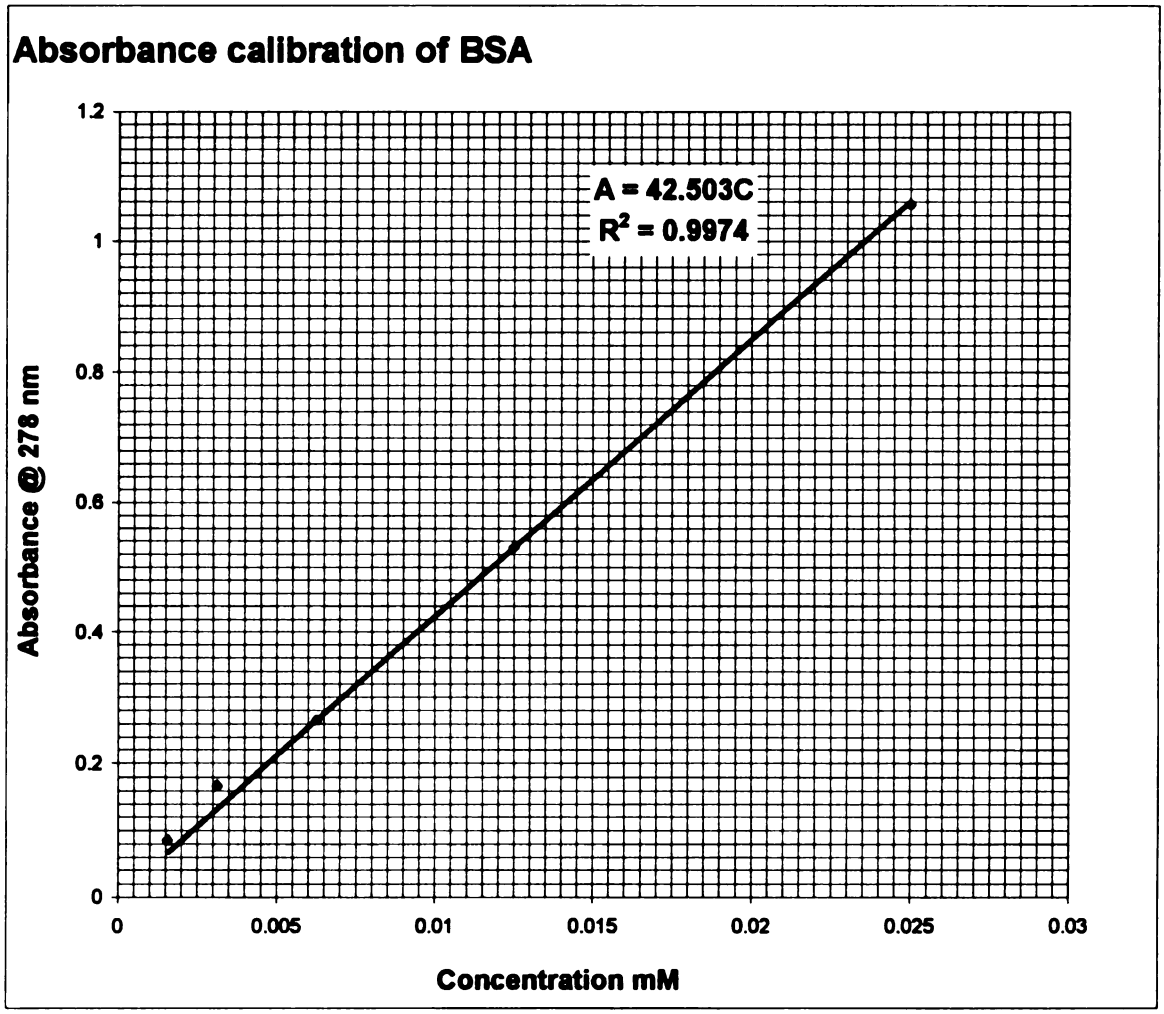

Figure 8.4. Absorbance versus concentration of BSA in pH 7.4 PBS buffer, measured with a diode-array spectrophotometer (8452A Hewlett Packard)

8.4.2 FITC at pH 5.1, acetate buffer

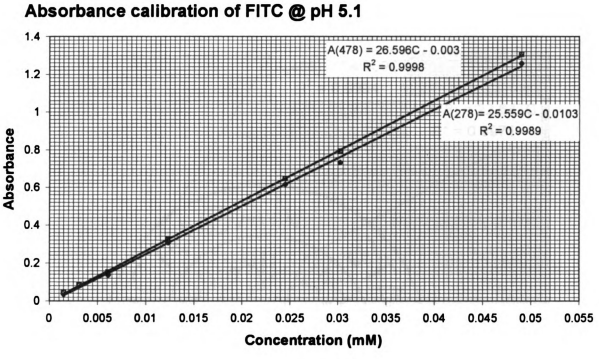

Figure 8.5. Absorbance versus concentration of FITC in pH 5.1 acetate buffer, measured with a diode-array spectrophotometer (8452A Hewlett Packard)

8.4.3 FITC in pH 7.4, PBS buffer

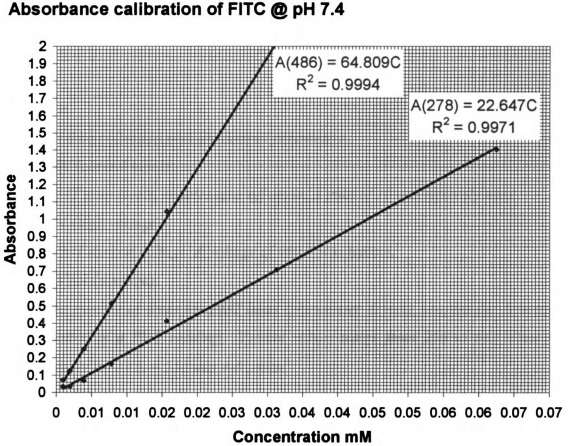

Figure 8.6. Absorbance versus concentration of FITC in pH 7.4 PBS buffer, measured with a diode-array spectrophotometer (8452A Hewlett Packard)

8.5 Appendix E: Data collection program

The Viewdac program code for reading data from the PMT head memory is listed below. An explanation of the code is presented in italics.

The PMT head is interfaced to an IBM 386 computer using an RS-232 interface with RTS/CTS handshaking protocols. The baud rate of data transfer is 9600 bytes/ sec.

Start P

Begins data collection with the desired parameters

Set CW (control word)

Sets PMT gain levels, enables sync off mode. A gain of 10 was typically used.

Set HV (high voltage)

Sets PMT dynode voltage. A voltage of 800 V was typical.

Set AVER (average)

Sets the number of times the PMT head (photometer device) samples the detector in the calculation of a PMT reading. Typical values range from 256 to 64. Time for one reading for an AVE = 256 was 4-6 μsecs.

Set INTER (time interval)

Sets the time interval between PMT readings, i.e. the time the PMT head rests between sampling cycles of the detector. Typical values ranged from 1 ms, for photobleaching experiments to 150 ms for experiments monitoring the timescale of equilibrium adsorption.

Set COLQTY (collection quantity)

Sets the number of readings to be taken by the PMT. Typicaly values ranged from 8000 to 20000.